MULTI-SCALE REMOTE SENSING TECHNIQUES FOR VEGETATION STRESS
DETECTION

By

JOHN C. CRAIG

A DISSERTATION PRESENTED TO THE GRADUATE SCHOOL
OF THE UNIVERSITY OF FLORIDA IN PARTIAL FULFILLMENT
OF THE REQUIREMENTS FOR THE DEGREE OF
DOCTOR OF PHILOSOPHY

UNIVERSITY OF FLORIDA
2001

Dedicated to my parents
Robert Thomas Craig and June Rose Craig
and to the late Sun-Fu "Tony" Shih

ACKNOWLEDGMENTS

This work is dedicated in part to Professor Sun. F. "Tony" Shih who, while chair of my supervisory committee, passed away suddenly on June 14, 2000. Professor Shih provided wise and helpful insights, support and encouragement. I would also like to thank my current committee chair, Jonathan D. Jordan, who, as a former student of Dr. Shih himself, provided greatly needed continuity and support for my doctoral program. Among my other committee members, Brian J. Boman helped tremendously by providing access to the citrus experimental site, which he designed and directed, and taught me a great deal about citrus production, irrigation and instrumentation. Many thanks to Mark T. Brown, who as chair of my master's program in environmental engineering sciences has remained a friend and advisor. Thanks to Professor Larry Bagnall who served on my supervisory committee, and to all my other teachers at the University of Florida and everywhere else I studied and learned. A Chinese proverb states that whoever teaches you for one day is your teacher for life.

I owe a special thanks to Gregory Carter of the John C. Stennis Space Center, my mentor under the NASA graduate student researchers program. Dr. Carter and the Earth Systems Science Office at the Stennis Space Center also helped provide access to airborne multispectral and hyperspectral imaging of our research sites, and other facilities and equipment. Thanks also to Ramesh Shrestha, Bill Carter and Grady Tuell of the

iii

TABLE OF CONTENTS

LIST OF TABLES

LIST OF FIGURES

Abstract of Dissertation Presented to the Graduate School
of the University of Florida in Partial Fulfillment of the
Requirements for the Degree of Doctor of Philosophy

MULTI-SCALE REMOTE SENSING TECHNIQUES FOR VEGETATION STRESS
DETECTION

By

John C. Craig

May, 2001

Chairperson: Jonathan D. Jordan
Major Department: Agricultural and Biological Engineering

The quantity and quality of available water resources impose limits on the use of

water for agricultural, industrial and domestic consumption. The effects of such limits

appear as stresses in agricultural crops and natural ecosystems. This study evaluated the

use of various remote sensing techniques to detect stress at three local scales in an

agricultural system (individual leaves, tree canopies, and an entire citrus grove), and at

regional scale, in natural wetland ecosystems.

The use of multispectral digital imagery is evaluated to identify stressed grapefruit

(Citrus paradisi) trees within an experimental grove in southeastern Florida. Salinized

irrigation water at four salinity levels and three different fertilization regimes were

applied to trees grown on four different rootstock varieties. Spectral reflectance analysis

of individual leaves, and multispectral images of single trees and of the whole grove were

used to assess stress effects by comparing reflectance in specific spectral bands from trees that received different experimental treatments. A separate citrus grove located in Vero Beach, Florida was used to assess remote sensing methods including airborne laser terrain mapping and leaf area index mapping

The study of stress effects on a regional scale in cypress *(Taxodium spp.)* wetlands uses a database containing quality rankings of over 200 sites in the Northern Tampa Bay Region of Florida to investigate the individual and cumulative effect that regional groundwater use and other external factors have on the wetlands. The wetlands were evaluated by field biologists from the Southwest Florida Water Management District based on a qualitative assessment on a 1 to 5 scale of factors such as hydrology, wetland vegetation and wildlife usage. Landsat imagery was used to assess wetland health throughout the region according to reflectance characteristics of the monitored wetlands.

CHAPTER 1
INTRODUCTION

1.1 Remote Sensing of Vegetation Stress

At the dawn of the 21st century, humanity is in the position as never before to profoundly alter the earth's environment. Nations throughout the world are looking for means to satisfy the demand for food and material goods of their growing populations. Scientists and engineers are called upon to provide an understanding of the processes of nature and deliver solutions that allow us to meet human needs and minimize harmful impacts on the natural environment. An important element in this effort is the ability to effectively monitor the impact our activities have on the environment. Among the tools that are used to monitor human activities on a large scale are remote sensing and related technologies, such as Geographical Information Systems (GIS). Remote sensing technologies have proven themselves indispensable for some applications, and useful for others. The effectiveness and the degree of utilization of remote sensing technologies are likely to continue to increase as time goes on, since the underlying technologies involved are becoming more powerful and less expensive, and research continues on their application to real-world problems.

This study focuses on the application of current and developing remote sensing technologies to monitor and evaluate vegetation stress in crops and in natural wetland

vegetation. Citrus groves were chosen as the tree crops to study, and the natural areas are Florida cypress *(Taxodium spp.)* swamps. The principal questions asked in this study include

1.   What is the spectral reflectance response of certain vegetation types to stress?

2.   How does the reflectance response change when observed at different spatial scales?

3.   What are some effective means for the remote detection of stress conditions in crops and plant communities?

The remote sensing technologies used in this study include spectral radiometry, land based and airborne digital multispectral imagery, airborne hyperspectral imagery and Landsat satellite imagery.

1.1.1 Location

Studies were conducted at three areas in east-central and west-central Florida. The primary site for citrus stress study was at the Indian River Research and Education Center, Ft. Pierce, Florida located at 28°28' North latitude, 80°23' West longitude. A secondary citrus research site located at the Kerr Center for Sustainable Agriculture, Vero Beach, Florida was also used. Its geographic location is 27°39' North latitude and 80°28' West longitude. The area for research on regional water stress detection in cypress wetlands is located in a 2000 km² region in Hillsborough, Pasco and Hernando counties, north of Tampa, which extends between 28°0' and 28°23' North latitude and 82°15' and 82°45' West longitude (see Figure 1.1).
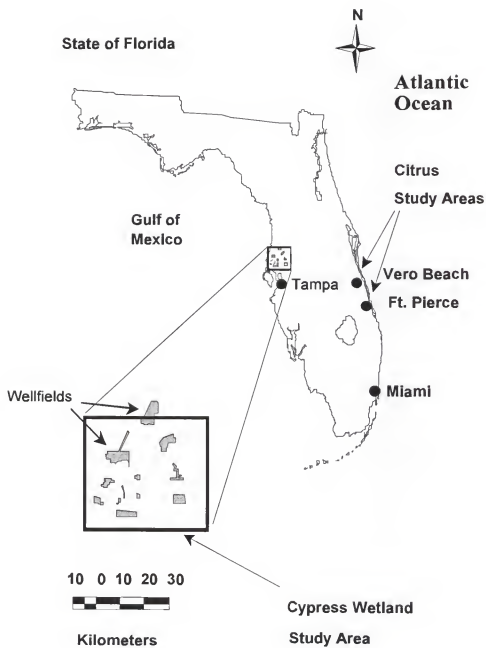
Figure 1.1 Locations of study areas: Citrus studies in Ft. Pierce and Vero Beach, and the Cypress study area in the Northern Tampa Bay area.

1.1.2 Spatial and Temporal Scale Dependance

It will be shown that the successful application of remote sensing technologies is largely dependant on the scales in several dimensions on which the processes that are being detected operate, and the scales on which instruments used to detect them operate. The dimensions of interest are spatial (such as length, width and height), temporal, and spectral. This work is organized into several parts which highlight a study of vegetation stress at a particular spatial scale. The stress detection techniques studied are each applicable at the indicated scale, but further allow the study of cross-scale behavior of spectral reflectance response. The approximate spatial scales are:

(1)   single leaf (1 cm-10 cm)

(2)   tree canopy (1 m-5 m)

(3)   grove (100 m-1000 m)

(4)   region (10 km-100 km)

Ths smallest scale studied (1) is that of individual leaves, where leaves were sampled from 24 trees in an experimental citrus grove at the University of Florida Indian River Research and Education Center at Fort Pierce, Florida. The trees have 'Ray Ruby' grapefruit scions planted on 'Swingle citrumelo' rootstocks. The trees selected for single-leaf scale study were differentiated in that they had received irrigation water with either high or low levels of salinity, and represented samples of three different fertilizer treatments, as specified in Chapter 2. Spectral reflectance measurements of a number of

leaves from the trees representing each experimental treatment were compared statistically to determine the wavelengths which show the greatest differences. While irrigation water quality and soil salinity are known to be factors which can produce stress in Citrus trees (Syvertsen et al. 1989), it is not suggested that spectral reflectance can show "stress" directly. It is, however, suggested by the experiments that the effects of vegetation stress may cause differences in spectral reflectance, and that citrus trees that had been exposed to stress factors may be distinguished from those which had not been so exposed by analyzing their spectral reflectance response.

The tree canopy scale experiments utilized the same trees that were studied in the single-leaf experiments. The intention of the canopy-scale study was to determine if multispectral imaging of citrus trees can be used to differentiate trees which had been exposed to stress factors. Additionally, the single-leaf and canopy scale measurements of the same trees can be used to show cross-scale effects, where reflectance in specific wavelengths may behave differently at different spatial scales. In the case of tree leaves and canopies, the differences may arise from the positioning of leaves at many varying angles in a canopy, whereas single-leaf measurement is done at one angle only. Furthermore, in tree canopy images, there may be gaps between leaves where other materials are visible, such as tree branches, or there may be areas in the canopy that are heavily shaded by other portions of the canopy. Such differences in reflective surfaces (relatively homogeneous leaf surface compared with a more heterogenous tree canopy) are unavoidable in any realistic remote sensing application. It may be noted that leaves

can be regarded as heterogeneous reflective surfaces at millimeter scales, since they may contain variegations, veins and spots.

At the grove scale, aerial multispectral and hyperspectral images were used, in addition to Landsat images. Aerial images were collected in May, 1999, at the Fort Pierce experimental site, and in May, 2000, at the Fort Pierce site in addition to two other citrus groves in Florida, in Vero Beach, some 60 km to the north of Fort Pierce, and at Hickory Branch, about 80 km to the west. The grove scale is perhaps the most useful for individual growers to assess the degree of damage to their crop and potential impact on harvest. A synoptic aerial view allows a comparison of different sections of a citrus grove and identification of factors that may be reducing growth and productivity in portions of the grove.

The regional scale study was done using Landsat imagery. Landsat images differ from the aerial images used in terms of spatial scale, as well as spectral scale and range, as well as the timing and repeat rate of successive imaging passes. While airborne imaging platforms can avoid cloud contamination of images by choosing clear days to fly, satellite sensors are limited to capturing images on the specific dates and times that they overpass a particular area. This makes the capture of Landsat satellite images during the rainy season a matter of luck, and as a result, all of the images used in this study were captured during cloud-free periods, between January and March.

To provide a clear understanding of the dimensions used in this study and the effects of scaling on observations, they will be briefly discussed here. The dimensions within the plane of the earth's surface (length and width) are most closely related to the

spatial resolution (pixel size) of the imaging device and the area covered by the objects of interest on the ground. If the objects are considerably larger than the pixel size, their shapes can be easily discerned, and if they are homogeneous, the reflectance observed in the pixels that fall within the object will be easily identifiable as that of the target object. On the other hand, if the pixel size is larger than the target object, its shape cannot be detected, and the reflectance observed within the pixel will be a mixture of that of the object together with surrounding material. Where the size of the objects in an image are approximately equal to the pixel size, the image will exhibit a greater index of spatial variability than if the objects were larger or smaller than the pixel size on average (Cao and Lam 1997).

The height dimension relates to the vertical variation within the image and may be negligible if the height of the target objects is much smaller than the pixel size of the image, for instance in 30 meter resolution Landsat imagery of peninsular Florida, where the topography rarely varies by more than a few meters within a 30 meter pixel area. Effects due to variation in height or elevation, known as topographic effects, become significant where object heights are much larger than pixel size, such as a Landsat image of mountainous terrain, or low altitude aerial imagery. When an accurate digital elevation model (DEM) is available of the target area, it can be used to terrain correct the image to remove geometric distortion by projecting the 3 dimensional land surface onto a 2 dimensional plane, and to correct radiometric distortions by adjusting the pixel values to accommodate variations in sun angle and shading (ERDAS 1999). In the present study there are significant shading effects in the aerial imagery of citrus trees, however, lacking

an accurate digital model of the tree canopies, the use of standard terrain correction techniques is not possible. Instead, analysis of tree canopy reflectance was restricted to the portions of the tree canopies that were not shaded.

The time dimension, as it applies to remote sensing of vegetation, relates the rate of change of vegetation characteristics that are being assessed to the frequency of repeated imaging of the targets. In order to detect seasonal changes, for example, images must be captured several times during the year, at least once during each season. If it is desired to detect changes that occur on a fairly short timescale, such as a brief flowering period, image capture must be timed appropriately (Steven 1993). In the case of the present study, imagery was obtained at ground level at sufficiently small time intervals to observe the onset of stress in citrus trees during the dry season, however airborne images could only be obtained once per year over 2 years, and therefore could not record seasonal change or the onset of stress, however they do allow comparison from one year to the next. Landsat images of the citrus grove were available for three periods over ten years. Although the coarser spatial scale of the Landsat imagery does not allow the identification of individual trees, it does allow the observation of the growth of groups of trees over a ten year period. Landsat imagery was also used in the Cypress wetland study, and the two images captured in 1992 and 1994 allowed for a comparison between years.

The spectral dimension relates the wavelengths of the radiant energy reflected by the objects being studied to the sensitivity of the remote sensing device in various wavelengths and its ability to record the measured reflectance in discrete bands. The

methods used to acquire and interpret spectral reflectance data are areas of intensive research at the present time, and form an important part of this study.

1.1.3 <u>Florida Citrus History, Stresses and Remote Sensing</u>

The various species and varieties of citrus can probably trace their origins to the Malay Archipelago some 20 million years ago. It gradually developed into an edible fruit in Southeast Asia, and the earliest record of its cultivation appeared in China. By the 4th century BC it had made its way to classical Greece, and was cultivated throughout the Mediterranean region by the Arabs. Columbus was known to have brought the first citrus seeds to America on his second voyage, and it was likely brought to Florida from Hispañola by Ponce de Leon. Various edible varieties, however, continued to be introduced directly from China and other regions. Citrus readily hybridizes with close relatives, and hundreds of varieties are known to exist at present.

The grapefruit has its probable origin from the pummelo *(Citrus maxima)* or shaddock *(Citrus decumana)*, which were brought from Southeast Asia to the West Indies in the 17th century. Grapefruit was first described by Griffith Hughes in 1750, who called it the "forbidden fruit." James MacFayden gave it the botanical name, *Citrus paradisi Macf.,* in his book *Flora of Jamaica*, in 1837, believing it to be a spontaneous sport of the pummelo. By the middle of the 20th century, citrus specialists began to suggest that the grapefruit was not a sport or mutation of the pummelo, but rather an accidental hybrid between the pummelo and the orange (Morton 1987).

The grapefruit was introduced to Florida in 1806 by the one time chief surgeon of Napoleon's navy, Count Odet Philippe, who established a grove in the Tampa Bay area in the 1820's, although it did not gain commercial acceptance until later in the century. The first commercial shipments of grapefruit from Florida and the West Indies to the northeastern United States took place in the 1880's. Its cultivation spread throughout the southern US as well as to South America and Israel by the 1940's. Grapefruit sales had increased in volume and price to become Florida's most valuable export crop by 1980 (Morton 1987). By the mid 1990's the industry had suffered from overproduction worldwide and weakened demand, but by the end of the decade, profitability had improved and grapefruit lands have increased in value.

One of the principle regional environments in which citrus is commercially produced in Florida is the coastal flatwoods region. It is characterized by shallow sandy soils overlaying a nearly impermeable spodic zone, or "hardpan" (Myers and Ewel 1990). Water management in this region requires careful control of water table depth, as the impermeable zone can cause heavy rainfall to quickly saturate the soil, and cause flooded citrus root systems to die. As a result, citrus production requires the formation of raised beds with drainage ditches between them to prevent the root zone from saturating. As a result, the root systems are kept relatively shallow (often 1 meter or less), and this contributes to the second main problem of water management in the flatwoods region, that of providing sufficiently frequent irrigation to prevent water stress during dry periods. The design and implementation of irrigation programs for citrus production in

the coastal region is further complicated by the sometimes poor water quality available for irrigation.

Water in the Upper Floridan aquifer, which underlies the entire state, and provides the largest source of fresh water in Florida, varies greatly in salinity, or dissolved solids concentration, from one region to another. Dissolved solids concentration is the sum of all cations and anions in solution in the water. The most common cations include sodium, calcium and magnesium, and the most common anions include chloride, bicarbonate and sulfate. Two factors principally determine the concentrations of dissolved solids in the aquifer: the ground water flow system, and the proximity to seawater (Miller 1990). Therefore, the regions which have the highest dissolved solids concentrations are those further south since they have the longest flow paths and have had the most time to dissolve minerals from the aquifer, and areas near the coast since seawater can intrude inland and mix with the freshwater, especially during dry periods when outward flow is reduced, or where there is excessive public water usage.

1.1.4 Salinity and Citrus Stress in Florida

Citrus is considered to be a salt sensitive crop because reduction of growth and fruit production occur at relatively low salinity levels (Tozlu 1997). Stress effects that are commonly reported include reduction in vegetative and generative growth due to reduced osmotic potential in the root zone (Dasberg et al. 1991) and leaf injury or loss due to the toxic effects of Cl^- accumulation (Storey 1995).

While most of the early studies on the effects of increased salinity in citrus or the salinity tolerance of citrus rootstocks were done in a laboratory or greenhouse, the present study was conducted at a long-term experimental site exposed to ambient rainfall and weather conditions. During the dry season (March-June), there is relatively low rainfall, and salt accumulates in the soil receiving saline irrigation. There are various visible acute effects of the increased salinity during the dry period, such as delayed leaf formation and leaf drop, delayed flowering and fruiting, and reduced fruit production and quality. During the rainy season, salts are leached from the soil, and stressed trees are able to recover foliage and growth. Chronic or long-term effects of this regime of periodic salinity stress include lower canopy volume due to slower growth rates, and reduced production (Boman 1993).

1.1.5 Cypress Wetlands in Florida

Some of the most common forested wetland ecosystems in Florida are dominated by *Taxodium distichum* (L.) Rich., known as baldcypress, or simply as cypress. Cypress is a deciduous conifer in the family *Taxodiaceae*, which includes 14 species found in China, Japan, Taiwan, Tasmania, and North America. In the United States, cypress's only other relatives are the *Sequoia* and *Sequoiadendron* genera which include the giant redwoods and sequoias of California (Duryea and Hermansen 2000). There are two common subspecies in Florida, baldcypress *(Taxodium distichum*(L.) Rich. var. *distichum)* and pondcypress *(Taxodium distichum*(L.) Rich. var. *nutans)*. Some taxonomists refer to pondcypress as a separate species, (*Taxodium ascendens* (Brongn.). Baldcypress can grow

up to 50 meters tall and more than 2 meters in diameter. Its leaves are flat, 10-15 mm long, and grow on both sides of small branchlets that extend horizontally. Pondcypress is a smaller tree with smaller scale-like leaves pressed close to its branchlets, which tend to hang downward somewhat. The differences between the two varieties are sometimes distinct, sometimes not, as they can interbreed readily, and both characteristics can appear on the same tree. Brandt and Ewel (1989) have summarized the differences between the growth characteristics of the two varieties as follows: baldcypress grows at low stem densities in locations with moderate water flow, high-nutrient availability, and rare forest fires. Pondcypress grows at high stem densities on sites with slow-to-stagnant water, low-nutrient availability, and occasional forest fires (Brandt and Ewel 1989). Both varieties have characteristic trunks that thicken at the base, buttress roots and structures known as "knees" which grow upward out of the root systems, up to nearly a meter above ground.

Cypress grows throughout the coastal plain of the southeastern United States from Delaware to Texas, and in the Mississippi Valley as far north as southern Illinois. Although cypress can tolerate a wide variety of climatic conditions, ranging from dry soils to permanently flooded lakes and streams, it is unlikely to reproduce and thrive except in very poorly drained, intermittently flooded soils. Although the most common means of seed dispersal for cypress is by water, the seeds do not germinate underwater, only when the waters recede and the moist soil is exposed to air (Wilhite and Toliver, 1990).

Cypress swamps and other types of forested wetlands that are periodically flooded receive nutrient subsidies from the floodwaters and as a result are some of the world's

most productive ecosystems. The annual above-ground production of biomass in a baldcypress-ash floodplain forest in Florida was 15,700 kg/ha (Brown 1981). In comparison, terrestrial forest communities in the temperate region often produce 12,300 to 15,000 kg/ha annually (Connor and Day 1976). Forested wetlands that do not receive nutrient subsidies from floodwaters, such as oligotrophic swamps located in drainage basin headwaters, have gross primary productivity rates comparable to, or lower than, those of terrestrial forests. Such wetlands, however, offer additional benefits such as wildlife habitiat (Wilhite and Toliver 1990), and storage of water and peat (Brown 1981).

During the first half of the 20th century, logging removed the majority of the large, old-growth baldcypress trees in virtually all the swamps in Florida, encouraged by the expansion of the railroad system throughout the nation (Duryea and Hermansen 2000). Cypress was used in products such as railroad ties, shingles and siding for buildings, pilings, ladders, soft-drink cases, fenceposts, and stakes. The Southern Cypress Manufacturers Association had claimed that these cypress products were protected from termites for 300 years. Cypress knees were marketed as beehives and birdhouses (Brandt and Ewel 1989). Due to its ability to tolerate dampness without affecting a liquid's taste or odor, cypress was ideally suited for water tanks and cisterns (Burns 1980). These new marketing tactics increased demand which increased the production of cypress lumber from 495 million board feet in 1899 to its peak in 1913, when more than one billion board feet were milled (Williston et al. 1980).

Cypress harvests dropped severely during the Depression years, and have never regained the former quantities. The virgin stands harvested during the peak years had

trees that were up to 1,000 years old, and commonly produced yields of 112 to 196 m³/ha. Under forest conditions, baldcypress trees require about 200 years to reach sufficient size to yield a high proportion of heartwood lumber (Kennedy 1972). While it would take another century for most of the previously harvested old-growth swamps to reach that size, cypress harvesting is on the rise again. From 1979 to 1987, 32 million cubic feet (906,000 m³) were harvested annually in Florida; from 1987 to1995 the annual harvest was 42 million cubic feet (1,189,300 m³) (Brown 1987, 1995) while board feet of sawtimber produced in the '90s decreased, the increased total annual harvest (from 32 to 42 million cubic feet) most likely reflects the growth in the mulch market. Though it tends to be smaller in size and provide lesser quality wood, much of the cypress harvest at present is of the pondcypress variety, because it is most abundant (Duryea and Hermansen 2000).

Many cypress-dominated wetlands are commonly referred to as domes, since the trees in the center of the stand are tallest, and those near the edges are smaller, giving the closed canopy structure a dome-shaped profile. In such areas, the upper canopy may be completely dominated by cypress, although many smaller herbaceous or woody plant species are found in the understory. These may include buttonbush *(Cephalanthus occidentalis)*, muscadine grape *(Vitis rotundifolia)*, Spanish moss *(Tillandsia usneoides)*, cattail *(Typha latifolia)*, lizardtail *(Saururus cernuus)*, and various hollies *(Ilex spp.)*, viburnums *(Viburnum spp.),* lyonias *(Lyonia spp.)*, orchids, bromeliads, sedges, grasses, and ferns (Barry 1980).

In other cypress-dominated wetlands, the upper canopy may be shared with a percentage of other wetland tree species, such as water tupelo *(Nyssa aquatica)*, swamp tupelo *(N. sylvatica* var. *biflora)*, red maple *(Acer rubrum)*, sweetbay *(Magnolia virginiana)*, southern magnolia *(M. grandifolia)*, sweetgum *(Liquidambar styraciflua)*, water oak *(Quercus nigra)*, ashes *(Fraxinus spp.)*, and some pines *(Pinus spp.)* (Wilhite and Toliver, 1990).

1.1.6 Impacts on Wetlands in the Tampa Bay Region

The principal large scale factors that affect wetlands in the Tampa Bay region, and contribute to their degradation, include the conversion of wetlands to urban or agricultural use, and indirect impacts from urban and agricultural zones due to ground water depletion. The interaction of wetland, urban and agricultural systems with the essential environmental inputs such as rain, wind and sunlight are shown in an energy systems diagram (Figure 1.2). The symbols used, and their definitions are given in Appendix B. The main interactions are shown at the numbered locations in the diagram. Sunlight (1) supports plant life in the wetlands and natural upland areas as well as agricultural fields. Rainfall (2) brings water to those systems, part of it recharges the groundwater, and part leaves the area through runoff. The wind brings in air, including oxygen and CO_2 as well as water vapor, and carries out water from the evapotranspiration of plants. The groundwater (4) is necessary to maintain wetland hydrology, although part is withdrawn in public wellfields, and some withdrawn from private irrigation wells to supply the agricultural system. Natural upland areas contribute to the support of wetlands, as shown
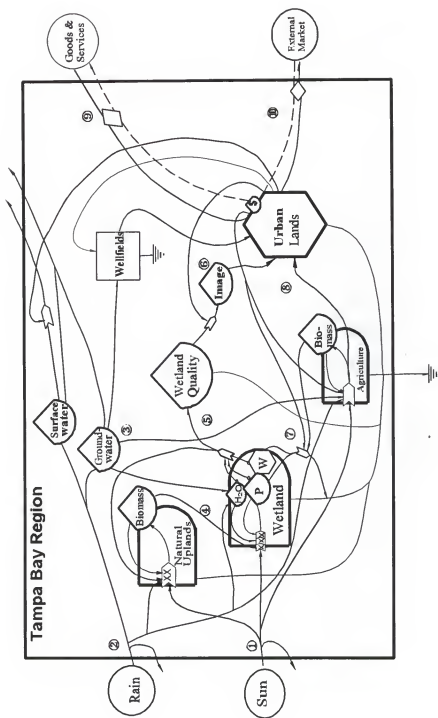
Figure 1.2 Energy systems diagram of the major causes of stress on wetlands in the Tampa Bay region (from Craig 1996). The interactions indicated by numbers are explained in the text.

in pathway (5) and wetlands contribute as well to the natural upland areas. This symbiotic relationship is manifest in many ways, including the exchange of wildlife between natural and upland areas, including animals that live in upland forests but feed in the wetland, or some bird species which nest in wetlands but feed elsewhere. Wetland quality (6) is a composite of several factors including hydrology, wetland plants and wildlife. The accumulation of "image" (7) is related to the way human society perceives wetlands and is a measure of the aesthetic value they have for society. The urban population (8) receives inputs from agriculture as well as imported goods and services, water, and aesthetic (or recreational) values. People also provide the necessary labor input to agriculture, sell goods and produce in exchange for money, which they use to buy other goods and services. Both the urban population and the agricultural lands are depicted in this model as contributing to the destruction of wetlands (9) by reducing both plant life (P) and wildlife (W). Pathway (10) shows the flow of goods and services into urban areas, and out to the markets in exchange for money.

1.2 Review of Literature

1.2.1 Interpretation of Airborne Imagery

Prior to the existence of aerial photography, natural resource mapping was a far more tedious and less accurate process than it is today. Aerial photography developed significantly during World War I, and after the war, civilian use, particularly for agriculture, forestry and mineral exploration, became commonplace. Color infrared film

was first introduced during World War II as "camouflage detection film" because of its ability to distinguish living vegetation from green camouflage coverings (Lillesand and Kiefer 1994). While digital multispectral imaging equipment is starting to become commonly available on aerial platforms, color infrared and natural color film is still the mainstay of airborne photography and photogrammetry.

The growth habits of cypress and other forest species have an impact on the methods used to map and quantify forested areas with remote sensing. Photointerpretation is key to making effective use of aerial images for natural resource mapping. It must be done with knowledge of the characteristics of various ground cover types as they appear in the photographs, including colors and hues, shadows, textures, shapes, sizes, patterns and, importantly, associations of different ground cover types that commonly appear together. The success of airphoto interpretation depends on the skill and training of the interpreter, the quality of the photography and the nature of the objects or phenomena being observed (Lillesand and Kiefer 1994).

Digital images such as those from satellite sensors capture and present image data in computer readable format. Among other goals, much effort has been applied to developing computer algorithms to automatically "interpret" the images and list the ground cover types present in the image, and the area covered by each. While many advances have occurred on this front, there is no general method that is as accurate as human interpretation to precisely identify all of the objects that appear in an airborne or satellite image. Automated classification methods have the advantage of processing an image with far greater speed and consistency than is possible by a human. Even to do

this, however, the classification programs require considerable human intervention to provide information about context, and specify the number and define the types of land cover classes that a computer program will identify in the image (Lillesand and Kiefer 1994) .

1.2.2 Collection and Interpretation of Canopy-scale Imagery

The capture of images only a few meters or so from the subject defies the common notion of remote sensing, although it is frequently used in industrial processes, such as product inspection (Kaplan 1996). Image capture at the tree canopy scale is generally done to determine the spectral characteristics of the trees, and the bands or band ratios that are most sensitive to the phenomena in question as a preliminary step to developing airborne imaging techniques (Carter et al. 1996a, Craig and Shih 1998). Some of the difficulties involved with canopy scale imaging include the effects of sun angle on the trees, which may be resolved by capturing the images in the morning or afternoon on the illuminated side of the trees, and to capture images at the same time of day to maintain a consistent illumination angle and camera angle (Carter et al. 1996b). Image analysis must be done with care, so that comparisons between trees or the same tree at different dates are based on images of comparable sections of the tree canopy. Carter et al. (1996a) selected portions of tree images for analysis which corresponded to the central 1 m^2 of the canopy in each case. Radiometric correction can be done using a set of grey shaded panels placed in each image to provide a reflectance reference, and calculating a

reflectance image using some form of an empirical line method, where a calibration curve
is developed based on the known reflectance of the shaded panels. (Carter et al. 1996a).

1.2.3 Citrus Leaf Structure

Citrus trees are evergreen, woody, broadleaf plants, which have a leaf structure as
follows: single leaves are attached to the stem or twig by a petiole which supports the leaf
and transports water, nutrients and photosynthates to and from the leaf. The vascular
system continues into the midrib, and smaller vascular bundles extend from the midrib to
other parts of the leaf. Leaf tissue is composed of several layers (see Figure 1.3). The
upper surface is covered with a waxy cuticle (C) which reduces water loss. Below that,
and also on the bottom surface, is the epidermis (E), which is dotted with stomata (S), or
small openings that allow for gas exchange, and through which most of the transpiration
occurs. There are normally many more stomata on the bottom surface of the leaf than the
top surface. The stomata have a pair of guard cells that open and close to regulate gas
exchange and water loss. Below the upper epidermis are the palisade cells (P), which are
cigar shaped and arranged vertically. They contain most of chloroplasts in the cell and are
responsible for photosynthesis. Below the palisade layer are spongy mesophyll cells (M),
which also contain chloroplasts. Between the mesophyll cells, and to a lesser extent,
between the palisade cells, are air spaces that allow air to circulate within the leaf.
Vascular bundles (V) are interspersed in the mesophyll just below the palisade
layer.Liquids are transported to and from all the cells in the leaf through their cell walls,
which are in contact with each other.
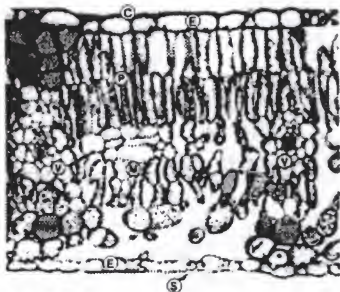
Figure 1.3 Light micrograph of a cross section of a *Populus* leaf. Adapted from Salisbury and Ross (1992). The labeled structures are cuticle (C), epidermis (E), stomata (S), palisade cells (P), mesophyll (M) and vascular bundles (V).

1.2.4 Plant Water Content

Water makes up as much as 90% of herbaceous plant matter and 50% of woody tissue by weight. By maintaining cell turgor, it keeps herbaceous portions of the plant erect and extended. It also serves an essential role as a solvent that carries minerals and gasses throughout the plant, and as a temperature regulator by cooling leaves through evaporation. Water is essential for photosynthesis, although only a small portion of the water taken into a plant is used as a reagent. The majority, about 95%, is transpired, transporting solutes and cooling the plant, while less than 5% of the water is used for growth and metabolism (Kramer 1983).

The water potential of plant tissue is an important physiological indicator. Water potential (ψ) is defined by Salisbury and Ross (1992) as "the chemical potential of water, expressed in units of pressure and compared with the chemical potential (also in pressure units) of pure water at atmospheric pressure at the same temperature and height, with the chemical potential of the reference water being set at zero." The currently used SI units for water potential are Megapascals (MPa), although it was common until recently to express it in bars, where 1 bar = 0.01 MPa.

A more precise representation of water potential is given by Beadle *et al.* (1993), where it is expressed as the potential energy in joules of water in the plant (μ_w) per unit partial molal volume of water (V_w), with reference to pure water at zero potential (μ_w^0), as seen in equation 1.1.

$$\psi_w = \frac{\mu_w - \mu_w^{\,o}}{V_w} \tag{1.1}$$

Moist soil has slightly lower potential due to the presence of solutes and adhesion to soil particles. An increasingly negative water potential gradient must exist in the plant from its roots to its leaves to allow for the transport of water upward, against gravity, although water transport is facilitated by capillary action in the narrow tracheids of xylem tissue. It is by virtue of the strongly negative water potential of unsaturated air that water and nutrients are drawn up through the plant from the soil, making photosynthesis possible.

Water potential observable in plant tissue is the result of a combination of factors. The main source of water potential depression in xylem tissue is hydrostatic tension that results from water being removed from the stomata by transpiration, denoted by ψ_p. Within plant cells, solute concentration is high and contributes significantly to lower the water potential. Osmotic potential (always negative) is indicated by ψ_n. Another source of water potential depression in plant tissue is matric potential, which results from the adsorption of water by hydrophilic surfaces such as cell walls, and is indicated by ψ_m. Dry hydrophilic surfaces can have an extremely negative water potential, which becomes less negative as they imbibe water, and reaches zero potential when they are saturated. Within cells, the contribution of matric potential depends on the water potential that results from osmosis, which prevents hydrophilic surfaces from becoming saturated. Another component of water potential within plant cells is the hydrostatic pressure that results in cell turgor, also denoted as ψ_p. Turgor pressure is the result of water entering the cell by osmosis, forcing the cell membrane against the relatively inelastic cell wall. It is positive hydrostatic pressure, counteracting to some extent the pressure reduction that results from

osmotic and matric effects. The final component of plant water potential is the potential energy of water due to gravity, ψ_g. This can be significant in tall trees, although in most crop species it is small enough to be neglected. The resulting water potential in plant tissue can be expressed as:

$$\psi_w = \psi_p + \psi_\pi + \psi_m \qquad (1.2)$$

Since solute concentrations are relatively low in the xylem, osmotic and matric potentials are negligible, and the only source of water potential depression is negative hydrostatic pressure due to transpiration loss, so that $\psi_w = \psi_p$.

1.2.5 Light Absorption and Photosynthesis

Light is the essential source of energy for all green plants. The radiant energy reaching the earth from the sun is distributed across the electromagnetic spectrum from about 200 to 10,000 nanometers. according to the black body radiation curve at 5,800 °K, with a peak at approximately 500 nm. The earth's ozone layer absorbs radiation in the ultraviolet region (<350 nm), while water vapor and other atmospheric constituents absorb radiation in the infrared (>750 nm) and, to a lesser degree, in several parts of the visible region (Court 1997). The net radiation reaching the earth's surface is, therefore, highly concentrated in the visible region. It should not be surprising, then, that plants (and for that matter, animal eyes) have evolved photoreceptor systems that operate in the visible part of the electromagnetic spectrum..

Photosynthesis occurs within the chloroplasts in the cells of green plants. The chloroplast contains a complex network of gel-like material called the stroma. Embedded in the stroma are flattened membrane complexes called thylakoids, in which the basic reactions of photosynthesis take place. The pigments which intercept light energy most commonly include two types of green chlorophylls, known as chlorophyll *a* and chlorophyll *b*, as well as yellow-orange pigments called carotenoids. Carotenoids are of two main types, carotenes, and xanthophylls, with several varieties of each (Salisbury and Ross 1992).

Chlorophyll molecules and all or most carotenoids are embedded in the thylakoid membranes and are attached by noncovalent bonds to protein molecules. The pigment molecules may absorb only one photon at a time, and the energy causes the excitation of one electron. The pigments can remain in an excited state for only a brief period of time, usually one nanosecond or less. The energy may be released from the pigment in two different ways, by heat loss, the release of light energy through fluorescence, or a combination of the two. Regardless of the color of the light intercepted by a chlorophyll molecule, the fluorescence it produces involves only deep red light, with spectral peaks at 685, 695, and 735 nm. In the light harvesting complexes, the light absorbed by one pigment molecule is transferred to another adjacent molecule, and to another and so on, until it reaches an energy collecting pigment located at a reaction center. The reaction centers are composed exclusively of chlorophyll *a* molecules in association with certain proteins and other membrane components (Salisbury and Ross 1992).
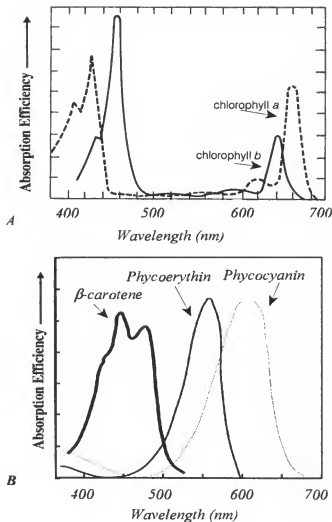
Figure 1.4 Absorption spectra of (a) chlorophyll *a* and chlorophyll *b* and (b) β-carotene, phycoerythrin and phycocyanin. Each pigment was extracted from plant matter with organic solvents, and so the effects of chloroplast structure on absorption is not present. Part (A) adapted from Salisbury and Ross (1992); part (B) adapted from Jensen (2000).

As can be seen in Figure 1.4, Chlorophyll molecules absorb blue and violet light (~450 nm) quite efficiently, and red light (~650 nm) with somewhat lesser efficiency, but green wavelengths (~550 nm) are hardly absorbed at all. Carotenoid pigments effectively absorb light in a somewhat broader band in the violet to blue region, and transfer their excitation energy to the same reaction centers as do chlorophyll molecules. Since they do not absorb much green or red light, they have a yellow-orange appearance, whereas chlorophylls appear green because they absorb blue and red light, and reflect or transmit green light. Two other classes of pigments also absorb light in the green and yellow regions. They are phycoerythins, which absorb light from 450 nm to 570 nm, and phycocyanins, which are sensitive in the region of 560 nm - 650 nm (Jensen 2000).

At the reactions centers, there are two coupled photosystems (see Figure 1.5), both containing chlorophyll *a* in association with other molecules, which receive light energy either directly, or transferred from other pigments. Photosystems I and II are both able to make use of a broad spectrum of light for photosynthesis, due to the combinations of pigments present in them (Salisbury and Ross 1992).

Since light at shorter wavelengths has more energy per photon than light at longer wavelengths, the additional energy imparted by blue light to excite a chlorophyll molecule must be dissipated as heat, where as red wavelengths at 680 nm provide exactly the amount of energy to drive photosystem II, and red light at 700 nm is able to drive photosystem I, but does not have enough energy to drive photosystem II.
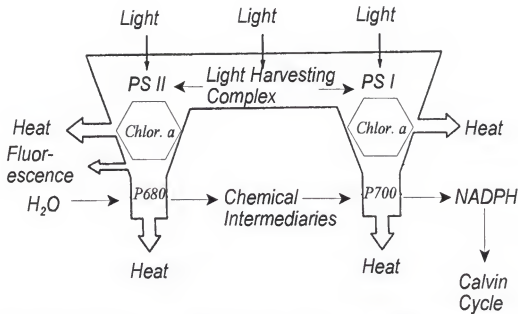
Figure 1.5 Schematic representation of the two photosystems together with associated light harvesting complexes. Adapted from Schreiber (1997).

The highest efficiency of photosynthesis is obtained with red light below 680 nm. When a plant is unable to utilize all of the light energy it receives one of the results is fluorescence, whereby light that would normally drive photosynthesis is re-emitted by the pigment at a different wavelength. For this reason, estimates of carbon assimilation rate in a plant are generally inversely proportional to fluorescence (Salisbury and Ross 1992). Emission of excess light energy by fluorescence reduces the generation of heat slightly.

1.2.6 Salinity Effects on Citrus

Increased soil salinity has been shown to reduce root development below 0.3 m and increase roots near the surface. Water uptake in the 0.6-0.9 m layer was reduced 20% as salinity increased from 2.0 to 5.6 dS m^{-1} (Bielorai et al. 1978). Citrus trees are highly

dependant on vesticular arbuscular mycorrhizae (VAM) to increase water absorption in the roots, although the relationship between root conductance and VAM appears to be complex, as experiments have shown a stronger relationship between VAM and stomatal conductance than root conductance. VAM infestation appears to be reduced by excessively wet or dry soil conditions. Citrus roots are highly susceptible to flooding, and will die back if the water table rises into the root zone. For this reason, citrus is normally planted in well-drained soils.

Rootstock variety has a significant effect on salinity stress, with 'Cleopatra mandarin' and 'Rangpur lime' showing the greatest resistance to salt uptake and lowest Cl^- accumulation in leaves, while rough lemon and sour orange had moderate resistance, and sweet orange and citrange were most susceptible to stress (Shalhevet and Levy 1990). All rootstocks have an absorption differential between Na^+ and Cl^-, some are better Cl^- excluders, and others exclude Na^+ better. Toxicity and leaf damage results only from Cl^-, rather than Na^+, concentration in leaves. When saline water is sprayed directly on leaves, however, both Na^+ and Cl^- were shown to injure the leaves (Shalhevet and Levy 1990).

There are two principal mechanisms by which salinity can stress citrus trees and reduce yield. They are the effect of reduced osmotic potential in the root zone, which results from the total dissolved solids content in the soil water, and the toxicity effects of chloride. In cases where Cl^- is the dominant anion in the soil water and the root stock cannot efficiently exclude it, chloride toxicity overshadows the effect of total salt stress (Shalhevet and Levy 1990).

1.2.7 <u>Spectral Response of Leaves</u>

The light intercepted by a leaf may be absorbed, transmitted, or reflected from the surface or its interior (see Figure 1.6). Absorbed light may be used to drive photosynthesis, produce heat, or may be fluoresced (emitted from the leaf at a different wavelength than it had when it was absorbed), although the great majority of absorbed radiation heats the leaf, and only a small quantity is actually used to drive photosynthesis or is fluoresced. All healthy leaves have a similar general response. Light is mostly absorbed by chlorophylls, xanthophylls and other pigments in the chloroplasts within photosynthetic cells. Most absorption occurs in the blue and red wavelengths, and less so in green wavelengths, which results in the green appearance of healthy leaves. Some light is transmitted as well, the pigments in the leaves. Most of the near infrared energy which falls on healthy leaves is internally reflected, due to the internal structure of leaf tissue. This results in the characteristically bright appearance of healthy vegetation in infrared bands. Surface reflection from the leaf is relatively independent of wavelength, but its quantity is related to shininess of the surface, especially in leaves that have a waxy cuticle.

The resulting reflectance spectrum that is typical of healthy vegetation compared with that of stressed or damaged vegetation, and dry, dead leaves is shown in Figure 1.7. It shows typically low reflectance in the blue range, higher reflectance in the green, lower red reflectance, and high infrared reflectance for a healthy leaf. The damaged leaf shows similar reflectance in the blue range, but much higher reflectance in the red and lower
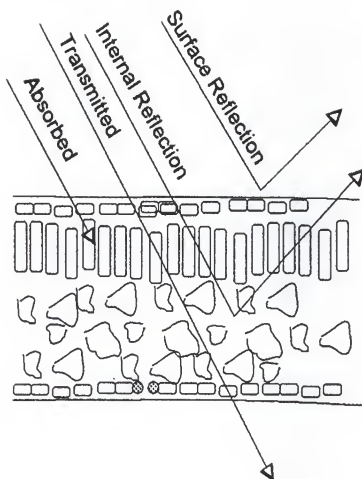
Figure 1.6 Pathways for incident light on a leaf, including absorption, transmission, internal reflection and surface reflection.

reflectance in the infrared. This is typical of severely damaged or necrotic leaves. Completely dead, brown leaves show none of the characteristics of living vegetation; their reflectance spectra appear more similar to that of dry soil.

1.2.8 Vegetation Indices

Several different vegetation indices can be calculated from remotely sensed data. The simplest is sometimes called the Simple Vegetation Index, and is the arithmetic difference between the near infrared (IR) band and the red (R) band (IR-R). The exact wavelengths used depend on the sensor. In Landsat TM imagery, this corresponds to Band 4 (760-900 nm) – Band 3 (630-690 nm), in SPOT imagery, it is Band 3 (790-890 nm) – Band 2 (610-680 nm), in AVHRR imagery, it is Band 2 (720-1100 nm) – Band 1 (580-680 nm). The simple vegetation index will produce high values for healthy, green vegetation, and low values for sparse, injured or dead vegetation. It will also produce negative values when applied to objects that have higher red than infrared reflectance, such as water bodies and clouds.

To normalize the index for images with different incident radiation values, the Normalized Difference Vegetation Index (NDVI) was developed (Rouse et al. 1974). It is defined as (IR-R)/(IR+R). NDVI produces a range of values from 0 to 1. In some practical implementations in remote sensing interpretation software, such as ERDAS Imagine ™, the resulting values are then stretched to cover the range of 0 to *255,* so that the results can be displayed as an 8-bit integer raster image.
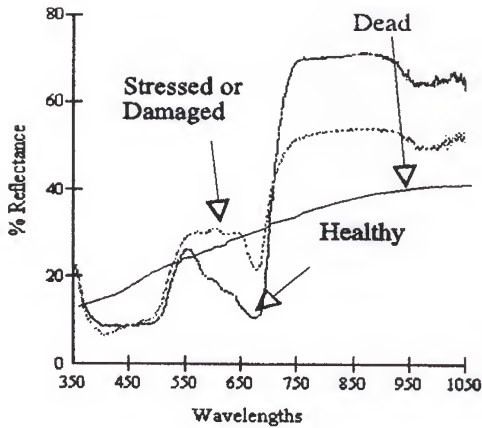
Figure 1.7 Reflectance spectra from healthy, stressed and dead citrus leaves. These spectra were captured in full sunlight, with freshly picked healthy and stressed leaves.

Other types of standard indices or transformations have been developed for specific purposes, such as the Tasseled Cap transformation which is applied to Landsat TM imagery. It consists of a matrix of empirically derived values that, when combined with the 7 Landsat bands using matrix multiplication, it results in 6 transformed bands, called Brightness, Greenness, Wetness, Haze, Fifth and Sixth. The Greenness band can be used as a vegetation index.

Vegetation indices, especially NDVI can be very useful in assessing differences between citrus trees, especially differences in canopy density. In effect, the canopy volume and density integrates growth over a period of several years. Leaf response operates over a shorter time scale, a period of several weeks or months.

The application of NDVI to cypress stress detection is also of interest. The application in this case is not obvious, since the Landsat images used are all captured in the winter, when cypress has its leaves off, and would normally present low NDVI values. Many of the stressed cypress domes that have been observed in the Landsat imagery have unusually high NDVI values, and it is assumed that this results from non-wetland plant species that are invading the understory of the stressed cypress stands.

1.2.9 Types of Vegetation Stress

The term "stress" has several common meanings, which may lead to some confusion about its applicability to vegetation. The American Heritage Dictionary (Houghton Mifflin 1996) cites 10 distinct definitions, none of which apply to vegetation

directly. They include a humanistic definition of stress as a mentally or emotionally disruptive or upsetting condition occurring in response to adverse external influences, and a physical definition of stress as a force or system of forces acting on a body which tends to strain or deform it. As applied to vegetation, stress generally signifies the presence of one or more environmental factors which are injurious to the plant, or the lack of one or more factors necessary to the plant's well-being. These may include the insufficient availability of water, light, oxygen, carbon dioxide or nutrients to the plant, excess heat, cold, light or moisture, or the presence of toxins, salinity, excessive alkalinity or acidity, grazing insects, diseases or competition from other plants (Christiansen 1979).

Plant physiological responses to stress are so varied as to be difficult to characterize generally. The long-term responses include reduction or retardation of growth and development, damage or loss of leaves, roots, stems or fruit, and the reduction of fruit or product quality and quantity. These effects may result from more subtle physiological changes, such as the reduction of efficiency of photosynthesis, water or nutrient uptake, reduced water potential in the plant. Depending of the type and severity of these effects, they may be readily detectible to a trained eye. It is generally desirable to detect such changes as early as possible, however, preferably, early enough to avoid any long-term damage or loss.

Carter (1993) conducted a series of experiments to determine how the spectral reflectance of certain plants may change in the presence of specific vegetation stresses. The plants and stresses that were studied were: loblolly pine (*Pinus taeda* L.) under competition stress, golden eunonymus (*Eunonymus japonica* var. Aureo-marginata) under

powdery mildew stress, slash pine (*Pinus elliotii* Engelm.) under stress from the lack of
ectomycorrhizal fungi in the root system, live oak (*Quercus virginiana* Mill.) under stress
from senescence, persimmon (*Diospyros virginiana* L.) exposed to herbicide (DCMU),
loblolly pine exposed to high atmospheric ozone, slash pine exposed to high salinity and
sandy soils of a barrier island compared with mainland slash pine, and switchcane
(*Arundinaria tecta* [Walt.] Muhl.) exposed to short-term dehydration (Carter 1993).
Results from these experiments were expressed as bands of light wavelengths in which a
plant's reflectance showed a significant change when exposed to a given stress.
Significance ($p \leq 0.05$) of the reflectance difference was determined by ANOVA and
Dunnett's means test. The results are summarized in Table 1.1. Another interesting result

Table 1.1 Wavelengths at which spectral reflectance changes in response to stress
for several species and stresses (Carter 1993).

Plant	Stress	wavelengths (nm)
loblolly pine	competition	403-409, 525-650, 868-728
euonimus	powdery mildew	405-418, 428-738, 1390-1595 1743-185, 1856-2508
slash pine	insufficient micorrhyzae	415-760
live oak	senescence	498-715
persimmon	herbicide	405-409, 519-573, 688-735, 1384-1401 1875-1905
loblolly pine	ozone	506-661, 680-723, 1865
slash pine	barrier island	409-413, 420-436, 445-468, 491-667, 681-742

from this study are the maximum and minimum values of spectral reflectance differences

in certain regions of the spectrum (Table 1.2), in particular, the maximum in the green

range (around 550 nm), the minimum in the red range (near 700 nm) and the maximum at

the "red edge" (near 700 nm). These features appear in each of the reflectance

comparisons, and the similarity between the two slash pine treatments and the two

loblolly pine treatments seems to indicate species-specific stress response characteristics.

Table 1.2 Wavelengths at which minimum or maximum spectral reflectance changes appear near the green maximum, red minimum and red edge reflectance features in green vegetation.

Plant	Stress	Green max./ Red min./Red edge		
loblolly pine	competition	551	671	716
loblolly pine	ozone	551	672	710
slash pine	insufficient micorrhyzae	549	670	718
slash pine	barrier island	562	674	717
live oak	senescence	560	672	703
persimmon	herbicide	540	672	715
euonymus	powdery mildew	545	672	708
switchcane	dehydration	584	667	706

1.2.10 Sources of Error in Remote Sensing

The principle sources of error in the process of acquisition and application of

remotely sensed can be categorized by the phase of the process in which they occur. The

phases identified by Lunetta et al. (1991) include acquisition, data processing, data

analysis, data conversion, error assessment, final product presentation, decision making and implementation.

The acquisition of remotely sensed data is constrained by the attributes of the sensor used, including spectral sensitivity, bandwidth, number of bits per sample, and number of channels in the system. The attributes of the platform on which the sensor is flown also play an important role. The altitude of the platform, together with the optical assembly on the sensor, determine the spatial resolution of the data. Satellite-based sensors move in an almost frictionless environment, so they are not susceptible to the instabilities that affect aircraft-based systems due to air turbulence. Corrections for the rotation of the earth do need to be applied accurately to spaceborne data. In addition, geometric distortions are caused by the distance from sensor to target, which differs at the edges of the image from that in the image center. Topography of the land surface will also distort the image, because of shadows that are cast by vertical features and because of the differing distance from the sensor to the ground features. Topographic distortions are usually more significant in airborne data than satellite-based data. The local time of day in which the data are acquired is significant, as it affects the intensity, spectral attributes and angle of the incident light. Finally, the atmosphere and any clouds or pollution in it can greatly affect the quality of the data acquired.

Once the data have been acquired, many of the distortions in it due to sensor attributes or local conditions can be corrected in the processing of the data, provided that accurate information about those attributes and conditions is known. Geometric correction or rectification is the process by which the raw data are projected onto a plane

and transformed spatially so that the elements in it are in positions that correspond to the real objects they represent in some recognized projection system (ERDAS 1994). Radiometric correction involves altering the intensities of the data elements to compensate for the sensor attributes, solar angle, and atmospheric conditions at the time of image capture. Correction for topographic effects may require both geometric and radiometric correction, to remove distortions and shadows, using information about topography and sun angle. Data processing can also involve transforming the corrected data into specific formats for use and distribution, and this could introduce errors if not done correctly.

Data analysis involves many processes by which meaningful interpretations are given to remotely sensed data. This is perhaps the area that is most susceptible to the introduction of errors. Some of the types of data analysis include quantitative analysis, classification, and data generalization (Lunetta et al. 1981). Quantitative analysis of an image may involve determining the absolute quantity of reflected or emitted radiation within the scene at ground level, which requires radiometric calibration of the image. Quantitative analysis of relative reflectance may be done without absolute radiometric calibration, as long as there is no exposure falloff, vignetting or similar non-uniformity within the image. By this method, the digital numbers from certain portions of the image are compared with those of other portions of the same image. If individual objects are identifiable, the reflectance of these objects may be compared. Comparisons between different images cannot be made without radiometric calibration or normalization, however.

1.2.11 <u>National Map Accuracy Standards</u>

For maps on publication scales larger than 1:20,000, not more than 10 percent of the points tested shall be in error by more than 1/30 inch, measured on the publication scale; for maps on publication scales smaller than 1:20,000, at least 90% of the points must be in error by less than 1/50 inch (USGS 2000). These standards imply the following spatial accuracies for maps and imagery that follow these standards (see Table 1.3).

The federal standards for spatial accuracy in digital data are currently under development. The Federal Geographic Data Committee has set standards for metadata formulation for digital data.

Table 1.3 Maximum spatial error allowed by the National Map Accuracy Standard.

```
Scale                       Maximum error
1:12,000      12,000*(1/30)*(1/12) = 33.3 ft.    (10.15 m)
1:24,000      24,000*(1/50)*(1/12) = 40 ft.      (12.19 m)
1:250,000    250,000*(1/50)*(1/12) = 416.7 ft.   (127 m)
```

In addition to positional accuracy, the accurate identification of types of land cover or land use is of paramount importance in determining the usefulness of GIS data It is not possible to have a perfect classification system for all purposes, and several classification systems have been adapted to meet specific needs. Some classification systems one may see include:

1. Florida Land Use and Cover Classification System (FLUCCS), a four-level system published by the Florida Dept. of Transportation and adapted and extended by Florida's Water Management Districts (FDOT 1985).

2. Standard Digital Line Graph Attribute Coding, which codes all area, point and linear features of DLG data, from the U.S. Geological Survey (USGS).

3. Hydrologic Unit Codes, used to identify watershed boundaries, rivers and streams, also published by USGS.

4. National Wetlands Classification System, used in the National Wetlands Inventory digital data published by The U.S. Fish and Wildlife Service.

5. Soil Type Classification systems, used in soils maps, generally published by county in the United States, used by the Natural Resources Conservation Service.

6. Property boundaries, use and ownership (cadastral information), used by State and local governments to keep land records.

CHAPTER 2
METHODS

2.1 Study Areas

2.1.1 Fort Pierce Citrus Site

The University of Florida Indian River Research and Education Center is an agricultural research and education unit of the University of Florida's Institute of Food and Agricultural Sciences (IFAS). The experimental citrus plots used in this study were developed to study the growth and production of a grapefruit variety planted on four common rootstocks in response to irrigation water salinity and fertilizer treatments (Boman 1993).

A total of 960 trees were planted in the plot in 1991 at a density of 255 trees per hectare. Four different rootstock varieties were used in the experimental plot: 'Swingle citrumelo', 'Carizo citrange', 'sour orange' and 'Cleopatra mandarin'. All of the trees were grafted with 'Ray Ruby' grapefruit scions. The experimental treatments included four levels of salinity used in irrigation water, crossed with three different fertilizer applications. The salinity levels used had conductance values of 0.7 dS/m, 2.3 dS/m, 3.9 dS/m and 5.5 dS/m, corresponding to approximately 500, 1600, 2700 and 3800 ppm total dissolved solids (TDS), respectively. The salinity levels were achieved by mixing sea

43

water with local ground water. The fertilizer treatments were obtained by applying

equivalent amounts of three different types of fertilizer, (A) NH_4NO_3 & KCl, (B)

$Ca(NO_3)_2$ & KNO_3 and (C) NH_4NO_3 & KCl (dry). Fertilizers (A) and (B) were applied by

fertigation, 15 times per year, while fertilizer (C) was broadcast 3 times per year. The

application rates were 140 kg/ha N and 140 kg/ha K for all methods. Other cultural

operations such as weed and insect control were identical for all the treatments (Boman

1993). Data collected annually from the experiment include leaf chlorophyll, nitrogen,

potassium, phosphorus and chloride content, averaged among trees receiving the same

treatments, as well as yield of fruit from each tree and fruit size.

2.1.2 Vero Beach Citrus Grove.

The Vero Beach Research Station (VBRS) is the subtropical research station of

the Oklahoma-based Kerr Center for Sustainable Agriculture, Inc. Approximately 35

acres (15 ha.) of citrus groves are used for research in "sustainable" agricultural

practices, including methods of insect control such as growth regulators, attractants,

parasites, and natural predators. In recent years, virtually all of the citrus groves in the

Vero Beach area, including those at the Kerr Center, have become infested with

Diaprepes abbreviata root weevil, or are in danger of becoming infested.

Airborne multispectral and hyperspectral imagery were obtained covering the

research groves, and a digital elevation model was constructed from point elevation data

collected by the UF/FIU Airborne Laser Swath Mapper (ALSM) (Shrestha and Carter,

1998). Research on infestation, root biomass and leaf area index (LAI) was conducted on

some 60 eighteen month old 'minneola' orange saplings that were planted near a mature

grove that is partly infested with *Diaprepes abbreviata* root weevil.

2.1.3 Regional Study site: Cypress Wetlands

The Northern Tampa Bay Region is an area rich in lakes and wetlands. The area

used in this study contains nearly 6,000 depressional cypress wetlands, with many

hardwood swamps, marshes, and open-water lakes as well. These surface hydrological

features are strongly influenced by the water table in the surficial aquifer, which is also

influenced by the potentiometric surface of the Floridan aquifer, despite the presence of a

confining layer, which partially isolates the two aquifers. In their 1996 report, the

Southwest Florida Water Management District showed that the water table elevation

follows surface topography while being influenced as well by rainfall, evapotranspiration,

inflow and outflow. The annual high for the surficial aquifer usually occurs in September

at the end of the wet season. The annual low is generally in May, at the end of the spring

dry period. The rate and direction of ground water flow varies from one location to

another, according to local topography. The hydrologic gradient varies from a few feet per

mile (less than 1 m/ km) to about 10 feet per mile (2 m/km) (SWFWMD 1996).

Water use in the Northern Tampa Bay Region is predominantly for public supply,

75% of the estimated groundwater use in the area in 1990; the remainder going to

agricultural (12.6%), industrial (7.3%), and other uses (4.7%) (SWFWMD 1996). Public

supply groundwater and agricultural water use are almost exclusively derived from the

Upper Floridan aquifer. The 1990 annual average quantity of water withdrawn for all users was estimated at 349 mgd (SWFWMD 1996).

2.2 Sensors and Instruments

2.2.1 Spectroradiometer

Spectral scanning was done with a Geophysical and Environmental Research Corporation (GER) portable spectroradiometer model GER1500 (GER, 1996). This device has a spectral range of 350 nm to 1050 nm, including ultraviolet (UV) visible (VIS) and near infrared (NIR) wavelengths. It makes use of a silicon diode array, with 512 detectors. Light entering the device through the lens or a fiber optic probe is split by a diffraction grating and the resulting spectrum is projected onto the detector array, so that the spectrum is divided into 512 discrete bands. The device is calibrated at the factory to measure the intensity of light in each waveband in radiance units (watts per cm^2 per nm waveband per steradian of solid angle). Since solar illumination of a target can change significantly in a brief period of time, it is usually appropriate to measure the relative reflectance of vegetation or other targets rather than radiance. This is done using a calibration panel of some sort to compare the intensity of light reflected from the target with that reflected from the calibration panel.

A typical measurement is accomplished by first scanning a white reference plate such as those produced by Labsphere (Labsphere SRT-99-50) which is calibrated to diffusely reflect nearly 100% of incident radiation in the visible and infrared wavelengths.

With the reference scan stored in memory, a measurement is then made of the target, either a single leaf or a whole canopy, and the percent reflectance of the target in each of the 512 bands is automatically calculated. Nearly 500 measurements can be stored in the radiometer, and then downloaded to a computer for analysis. Alternatively, measurements can be made with a computer attached to the unit, the spectra displayed in real time, and stored on the computer's hard drive.

2.2.2 Canopy Analyzer

Citrus foliage density at Ft. Pierce and Vero Beach was measured using a SunScan Canopy Analyzer model SS-1 (Delta-T Devices, Cambridge, UK). This device makes use of photometers to measure light intensity inside and outside of the vegetation canopy simultaneously. The reference unit contains two photometers, one exposed to direct sunlight, the other shaded, so as to measure both total illumination and diffuse illumination, and calculate the ratio of direct to diffuse light. The sensor used inside the vegetation canopy consists of an array of 64 photometers 1 meter in length, to measure the quantity of light that penetrates the canopy and its variability along the length of the sensor. Information about sun angle is also provided based on the geographic location, the date, and the time of day at which it is used. These measurements are collected by a hand-held computer which runs a program to calculate leaf area index (LAI) and other parameters based on a particular light attenuation model. The model of light penetration used is that proposed by Whitfield (1986).

2.2.3 <u>Portable Area Meter</u>

The LI-3000A (LiCor, Lincoln, Nebraska) portable area meter is used to measure the total surface area of irregular flat objects such as leaves. It accomplishes this with a linear array of light emitting diodes mated with photodetectors on the opposite side of a long slot, so as to detect any obstruction between them. Leaves are pulled through the slot at a known speed, and the number of LEDs that are blocked is multiplied by the number of time intervals that pass as the leaf is pulled through, giving the total area of the leaf. A running tally of the total area of the leaves as they pass through the detector is kept until the counter is reset. Calibration testing of the machine using paper of known dimensions has shown the unit to be accurate to within 5% of the actual surface area.

2.2.4 <u>Narrowband Digital Camera</u>

A filter wheel digital camera was constructed for this study based on a model developed at the NASA Stennis Space Center (Carter et al. 1996). It consists of a monochrome Charge Coupled Device (CCD) video camera, model XC-77 (SONY, Park Ridge, NJ) mounted inside a black aluminum box, with an F-type lens mount on the front for interchangeable lenses. The camera has sensitivity in the spectral range of 400nm to 1000 nm. A disk is mounted inside the box which holds several light filters which are designed to pass specific narrow wavebands. The disk, or "filter wheel" places one of the filters between the camera and its lens to allow the capture of images in the waveband that is passed by that filter. The filter wheel is rotated to select different wavebands for

imaging. The filters used with this camera have bandpass center wavelengths at 443 nm, 550 nm, 675 nm, 698 nm and 790 nm, and bands of 438-448 nm, 545-555 nm, 670-680 nm , 695-701 nm, and 785-795 nm, full width half maximum (FWHM), respectively. The output of the camera is analog NTSC video, which is digitized using a frame capture device. During these experiments, The frame capture device used was a Snappy (Play Inc., Rancho Cordova, California), which captured image frames in the field as 640x480 pixel images in TIFF format when attached to a portable computer.

2.2.5 <u>Airborne Digital Multispectral Imager</u>

Aerial multispectral images of the citrus study sites were captured using an array of three Kodak Megaplus digital cameras with 12.5 mm focal length lenses and narrow bandpass interference filters (Mao and Kettler 1995). The spectral bands obtained were 10 nm FWHM, centered on 550 nm , 700 nm and 840 nm. For the 1999 images, imaging was done at a flying height of 5500 feet (1690 m) with a resulting pixel resolution of 0.9 m. For the 2000 images, imaging was done at 3300 feet (1006 m) with a resulting pixel resolution of 0.3 m. The imager is mounted on a light aircraft with a gyroscopically stabilized camera mount. The three cameras capture images simultaneously, although the individual band images must be coregistered in post processing, because of parallax effects and slight misalignments of the cameras. This postprocessing was done by the company that flew the missions, Geotek Aerial Data Services Company of Moselle, MS. The resulting images were delivered in digital format to the University of Florida Center

for Remote Sensing. Airborne imaging was done on two dates in late spring, May 26,

1999, and May 12, 2000.

2.2.6 <u>Airborne Digital Hyperspectral Imager</u>

    The hyperspectral imager used in this study was developed by the Institute for

Technology Development (ITD) at the NASA Stennis Space Center (Figure 2.1). It is

potentially able to capture images in up to 1024 bands from 395 to 905 nm wavelengths.

The number of bands captured may be reduced by combining adjacent bands, thereby
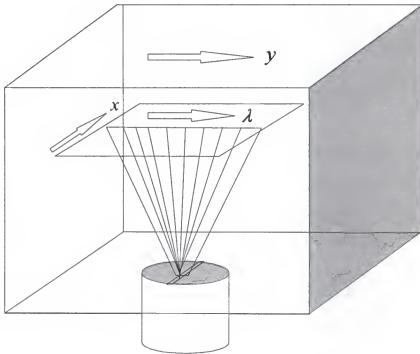
Figure 2.1 Schematic representation of the ITD hyperspectral imager.

allowing faster scan rates that are necessary to capture images at finer spatial resolution, while maintaining the necessary air speed and flying height. As configured for this study, 64 bands were captured, with band centers approximately 8 nm apart, at a nominal 1 meter spatial resolution. The method of image capture used by the hyperspectral imager is different than that of cameras. Instead of recording full-frame images in two spatial dimensions, the hyperspectral imager captures data in one spatial and one spectral dimension at each instant. Figure 2.2 shows schematically how the hyperspectral imager functions. A slit aperture allows light to enter the imager that corresponds to a line of pixels across the horizontal dimension of the image (x). The light is split into a spectrum of wavelengths, which is projected onto the vertical dimension of the focal plane of the imager, and represents the spectral dimension (λ). The vertical dimension of the image (along the flight path of the aircraft) is built up line by line as the aircraft moves forward (y). The resulting multi-layered data block is sometimes referred to as a hyperspectral cube.

One of the disadvantages of this approach is the sensitivity of the system to instability of the aircraft. Most aerial imaging platforms make use of a gyroscopically stabilized camera mount to compensate for rotations of the airframe in three orientation angles, ϕ, ω and κ, corresponding to the pitch, roll and yaw of the aircraft, respectively (Figure 2.2). Stabilized camera mounts are sufficient for fixed frame images, since these can be rectified using standard techniques. Imagers that scan a continuous swath, such as the hyperspectral imager used here, require an advanced inertial navigation system that records all movements and rotations of the airframe so that these can by used to
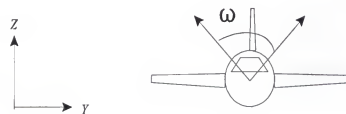
Figure 2.2 The three orientation angles, pitch (ϕ), roll (ω) and yaw (κ) of an airborne imaging system with Cartesian axes for reference.

geometrically correct the image data in post-processing. Such systems are now commercially available from companies such as Applanix (Hutton et al. 2000)

2.2.7 Landsat TM and ETM+ Imagers

Satellite images used in this study were obtained from the Landsat 5 Thematic Mapper (TM) sensor, and the Landsat 7 Enhanced Thematic Mapper Plus (ETM+) sensors. Landsat 5 was launched on March 1, 1984, and continues to operate today, well beyond its designed service life. It collects data in six multispectral bands at 30 m ground resolution, and also thermal infrared data at 120 m ground resolution. At present, it is only capable of direct data transmission to ground because its tape recording unit has failed, so it can only image areas that have a receiving station within range. The successor to Landsat 5 was launched in 1993, but failed to reach orbit and was lost. Landsat 7 was launched on April 15, 1999, and is now in operation. In addition to the multispectral and thermal bands available on Landsat 5, Landsat 7 has a panchromatic band with 15 m spatial resolution, and also its thermal band has 60 m resolution instead of 120 m available on Landsat 5. The spectral bands covered by the Landsat TM imager are shown in Table 2.1. There are three visible reflectance bands, sensitive to blue, green and red light, as well as one reflective near infrared band, and two reflective mid-infrared bands. The thermal band records emitted heat radiation, and so can be used to measure surface temperature.

Both Landsat 5 and 7 operate in sun-synchronous polar orbits, at an altitude of 705 km and inclination angle of 98.2°, with a local equatorial crossing time on each

Table 2.1 Landsat 4, 5 and 7 Sensor Wavelengths.

Band	Wavelengths	Color
1	450-520 nm	Blue
2	520-600 nm	Green
3	630-690 nm	Red
4	760-900 nm	Reflective Infrared
5	1550-1740 nm	Mid Infrared
6	10480-12500 nm	Thermal Infrared
7	2080-2350 nm	Mid Infrared
8*	520-900 nm	Panchromatic

* Available on Landsat 7 only

descending orbit of 10:00 AM, ± 15 min. The swath width of both sensors is 185 km, and the time period between passes over the same spot on earth is 16 days (Jensen 2000). Figure 2.3 shows the method of scanning and swath dimensions in pixels (A) and the polar orbit path of the Landsat satellites (B).

2.2.8 <u>Airborne Laser Swath Mapper</u>

The basic operation of an airborne laser swath mapper (ALSM) is produced by reflecting short pulses of laser light, commonly in the infrared band at around a 1 micron wavelength, off of the surface to be mapped, directed by a moving mirror. The precise time that each pulse is sent and its return detected is registered and the range to the target is calculated and stored on tape (Wehr and Lohr 1999). The approximate position

A

Instantaneous Field
of View (IFOV)
30 m pixel size.

Swath Width (Row)
(6600 elements)

Direction of Motion (Path)

Scene length
(typically
6000 lines)

B

Swath covered by polar
orbiting satellite.
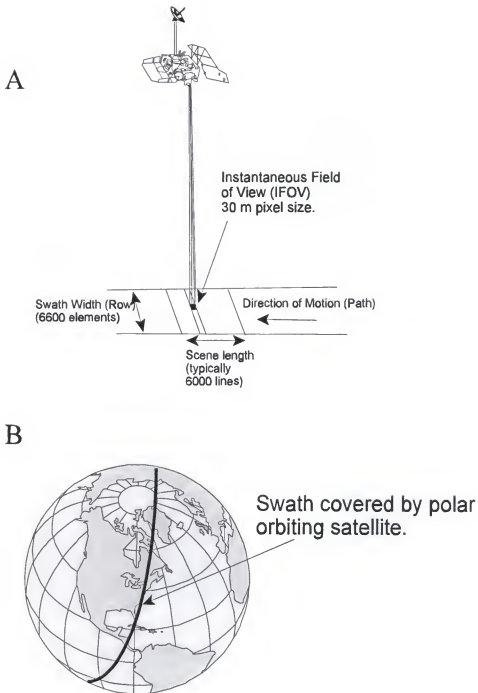
Figure 2.3 Method of data acquisition used by Landsat satellites. Instantaneous field of view swept by scanner (A). Swath covered by polar orbiting satellite (B).

and orientation of the aircraft at each instant is also stored on tape. After the flight, the precise position and orientations are determined by correcting the positional data using kinematic post-processing of carrier phase differential GPS data together with inertial navigation system (INS) data. The actual x, y and z coordinates of the terrain elevation points sampled by the laser are generated after the flight by combining corrected position and orientation data of the aircraft platform with the orientation of the laser pulse with respect to the airborne platform and the range value determined by the laser pulse, all obtained at the same instant in time. The return signal strength value provides additional information about the reflectance of the ground surface, and is also used to correct the range values for effects that result from different signal strengths.

2.3 Data Collection Methods

2.3.1 Single Leaf Measurement

In order to collect information about the spectral reflectance of citrus leaves in the presence of stress factors, leaves were sampled from the grapefruit plots at Ft. Pierce. In order to maintain consistency and reduce spurious readings, the leaves were imaged on clear days within two hours before or after solar noon. A total of 24 trees were sampled on each day, and the same trees were used for subsequent measurements. The trees chosen for measurement were in the first replicate block, all grown on the 'Swingle citrumelo' rootstock, and having received either the high (3500 ppm) or low (500 ppm)

salinity treatments, and examples of all three fertilizer treatments were used. All four

trees in each of the selected treatments were sampled.

Three leaves were picked at random from each tree and they were immediately

placed one by one on a flat black cardboard panel, which had 2-3% reflectance

throughout the visible and near infrared ranges. The radiometer was placed on a low

tripod, pointing downward at a 60° angle, with its objective approximately 20 cm from

the sample. The leaf was illuminated by full sunlight from the side, to prevent specular

reflectance from being measured. This produced a field of view that was 3 cm wide and

4.4 cm tall. After calibration with a reflectance standard (Labsphere SRT-99-50), the

spectral signature of the leaf was captured with an attached notebook PC. In this way, 12

spectral measurements were made for each treatment, 72 in all. The initial leaf spectral

reflectance measurements were made on December 19th, 1997, at the time when the trees

were laden with fruit, just before harvesting. Subsequent measurements were made in

February, March and April 1998 prior to the onset of the dry season.

2.3.2 Citrus Canopy Measurement

The filter wheel camera assembly was placed on a tripod and aimed at the western

side of the tree canopy as it received afternoon side illumination. A calibration placard

with four grey levels, with 80%, 50%, 20% and 5% reflectance, respectively, was placed

on a tripod in front of the tree to provide a standard to calibrate the images for canopy

reflectance. Monochrome images in five bands were captured with a video capture device

attached to a notebook computer. The bands used were 438-448 nm (band 1), 545-555 nm

(band 2), 670-680 nm (band 3), 695-701 nm (band 4), and 785-795 nm (band 5).

The individual single band images of a given treatment were calibrated by finding

the average pixel value in each panel of the calibration placard, determining what values

they should have in an image calibrated for reflectance, then performing a linear curve fit

to adjust the pixel values so they best correspond to a calibrated image. In some images,

the brightest gray level was saturated, meaning that the intensity of the light reflected

from the panel was higher than the maximum that can be accurately recorded by the

camera. Pixels in the images that were saturated were not used in calibration. After

calibration, the single band images for each treatment were coregistered to produce a five

band multispectral image.

2.3.3 Measurement of Canopy Volume

In order to precisely measure the actual volume of the tree canopies at the Ft.

Pierce citrus site, each of the nearly 960 trees still alive were measured with a 4 meter

long plastic pole marked in decimeters. Measurement was done in May-June, 1999,

shortly after the airborne image acquisition over the site. The height and diameter of each

tree was recorded. These values were entered into a database, together with the calculated

volume of the tree canopy. Given the irregular shape of actual tree canopies, some

judgement was used to avoid measuring the extreme ends of small branches which may

extend beyond the bulk of branches and leaves that form the canopy.

2.3.4 <u>Calibration of Leaf Area Index Measurements</u>

Leaf Area Index (LAI) is defined as the ratio of total leaf area in a vegetative

canopy to the area of ground it covers. The SunScan Canopy Analyzer field instrument

was used to measure the LAI of citrus trees for these experiments. The appropriate model

of light penetration to be used by the instrument depends on the canopy structure, which

differs from one plant species to another. In order to assure the accuracy of the leaf area

index recorded by the canopy analyzer, species-based calibration is needed.

To calibrate the field measurements of leaf area index for citrus, LAI

measurements were taken of 63 'Minneola' tangelo trees *(Citrus reticulata x C. paradisi)*

about 1 ½ years old. The trees had varying canopy condition, due to infestation with a

Diaprepes sp. weevil. The tree conditions had been visually assessed and given grades

from 1 (worst) to 4 (best) by Kerr Center director, Bob Adair. Of the 63 trees, eight were

chosen to calibrate the LAI measurements, including two from each of the four canopy

conditions.

The area of ground that the tree canopies covered was determined by measuring

their diameters in two directions, a and b, and calculating the area as an elliptical shape

with the formula Area = $1/4\pi ab$. The total leaf area of each tree was determined by

stripping all the leaves from the trees, packing them in airtight plastic bags and bringing

them to the laboratory, where there were run through an LI-3000A portable area meter

(LI-COR, Lincoln, NE). The leaves were weighed in the plastic bags, and a ratio between

the net weight of the leaves and their area was developed for each tree. For trees with

large numbers of leaves, the leaf weight times the area/weight ratio was used as a measure

of total area.

2.3.5 Airborne Data Collection

Airborne data were collected on two dates, May 26, 1999 and May 12, 2000 at Ft.

Pierce. The spectral bands obtained on May 26, 1999were 10 nm in width, centered on

550 nm , 700 nm and 840 nm from a flying height of 5500 feet (1690 m) with a resulting

pixel resolution of 0.9 m. Imaging was repeated with the same wave bands on May 12,

2000 at Ft. Pierce and also at the Vero Beach site, this time using 0.3 m resolution flying

at 3300 feet (1006 m). The time, location, heading, solar angle and solar azimuth for

Table 2.2 Time, location, and solar elevation and azimuth for each image frame
captured on May 12, 2000.

Local	UTC	No.	Loc.	Head.	Lat.	Long.	Elevation	Azimuth
8:50	12:50	1	FD	S	27°30'	80°42'	28.053	-97.092
9:00	1:00	2	FD	E			30.257	-96.081
9:10	1:10	3	VB	S	27°39'	80°28'	32.684	-94.868
9:15	1:15	4	VB	E			33.788	-94.347
9:20	1:20	5	VB	S			34.892	-93.822
9:35	1:35	6	FP	S	27°28'	80°23'	38.281	-92.311
9:40	1:40	7	FP	E			39.39	-91.767
12:20	4:20	61	VB	E	27°39'	80°28'	73.711	-58.168
12:22	4:22	65	VB	S			74.086	-57.116
12:25	4:25	69	VB	S			74.639	-55.452
12:27	4:27	73	VB	S			75.001	-54.281
12:30	4:30	77	VB	E			75.535	-52.427
12:40	4:40	81	FP	S	27°28'	80°23'	77.382	-45.52
12:43	4:43	85	FP	E			77.847	-43.005
12:46	4:46	89	FP	S			78.29	-40.308
12:50	4:50	93	FP	W			78.841	-36.40

each of the multispectral and hyperspectral images captured at the Fort Pierce and Vero Beach sites are given in Table 2.2. Similar data for the May 26, 1999 imaging were not available. These data are needed to determine the effects of shadows, or of the bidirectional reflectance distribution function (BDRF).

2.3.6 <u>Cypress Stress Data Collection</u>

For this study, Landsat TM images captured on March 24, 1992 and March 14, 1994 were used. Landsat 5 TM data are in 7 bands (3 visible and 4 infrared). The wavelengths of these bands and corresponding colors are given in Table 2.1. All bands have 30 meter spatial resolution except the thermal infrared band, which has 120 meter resolution.

Each vegetation type has a characteristic reflectance signature, composed of the three visible and four infrared bands of the Landsat image. The wetlands were separated according to land cover classification so that comparisons could be made between sites of different quality rankings. The remote sensing analysis was only done on the cypress wetlands, since they represent the majority of wetlands studied, and provided the largest sample size for statistical analysis.

This analysis of wetland quality ranking began with the creation of a spatial database which contained the locations of 297 depressional, cypress wetlands. Figure 2.4 shows two examples. These cypress wetlands were evaluated and ranked on a scale of 1 to 5 by Southwest Florida Water Management District personnel using a rapid assessment
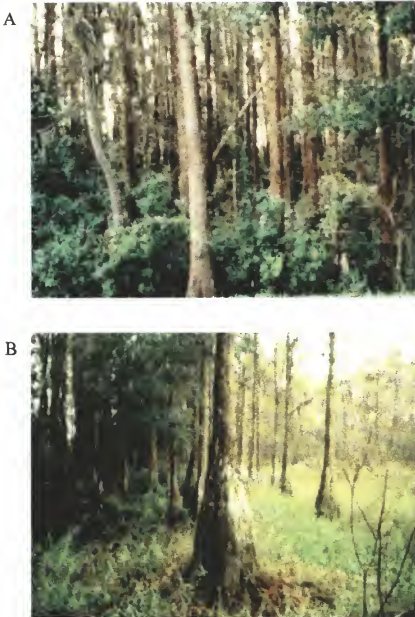
Figure 2.4 Examples of stressed and good condition cypress wetlands. The good condition wetland (A) has dense canopy, flooded soils for most of the year and no soil subsidence. The stressed wetland (B) has chronically low water levels, sparse canopy, some soil subsidence.

technique developed at the District (SWFWMD, 1996 and Rochow, 1994). The rankings for wetlands had nine levels, from 1 to 5 with 0.5 increments where wetlands with a ranking of 1.0 were considered in very poor condition and wetlands with rankings of 5.0 were considered in good condition. The factors that were assessed to determine the stress categories included:

1.1   Evidence of sufficient hydroperiod.

1.2   Presence of obligate wetland species in the understory and canopy and absence of upland plant species.

1.3   Soil integrity, lack of subsidence or severe fires.

1.4   Evidence of wildlife usage.

For the purposes of this study, the quality rankings were grouped into three quality categories: good (4.0 - 5.0), moderately stressed (2.5 - 3.5), and severely stressed (1.0 - 2.0). Wetlands were grouped and then used to develop the spectral signatures characteristic of each of the three groups. The locations of each of the evaluated cypress wetlands were entered into a GIS spatial database together with their quality rankings.

A vector GIS coverage containing only cypress wetlands was created from a land use/land cover coverage obtained from the Southwest florida Water Management District. The land use/land cover coverage was based on false color infrared aerial photography taken in 1990. All wetlands classified as cypress wetlands on the land use/land cover coverage were extracted and a cypress wetland coverage was constructed. Additionally, wetland GIS data were obtained from the National Wetland Survey, and processed with similar methods to the GIS data created by the SWFWMD, for comparison, and to

determine the relative effectiveness of using the National Wetland Survey data for this purpose.

The remotely sensed data were used to develop a regional assessment of cypress wetland condition. The picture elements (pixels) of the satellite image which lie within the boundary of the cypress dome were extracted by overlaying the corresponding cypress feature from the regional land use/land cover GIS layer.

2.4 Data Analysis Methods

2.4.1 Single-leaf Statistical Analysis

The 512 band reflectance spectra from individual leaf measurements made on the several sampling dates were analyzed in various groupings. The mean and standard deviation of each band in the spectra from three leaves of a single tree were found for all trees measured. The mean and standard deviation of all twelve measurements of each treatment (4 trees x 3 leaves) were also found, as well as the mean and standard deviation of all measurements from high-salinity and low-salinity trees, and for trees receiving each of the fertilization methods.

The unpaired t-test (McClave and Dietrich 1982) was used to compare the 12 reflectance readings obtained for each treatment with those of another treatment for each of the 512 bands from the spectroradiometer. The critical value of t used to test for significance was 2.2, for $\alpha/2=0.025$. One of the assumptions of the unpaired t-test is that the sets of values being compared have an approximately normal distribution. This was

verified by finding the skewness of the distribution of reflectance values from the twelve

leaves measured of each treatment in each of the 512 bands. The mean and root mean

square of the skewness values and the average of the standard deviations of the

distributions are listed in Table 2.3. For all treatments, the root mean square of the

skewness is on average less than one third of one standard deviation. These results

indicate that the data are approximately normally distributed.

Table 2.3 Summary of tests of skewness for distributions of leaf reflectance. Mean skewness is the average for 512 distributions, one in each band. RMS skewness is the root mean square of these values. Mean STD is the average of the standard deviations of these distributions. The column headings are treatment numbers. 1, 5 and 9 are low salinity; 4, 8, and 12 are high salinity.

	1	4	5	8	9	12
Mean skewness	-0.18	-0.45	1.05	0.11	0.31	0.01
RMS skewness	0.89	0.61	1.26	0.54	1.28	0.65
Mean STD	4.76	3.42	4.46	1.81	4.02	2.38

Since the instrument used to measure reflectance has a finite accuracy and errors

may compound when making multiple comparisons (Carter 1998), a second criterion was

used to determine significant differences in reflectance. Differences were only

considered to be significant when the measured difference was greater than 1%

reflectance. For the spectral bands that show significant differences, the measured

differences in mean were at least 4% reflectance or greater, so that the second criteria was also met.

A measure was also made of the sensitivity of the reflectance at each wavelength to salinization. Assuming that the reflectance of stressed trees is higher than that of unstressed trees at most wavelengths, the sensitivity measure was made by subtracting the reflectance of the salinized tree leaves from those of the unsalinized trees, then dividing the result by the reflectance of the unsalinized leaves (Carter 1994).

2.4.2 Citrus Canopy Analysis

Measurements of the height and diameter of the tree canopies were made during the period of aerial imaging, and canopy volume was calculated from these measurements, assuming a spheroidal shape for the trees using (2.1).

$$Volume = \frac{4}{3} \pi \frac{h}{2} \left(\frac{d}{2} \right)^2 = \frac{1}{6} \pi h d^2 \qquad (2.1)$$

Multispectral Aerial images were acquired from the site on May 26, 1999. Imaging was repeated on May12, 2000 at Ft. Pierce and also at the Vero Beach site, this time using 0.3 m resolution flying at 3300 feet (1006 m). The single-band images from each of the three cameras were co-registered, and radiometrically calibrated for reflectance by means of five grey level calibration targets, 4 m x 4 m in size, placed on the ground near the center of the study area (Figure 2.5). The calibration targets were made of fabric backed with black plastic to ensure opacity. The reflectance values of the

calibration targets were measured on the ground using a GER 1500 spectroradiometer (GER, Milbrook, NY) which was itself calibrated for percent reflectance using a Spectralon SRT-99-50 reference plate (Labsphere, North Sutton, NH). The reflectances of the panels were approximately 5%, 10%, 20%, 40% and 60% throughout the visible and near infrared range (Figure 2.6). The brighter panels have significantly lower reflectance in the ultraviolet range below 400 nm, however, these wavelengths are beyond the sensitivity range of the cameras and are not used.

2.4.3 Geographic information System

A geographic information system (GIS) was used to collect, manage and display the data for each tree, including directly measured, and remotely sensed data (Figure 2.7). The GIS was developed using Arc/Info®. A point coverage representing the location of each tree was created, and information about the treatment parameters of each tree (rootstock, salinity level, fertilizer) were added to the GIS database. Additional types of data that were available on a per-tree basis were also added, including canopy height and width and trunk diameter from 1991-93, canopy height and width only from 1994-96 and 1999, yield data (total fruit weight and fruit size) from 1992-96, plus 1999 and 2000. Not all of these data sets included data for all of the trees in the study area.

To collect reflectance values from each tree canopy, the GIS coverage was re-projected to fit the 3-band digital image. This was done, rather than rectification of the image, to avoid resampling the pixels, so that the maximum integrity of the image was retained. The fit of the tree centers over the trees in the image was within one pixel in

Figure 2.5 Placement of the ground calibration panels at the Ft. Pierce citrus grove. The reflectances of these panels were used to radiometrically calibrate the airborne images.

accuracy. The tree center locations in the GIS were then used to extract the reflectance values from a single pixel of the image within each tree canopy, and these were incorporated into the GIS database. In cases where trees were missing, the reflectance data extracted was actually that of the ground cover at the location where the tree used to be. Trees that died or were severely damaged by disease or stress were eventually replaced over the ten years in which the study progressed. The new trees, called resets, were planted with the same rootstock and scion type as the trees they replaced. The smaller size resulted in them appearing similar to severely stressed trees in the image.

The resulting database was then analyzed using a commercial statistics package (Minitab Inc., State College, PA) to determine relationships between the reflectance values from the tree canopies in the three bands acquired, or indices derived from them, and the treatment groups and measured parameters of the trees.

2.4.4 Hyperspectral Data Analysis

The digital images produced by the hyperspectral imager (Figure 2.8) are normally calibrated to units of radiance, such as $mWm^{-2}sr^{-1}$, which is the power of light radiation in each waveband, reflected off of a surface in a cone-shaped region defined by a certain solid angle. The radiance values obtained on a given day are highly dependent on the intensity of the sun's radiation on that day, and are affected by atmospheric conditions, sun angle, time of day, etc. In order to make the spectral data more independent of these factors, the images were calibrated for percent reflectance using the known reflectance values of the pixels that fell within the ground calibration targets. In a
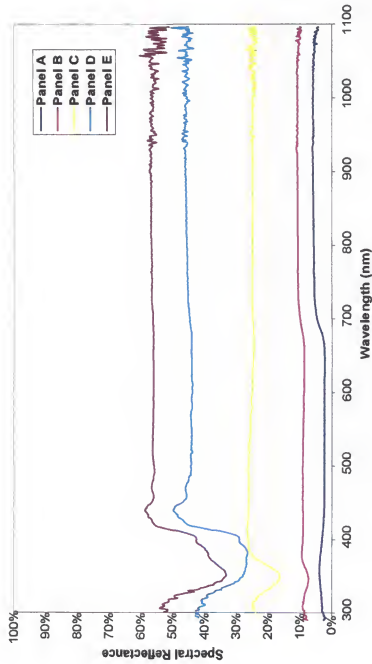
Figure 2.6 Spectral reflectance of the ground calibration panels. These values were obtained by placing the panels in full sunlight and capturing reflectance spectra from a height of 3 m directly above the panels.

Some Data Layers Contained in GIS

Calibrated Image

Salinity   Yield (1996)   Rootstock

0 – 10
10 – 45
45 – 60
60 – 75
75 – 85
85 – 95
95 – 110
110 – 125
125 – 145
145 – 281

1
2
3
4

- CA
- CL
- SO
- SW
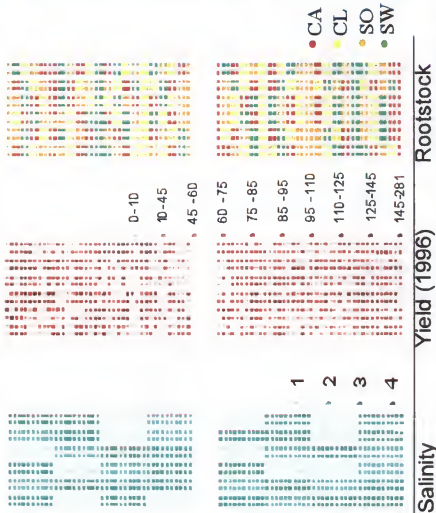
Figure 2.7 GIS layers and the 3-band image of the experimental site. In the Salinity layer, darker colors represent higher irrigation water salinity ranging from 500 to 3600 mg/L TDS. In the Yield layer, darker colors represent higher yield, ranging from 0 to 281 kg of fruit per tree. In the Rootstock layer, the different shades represent the four rootstocks used. 'Carrizo citrange' (CA), 'cleopatra mandarin' (CL), sour orange' (SO) and 'Swingle citrumelo' (SW) (Craig et al. 2000).

procedure known as the empirical line method (ELM), a regression line was fitted to the points representing the reflectances of the calibration panels in each of the 64 bands, and the equations of those lines were then used to find the calibrated values of all the pixels in the image.

Spectral calibration was done with two complimentary methods, using easily identifiable spectral features. First, a deep O_2 absorption band at 751 nm is identified in the radiance image, which fixes the infrared end of the spectrum, then the green peak at 550 nm and chlorophyll absorption band at 670 nm are identified in the radiometrically calibrated reflectance image, which determine the visible side of the spectrum, and allow the wavelengths of each band to be identified.

The extraction of reflectance data from the hyperspectral images proceeded in a way similar to that used for the multispectral images, except that the images contain 64 bands instead of 3. This process was more problematic for the hyperspectral image, however, because of the geometric distortions present in it. The placement of the tree center points over their respective locations in the hyperspectral image was a more laborious process, which involved manually adjusting the locations of the points. Once this was done, it was then possible to used the GIS to automatically extract a single pixel value in each band from the approximate center of each tree.

2.4.5 Hyperspectral Image Interpretation

Several methods were used to locate areas within the hyperspectral images that may correspond to normal citrus, stressed citrus, or other ground cover types. Two
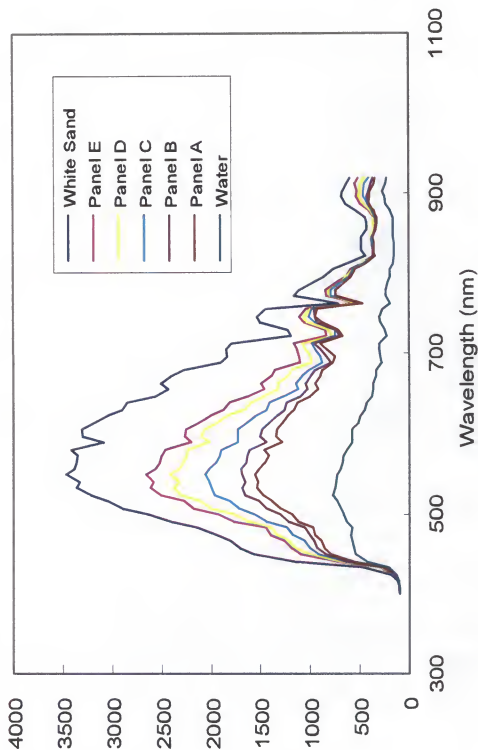
Figure 2.8 Radiance values of the hyperspectral image prior to reflectance calibration. Values are from the center pixel within each calibration panel, as well as areas of water and bright sand.

methods used were a maximum likelihood classifier, and a subpixel classifier.

Additionally, calculations were made to determine the approximate wavelength at which

reflectance in the image increases most rapidly with increasing wavelength (maximum

first derivative of the spectral curve with respect to wavelength), which is also known as

the " red edge position." The red edge position was shown to be correlated with canopy

chlorophyll concentration, an indicator of stress (Jago et al. 1999).

2.4.6 Maximum Likelihood Classifier

This procedure was done using ERDAS Imagine. Training areas are identified in

the image using the area of interest tool, and the per band statistics (count, minimum,

maximum, mean, standard deviation) are compiled for the values of the pixels included in

each training area to create what is known as a spectral signature. These spectral

signatures are then used to locate similar areas throughout the image on a pixel by pixel

basis. The "weighted distance" from the pixel to each of the signatures is calculated, and

the pixel is assigned to the class with the lowest weighted distance. The equation used to

determine weighted distance (D) is shown in equation (2.2) (ERDAS 1999),

$$D = \ln(ac) - [0.5 \ln(|Covc|)] - [0.5 (X - Mc) T (Covc - 1)(X - Mc)] \qquad (2.2)$$

where:

c = a particular class

X = the measurement vector (distance from zero in all bands) of the pixel

Mc = the mean vector of the sample of class c

ac = a priori probability that a pixel is a member of class c

Covc = covariance matrix of the pixels in the training signature of class c

|Covc| = determinate of Covc

T = transpose function.

2.4.7 Spectral Angle Mapper Classifier

This procedure was done using ENVI. The spectral angle mapper (SAM) is similar to the maximum likelihood method in that training signatures, or spectral "endmembers" are collected, and the vector of the distance from zero to each signature mean is calculated, however, the spectral angle mapper calculates the angle between the vectors in n-dimensional space, and assigns pixels to the class whose vector has the smallest angle to it. Pixels that have a distance vector greater than a certain minimum from one of the endmembers are not classified (Research Systems 2000). As with the maximum likelihood classifier, the output is a single layer thematic raster image, with pixel values which represent the class to which it is assigned.

2.4.8 Subpixel Classifier

Also performed using ENVI software, the "subpixel classifier" is different conceptually from the previous methods. Instead of attempting to determine the type of land cover that best represents what is found within a given pixel, it seeks to estimate the percentage of the pixel which is covered by each of several predefined endmembers. The endmembers are collected from regions within the image that are known to be purely

composed of a given ground cover, or may be imported from spectral libraries or spectra collected at ground level at the time the image was captured. (Research Systems 2000). The product resulting from the procedure is a set of continuous images of the same spatial scale as the original hyperspectral image, but which have pixels which contain the estimate of the fraction of the pixel which is covered by a particular type of ground cover. This method is used to detect the presence of objects which may be smaller than the pixel size, and would otherwise not be detected by any classification method. This is of particular interest in agricultural applications to find weeds, or perhaps portions of a crop smaller than the imaging pixel size which are affected by disease or stress.

2.4.9 Red Edge Position Detection

Vegetation studies have indicated that the red edge of the reflectance spectrum is particularly likely to change in response to early stages of stress (Carter et al. 1996, Craig et al. 1998, and has been positively correlated with the concentration of chlorophyll in vegetative canopies (Miller et al., 1990). In order to locate the wavelength at which reflectance increases most rapidly with increasing wavelength, an analytical method was used, which could be easily implemented in an image processing model in ERDAS Imagine, given in Appendix C, section C-2. The program calculates red edge position (REP) for each pixel and creates an image with these wavelengths as pixel values, as well as an image that does not contain wavelength numbers, but instead, relative values which are scaled to 8 bits (the numbers 0 to 255) to provide enhanced contrast.

The analytical solution to find the REP is shown in Figure 2.9. It is based on the assumption that the red edge curve is sigmoidal in shape, increasing gradually at first, then quickly, then leveling off at some point. Four values are needed to characterize this curve, and may differ according to the plant species of interest. For this study, the minimum was at 670 nm, the maximum at 743 nm, and two intermediate points at 686 nm and 719 nm, with reflectance values A, D, B and C, respectively. The point of maximum rate of increase is located at the intersection of a line between the minimum and maximum, and a line between the intermediate points (Guyot and Barret 1988).

2.4.10 Leaf Area Index Map Creation

In the Kerr Center citrus grove, the availability of calibrated leaf area index (LAI) measurements made possible the creation of an LAI map of the grove and surrounding vegetation. To accomplish this, a semi-empirical relationship between NDVI and LAI developed by Baret and Guyot (1991) was employed (Friedel 1997). The equation (2.3) relates the pixel NDVI to that of the surrounding bare ground ($NDVI_g$) and the asymptotic value at which LAI approaches infinity ($NDVI\infty$). Figure 2.10 shows a graph of this function, and calibration method.

$$LAI = \frac{\log\left[\left(NDVI - NDVI\infty\right) / \left(NDVIg - NDVI\infty\right)\right]}{-K_{NDVI}} \qquad (2.3)$$

The values K_{NDVI}, $NDVI_g$ and $NDVI\infty$ must be obtained empirically, and will differ according to factors such as the multispectral bands used, the radiometric

$$REP = 686 + \frac{\left(\dfrac{A+D}{2}\right) - B}{\left(\dfrac{C-B}{719-686}\right)}$$

670   686 REP 719   743
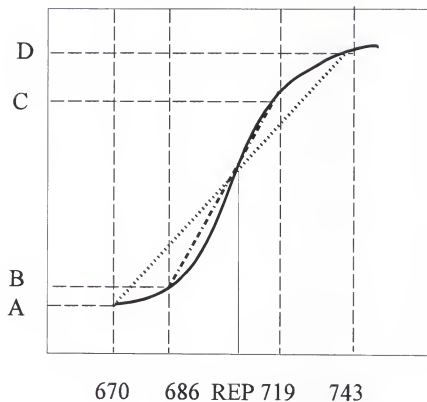
Figure 2.9 Formula, and graphical representation of method to find red edge position in hyperspectral images. The bottom axis shows center wavelengths of the bands used. The vertical axis shows the variables assigned to the digital numbers in those bands.

calibration of the image, the type of soil or ground cover, the type of vegetation, and seasonal variations. To obtain these values, LAI values obtained from the canopy analyzer validation study were used in conjunction with NDVI values calculated from pixels centered on the small trees, some of which were less than 1 m in diameter.

The pixel size of the multispectral image was 0.3 m, so for all but the most defoliated trees, there was at least 1 pixel centered within the tree canopy. Even where a pixel is entirely contained within the tree canopy there is some radiation scattered by the atmosphere from the surrounding pixels, which contaminates it. In order to overcome this effect, as well as that of pixels which partly fall on the grass surrounding the trees, the $NDVI_g$ parameter was obtained from the NDVI of the surrounding grass, rather than areas of bare soil. In effect, this set the LAI of the grass to zero, which was not a problem in this case, because the LAI of the grass was not of interest in this study.

The calibration of the K_{NDVI} parameter was mainly accomplished by performing a linear regression through the NDVI points plotted against measured LAI, since the lower portion of the curve is nearly linear. The LAI and NDVI data used to calculate the parameters are given in Table 2.3. The upper portion of the curve was calibrated using the NDVI values from the tall windbreak row of Australian pine (*Casuarina equisetifolia* L.) trees. It was assumed that these trees would have LAI values approaching the maximum found in dense forests, approximately 11 or 12. The resulting parameters values used in the LAI calculation were an $NDVI_g$ of 0.35, $NDVI\infty$ of 1 and K_{NDVI} of 0.1. The program used to generate the LAI map image in ERDAS Imagine is shown in Appendix C, section C.5.

Table 2.4 LAI and NDVI data used to calibrate LAI map calculation, as well as NDVI values obtained from canopy spectroradiometer readings.

| Tree	LAI	NDVI	$NDVI_{200}$	$NDVI_{670}$	Tree	LAI	NDVI	$NDVI_{200}$	$NDVI_{670}$
W1	1.68	0.53	0.69	0.9	E1	1.95	0.47	0.63	0.87
W2	1.73	0.5	0.66	0.9	E2	1.68	0.48	0.54	0.88
W3	1.45	0.48	0.72	0.89	E3	0.98	0.39	0.62	0.9
W4	0.13	0.43	0.51	0.72	E4	1.08	0.43	0.59	0.87
W5	1.13	0.43	0.69	0.91	E5	2.05	0.49	0.57	0.85
W6	1.45	0.54	0.55	0.83	E6	2.00	0.53	0.65	0.85
W7	1.40	0.46	0.7	0.9	E7	1.73	0.47	0.61	0.89
W8	1.35	0.51	0.74	0.89	E8	1.33	0.41	0.66	0.86
W9	1.33	0.38	0.67	0.87	E9	1.28	0.48	0.57	0.83
W10	1.23	0.39	0.65	0.88	E10	1.00	0.44	0.6	0.87
W11	1.48	0.44	0.66	0.85	E11	2.48	0.52	0.68	0.9
W12	1.13	0.41	0.66	0.89	E12	1.95	0.41	0.61	0.82
W13	1.05	0.36	0.63	0.81	E13	2.03	0.52	0.65	0.89
W14	0.68	0.48	0.63	0.87	E14	2.98	0.52	0.69	0.91
W15	1.63	0.45	0.2	0.13	E15	2.40	0.47	0.61	0.89
W16	1.83	0.46	0.67	0.89	E16	1.65	0.52	0.59	0.87
W17	1.15	0.46	0.57	0.84	E17	1.73	0.51	0.55	0.9
W18	0.95	0.45	0.6	0.86	E18	2.25	0.48	0.74	0.93
W19	n/a*	0.48	n/a	n/a	E19	2.53	0.52	0.67	0.87
W20	1.23	0.44	0.72	0.9	E20	1.10	0.49	0.62	0.88
W21	n/a	0.45	n/a	n/a	E21	1.30	0.49	0.53	0.76
W22	2.03	0.58	0.73	0.9	E22	1.55	0.49	0.6	0.85
W23	1.13	0.46	0.66	0.88	E23	1.05	0.49	0.78	0.92
W24	n/a	0.32	n/a	n/a	E24	2.75	0.55	0.67	0.93
W25	n/a	0.38	n/a	n/a	E25	1.63	0.49	0.62	0.85
W26	3.45	0.55	0.76	0.91	E26	2.55	0.5	0.66	0.9
W27	1.97	0.46	0.72	0.91	E27	2.20	0.5	0.65	0.9
W28	2.28	0.53	0.73	0.91	E28	2.08	0.48	0.67	0.9
W29	4.38	0.56	0.56	0.87	E29	2.15	0.46	0.73	0.93
W30	2.83	0.47	0.83	0.95	E30	3.10	0.58	0.61	0.86
					E31	2.40	0.51	0.66	0.92
* LAI and radiometer NDVI values not					E32	2.35	0.43	0.56	0.89
available because tree was defoliated.					E33	3.15	0.59	0.59	0.81

It may be noted from Table 2.4 that NDVI values calculated from spectra collected using the spectroradiometer are higher than those obtained directly from the calibrated image. This may be due to the scaling effect of imaging at 1000 m above the canopy , compared with close-up measurements. The $NDVI_{700}$ values were calculated using the 700 nm band as the red channel, whereas, the $NDVI_{670}$ values were calculated using the 670 nm band as the red channel. The red channel in the multispectral image is centered on 700 nm, hence the greater similarity to the $NDVI_{700}$ values.

2.4.11 <u>Multi-year Landsat Study of Citrus Growth</u>

As a bridge between the local scale studies in the citrus trees and the regional scale study of cypress wetland stress, an additional study was performed using Landsat imagery to observe the development of the experimental citrus grove at Ft. Pierce at three intervals during its first ten years of growth. Radiometrically and geographically corrected images from the Landsat 5 sensor from March 29, 1993 and March 21, 1996, and an image from the Landsat 7 sensor from February 5, 2000 were obtained for this purpose. Because of the superior capability of the Landsat 7 images for precise calibration, it was decided to perform a reflectance calibration procedure on the February, 2000 image, then reference the earlier Landsat 5 images to it for comparison.

The first step was to develop a calibration routine using the ERDAS Imagine model builder. Calibration for relative reflectance requires first finding the correct at-sensor radiance values. This is done by finding the gain and offset values that are

A
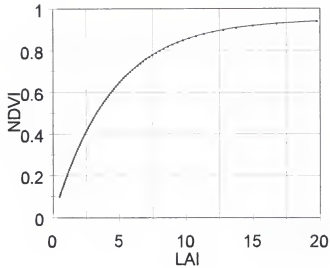
B
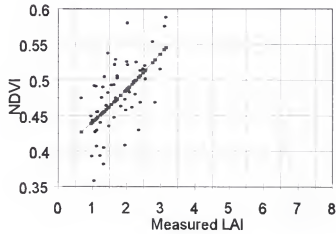
Figure 2.10 Hypothetical and actual relationship between NDVI and LAI. Curve showing the asymptotic relationship between LAI and NDVI is seen in (A). The measured LAI and NDVI values used to calibrate the lower portion of the curve (B).

particular to each band of the sensor for a given time period. For Landsat 5, pre-launch or revised calibration information is used. For Landsat 7, the latest values from NASA analysis of onboard calibration devices are found in the metadata file (CPF) which accompanies the image, or may be downloaded from the Landsat-7 web site. The gains A and offsets B are used in the following equation, where L is radiance in Watts per square meter per steradian per micrometer and DN is the digital number derived from the image:

$$L = A \cdot DN + B \qquad (2.3)$$

The next step is to convert the radiance values to apparent reflectance, which is the ratio of L (as defined above) to solar irradiance, the distance multiplicative factor (Earth-Sun distance) and the solar zenith angle. The formula (Arino et al. 1994) is:

$$P = \frac{\pi L}{d^2 E \cos\theta} \qquad (2.4)$$

where:

P = reflectance at the top of the atmosphere

π = 3.14159 .....

L = spectral calibrated radiance at top of the atmosphere

d = ratio of mean to actual Earth/Sun distance,

= 1.0 / (1.0 - 0.016729 cos(0.9856(Day ofYear-4)))

E = spectral solar irradiance at top of atmosphere (see Table 2.5)

θ = solar zenith angle

Table 2.5 Landsat ETM+ Sensor Calibration Parameters.

Band	Gain	Offset	Solar Irradiance
1	191.6	6.2	1970
2	196.5	6.4	1843
3	152.9	5.0	1555
4	241.1	5.1	1047
5	31.06	1.0	227
7	10.8	0.35	80.53

The overall view of the calibration procedure is shown in Figure 2.11. The six multispectral bands of the Landsat image are separated, then conversion to radiance is performed, then calibration for apparent reflectance (reflectance at the top of the atmosphere) is performed, then the image layers are rejoined. The program to perform these steps is given in Appendix C, section C-3.

After the year 2000 Landsat 7 image was calibrated, the 1993 and 1996 Landsat 5 images were normalized to it. This was done by locating points common to all three images which probably did not change in reflectance properties between the time periods of the images involved. Such points areas are usually man-made objects such as buildings, water towers, roads, etc. In this case, the roof of the equipment barn located at the Indian River Research and Education Center was used as a reference point.

The images were all cropped to include only the vicinity of the citrus grove and research center. The GIS point coverage of the citrus grove was overlayed on each image in turn, and the points which fall within a Landsat pixel were all assigned the value of that pixel, so the values were integrated into the GIS database. Then, the pixel values from
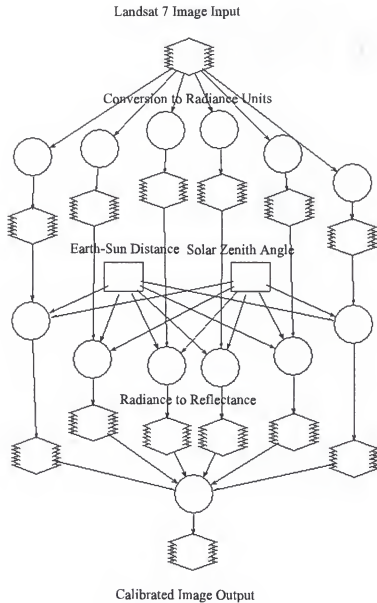
Figure 2.11 Reflectance calibration procedure for a Landsat 7 ETM+ image. Diagram shows the separation of the original image into 6 bands, application of calibration formula to each band, then recombination into a calibrated image, using the ERDAS Imagine graphical modeling environment.

within the roof of the equipment barn were extracted and copied into a spreadsheet.
These values from each band of the 2000 image were divided by the corresponding values
in the 1993 and 1996 images to obtain conversion multipliers. Then, the pixel values
from the citrus plots in the 1993 and 1996 images were multiplied by these values,
thereby normalizing them in reference to the calibrated 2000 Landsat 7 image. Finally,
NDVI was calculated from the band 3 and 4 values and integrated into the database.

2.4.12 Cypress Data Analysis

The set of numerical values derived from the various layers in a multiband image
which correspond to a certain ground cover type is known as a spectral signature. The
spectral signature usually includes statistical properties of the image pixels from which it
is derived, such as the mean and covariance matrix, of the values of several pixels. The
group of spectral signatures used to perform a classification is sometimes called the
training set. The larger the sample size of pixels in each signature of the training set, the
more reliable the final classification is likely to be.

Sample size of the training set is one of several factors that can affect the
reliability of the final classification. Other factors include the spectral separation of the
end classes, or the degree to which the spectral signatures are different from each other,
and also the spatial resolution of the image compared with the size of the areas of ground
cover that need to be placed in separate classes.

The classifications in this study were performed using a maximum likelihood
classifier. It should be noted that the maximum likelihood, or Bayesian classifier requires

that the histograms of pixel values in each band of the image have an approximately normal distribution. A histogram of an image represents the number of pixels in each band which have each of the 256 possible values plotted against the range of values. While the histograms for images covering the whole region are in some cases highly skewed, the images which include only cypress that were used in this study have histograms that are approximately normally distributed, satisfying this condition.

The classification of the images was done in ERDAS Imagine®, using Arc/Info® polygon coverages of wetland boundaries extracted from land use/land cover maps. First, using Arc/Info, a point coverage containing the locations of the assessed wetlands and their quality rankings from the Rochow study (Rochow, 1998) was used to overlay on the land use coverage and extract the polygons of the assessed wetlands into one of three groupings, Good (rank 4-5), Moderately Stressed (rank 2.5-3.5) and Severely Stressed (rank 1-2). Then, using ERDAS Imagine, the polygons were used to define an area of interest (AOI) in the image, which was used to copy the pixel values within that area to the signature editor. This process was repeated for each of the wetland quality groups, then samples of cloud and shadow were also extracted from the image into the signature editor. A supervised classification was then done on each image which had been masked to include only the cypress areas.

The overall procedure used to analyze the Landsat images is as follows:

1. Overlay Landsat image with GIS coverage to create an image containing cypress only.

2.   Identify monitored wetlands and create training signatures of stressed and
        unstressed cypress using GIS overlays

3.   Run supervised classification of image to identify areas with signatures similar to
        stressed wetlands.

        In order to test the robustness of the overlay method with respect to the land cover

data source used, the procedure was repeated using a GIS wetlands database published by

the U. S. Fish and Wildlife Service called the National Wetlands Inventory (NWI). Also,

a GIS data set was created that represents the intersection of the National Wetlands

Inventory database and the Southwest Florida Water Management District (SWFWMD)

database. In other words, the NWI cypress areas were overlaid on the SWFWMD cypress

areas, and only those areas which coincided were included in the new database. The

supervised classification was performed using the new data set also, and results from this

and the other two procedures were compared.

3.1 <u>Single-Leaf</u>

3.1.1 <u>Rainfall and Irrigation.</u>

As noted previously, the effect of saline irrigation water on the citrus grove at Ft. Pierce is largely dependent on the quantity of irrigation water applied during the dry season, as well as the frequency and intensity of rainfall events. March and April 1998 were unusually wet in Florida, with above average rainfall, so that irrigation had not been applied and the effects of acute salinity stress had not appeared. By the beginning of May, the rains had stopped, and an unusually dry period began with only occasional rainfall. This produced a substantial rainfall deficit, with the May 1998 rainfall less than half the average (see Figure 3.1B). The rainfall deficit was calculated by subtracting the 20 year average rainfall for each month from the 1998 monthly rainfall. Daily irrigations were applied during 12 days in April, 19 days in May, and 20 days in June with daily applications of 58 liters per tree, except for nine days in which 77 liters per tree were applied. The irrigations were sufficient to bring the total water available to the trees to levels similar to average rainfall years, although with increased salinity levels. The rainfall and irrigation quantities are summarized in Table 3.1. The resulting quantities of

salts added to the soil per tree are shown in Table 3.2. An operator error resulted in salinity not being applied in the irrigation water from the 13th to the 22nd of May; fresh water was applied to all trees during this period. Continued dry weather in June caused salinity to build up again. Long periods of dry weather cause salts to build up in the soil, although each rainfall event allows part of the salt to leach away. The quantities of rain in the heaviest rainfall event of each month are noted in Table 3.1. During the three driest months (April, May and June), the single heaviest rainfall event represented more than 50% of the total rainfall for that month. During January, February and March, the largest rainfall event represented much less than 50% of the total rainfall.

Table 3.1 Summary of rainfall and irrigation quantities (mm) for Jan.-June 1998.

	Jan	Feb	Mar	Apr	May	June
Heaviest rainfall	18.3	44.0	40.3	38.9	30.1	39.8
Monthly Total	48.4	124.7	116.6	54.3	53.2	69.1
Average	49.3	63.1	76.3	54.3	106.9	152.5
Difference	-0.9	61.6	40.3	0.0	-53.7	-83.4
Irrigation	0.0	0.0	0.0	44.2	64.6	74.9
Rain+Irrig.	48.4	124.7	116.6	98.5	117.9	143.9

Table 3.2 Estimated salinity loading due to saline irrigation water (kg per tree).

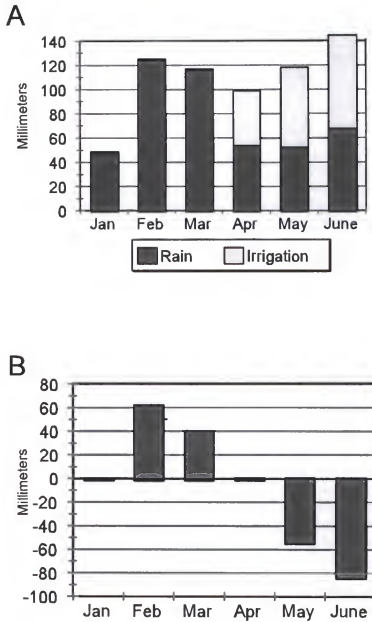| Salinity	April	May	June
3800 ppm	2.9	2.0	4.9
2700 ppm	2.0	1.1	3.5
1600 ppm	1.2	0.8	2.0
500 ppm	0.4	0.3	0.6

Figure 3.1 Rainfall and irrigation at Ft. Pierce for the first 6 months of 1998 (A). The rainfall deficit (B) was calculated by subtracting the 20 year average monthly rainfall from the monthly rainfall in 1998 (Craig et al. 1998b).

In order to observe the salinity increase in response to saline irrigation treatments, soil conductivity was measured in several different areas of the grove on three days in April, June and July, 1998. The areas measured were the ones where the trees used for leaf spectral reflectance measurements are located. They include areas treated with low salinity irrigation water, and areas receiving high salinity water, representing each of the three fertilizer methods used, for a total of six treatments. Four equally spaced measurements were taken in each treatment block with a soil conductivity probe. The average conductivity values from these readings are shown in Figure 3.2 (A). The average of all the low salinity measurements are compared with the average of the high salinity measurements in Figure 3.2(B).

One result that stands out from these measurements is that clearly, salinity had built up in the soil in response to saline irrigation water and the lack of rainfall. In all cases, conductivity increased from barely detectable levels in April to higher levels in June, and declined considerably by July, when seasonal rainfall had returned. There is also a difference in the soil conductivity in response to the quantity of salinity in the irrigation water, as indicated by average conductivity levels that are more than twice as high in the high salinity treatments compared with the low salinity treatments. One apparent anomaly is the conductivity level in treatment 5, which is similar to the high salinity values. This may be explained by the types of fertilizer used in treatments. Treatments 1 and 4 have NH_4NO_3 and KCl applied through fertigation 15 times per year, treatments 5 and 8 have $Ca(NO_3)_2$ and KNO_3 applied through fertigation 15 times per year, and treatments 9 and 12 have NH_4NO_3 and KCl applied dry, 3 times per year.
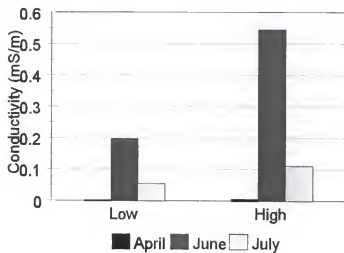
A
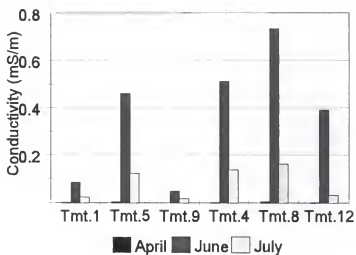
B

Figure 3.2 Soil conductivity as measured in April, June and July, 1998. Treatments 1,5 and 9 are "low"; treatments 4, 8 and 12 are "high" (A). Average conductivity among the low and high groupings are shown in (B) (Craig et al. 1998b).

Despite the fact that the $Ca(NO_3)_2$ and KNO_3 fertilizer treatment was used in order to reduce the salinity loading by avoiding the use of chloride, these results at least imply that the calcium nitrate and potassium nitrate do contribute to soil conductivity. In both the high and low salinity treatments, the highest conductivity values were from the plots where $Ca(NO_3)_2$ and KNO_3 are applied.

3.1.2 <u>Changes in Reflectance</u>

Single leaf spectral reflectance measurements taken from trees in the various treatments are shown in Figure 3.2. Despite some variability of measurements within a given treatment, the mean values were remarkably consistent. Reason for variability in spectral reflectance measurements may include differences in leaf texture due to infection by viral or fungal diseases, insect grazing, or perhaps effects of salinity stress that vary according to leaf age or location on the tree. Leaves were selected randomly to get an unbiased sample of leaves from each treatment, and a relatively large number of measurements were made so that effects due to factors other than salinity would appear in both salinity groups and not excessively skew the results.

Some notable trends were detected in single leaf reflectance measurements as saline irrigation began and the trees began to be stressed. Figure 3.4 shows the results of the paired t-test (McClave and Dietrich 1982) applied to compare the reflectances of high salinity and low salinity treatments at each wavelength in the range of 350-950 nm. In the pre-stress sampling period in Dec. 1997, the figure appears to indicate significant difference over the whole range, but this may be due to inconsistency in measurement at
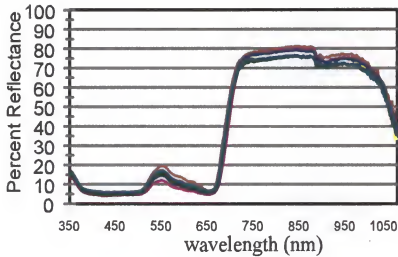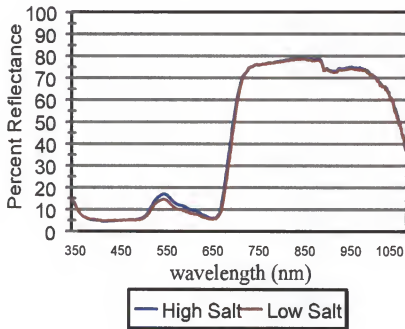
Figure 3.3 Spectral reflectance curves taken in June 1998 during a prolonged dry period. (A) Average values for 12 measurements for each treatment. (B) Average values for 36 leaves taken from trees of each salinity level. Slight but consistent differences appeared between high and low salinity treatments.

that time. For the other two sampling periods shown, a frame was designed to hold each leaf flat as it was being measured with the spectroradiometer, which allowed for more consistent results. In the May 1998 sampling period, a trend appeared to be developing which showed greatest difference in reflectance between high and low salinity treatments, and the final measurements in June 1998 showed the same trend but more pronounced, with significant differences in reflectance showing up near 700 nm, which corresponds to the "red edge" of the spectral curve, and in the green-yellow range of 500-600 nm. It should be noted that these differences are pre-visual, since no difference in appearance in the canopies of trees of different treatments was apparent at the time of measurement.

The unpaired t-test was used to compare the 12 reflectance readings obtained for each treatment with those of another treatment for each of the 512 bands from the spectroradiometer. The critical value of t used to test for significance was 2.2, for $\alpha/2=0.025$ (indicated by a horizontal line on the plots). One of the assumptions of the unpaired t-test is that the sets of values being compared have an approximately normal distribution. This was verified by finding the range of reflectance values from the twelve leaves measured of each treatment, dividing this range into seven equally spaced groupings, and counting the number of values that fall into each grouping. A normal distribution implies that the largest number of samples will have values near the group mean, and that equal numbers of samples would fall above and below the mean. This was done for different treatments at several different wavelengths, and the results indicated that the data were approximately normally distributed.

A
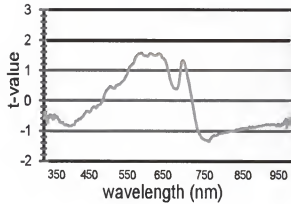
B

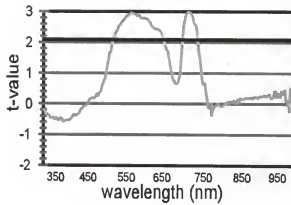Figure 3.4 Results of paired t-test comparing single-leaf reflectance of
high and low salinity groupings in each of 512 spectral bands on May 8,
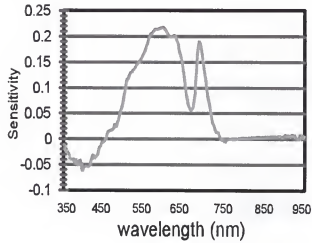1998 (A) and June 22, 1998 (B).
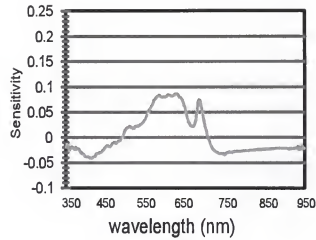
Figure 3.5 Sensitivity to change in reflectance in response to stress at each wavelength (Craig et al. 1998a). Reflectances from unstressed leaves are subtracted from those of unstressed leaves, and the result divided by the unstressed reflectances.

A measure was also made of sensitivity of each of the reflectance at each wavelength to salinization. Assuming that the reflectance of stressed trees is higher than that of unstressed trees at most wavelengths, the sensitivity measure was made by subtracting the reflectance of the leaves from trees exposed to highly saline irrigation water from the reflectance of the leaves from trees receiving lower salinity, then dividing the result by the reflectance of the low salinity leaves (Figure 3.5). This measure is simpler to calculate than the statistical t-test, and this example shows that the results in terms of revealing trends in spectral reflectance response to stress are similar.

3.2 Canopy-Scale Measurements and Images

Experiments done at canopy scale included multispectral image analysis, measuring and validating Leaf Area Index (LAI) and measuring tree height and canopy diameter for the whole experimental grove at Ft. Pierce.

3.2.1 Canopy-scale Multispectral Imaging

During the site visit of June 23, 1998, digital images of tree canopies from each salinity treatment were captured. This is done using a monochrome Charge Coupled Device (CCD) camera and narrow-band interference filters which pass the wavelengths of interest, and block all others. Monochrome images in five bands were captured with

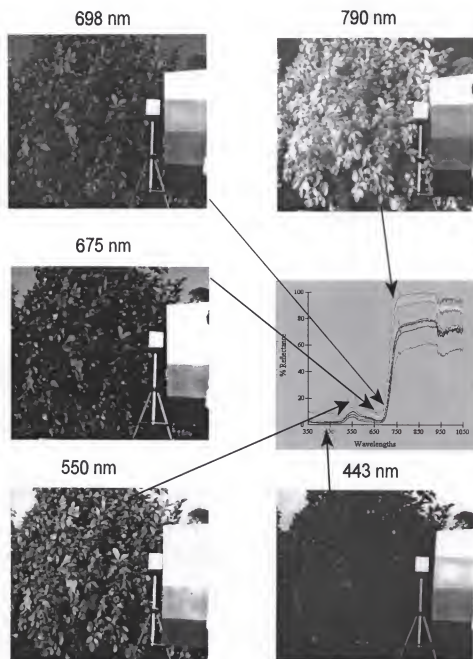**Figure 3.6** Five single-band images of a citrus tree (Craig and Shih 1997). Images were sequentially captured using a filter wheel camera. Band center wavelengths noted above each image.

a video capture device attached to a notebook computer. The bands used were 438-448 nm (band 1), 545-555 nm (band 2), 670-680 nm (band 3), 695-701 nm (band 4), and 785-795 nm (band 5).

The individual single band images of a given treatment were calibrated by finding the average pixel value in each panel of the calibration placard, determining what values they should have in an image calibrated for reflectance, then performing a linear curve fit to adjust the pixel values so they best correspond to a calibrated image. In some images, the brightest gray level was saturated, meaning that the intensity of the light reflected from the panel was higher than the maximum that can be accurately recorded by the camera. Pixels in the image that were saturated were not used in calibration. After calibration, the single band images for each treatment were coregistered to produce a five band multispectral image (Figure 3.6).

After processing and analyzing the images, it became clear that canopy-scale images of the type shown here present a great deal of variability in sun illumination angle, leaf angle, and as a result, highly variable reflectance characteristics. Variations in canopy reflectance in the five bands represented in the images may have resulted from differences of sun angle since the images were taken over a two hour period at the time when the sun was rapidly descending. Close spacing between rows of trees and variation in canopy size made it difficult to maintain the camera at a consistent angle and distance from the trees as well. Other experiments with multispectral imaging of tree canopies at close range have included stressed and unstressed trees within the same frame, so they were imaged under the exact same light conditions and angle (Carter et al. 1996).

Treatment 1　　　　Treatment 4

Treatment 5　　　　Treatment 8

Treatment 9　　　　Treatment 12

**Comparison of treatments using
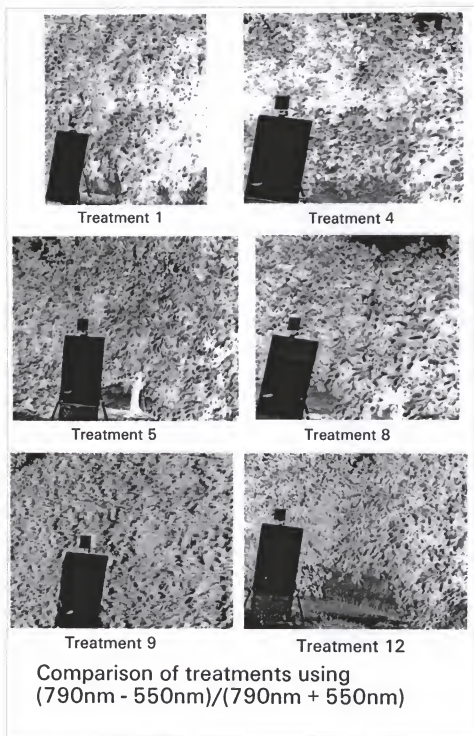(790nm - 550nm)/(790nm + 550nm)**

Figure 3.7 Comparison of canopy-level images using a normalized difference of 790nm and 550nm bands (Craig et al. 1998b)

This was not possible in this experiment, since the trees of different treatments were located in separate rows.

Another difficulty that arises from sequential capturing of images in different spectral bands is that unless the air is very still, there may be leaf movement between the capture of bands, which results in a lack of coregistration in certain areas of the frame. The image of treatment 8 shows this effect, in some leaves in the central part of the image. This difficulty is avoided in multispectral camera arrays that capture all bands simultaneously.

The slight differences in reflectance due to salinity stress were detected at the leaf level even though they were not generally apparent to an observer at the canopy level. Besides the fact that leaf angle and lighting conditions were easier to control at the leaf level than for the whole canopy, there is also a difference in the sensitivity of the spectroradiometer, with 16 bit dynamic resolution of spectral data compared to 8 bit per pixel dynamic resolution of the CCD camera system. In addition, the spectral resolution of the radiometer includes 512 bands, whereas the digital images were captured in only five bands. The sensitivity of a multispectral imaging system for detection of vegetation stress could therefore be improved by using cameras with a greater dynamic range, capturing images in more spectral bands, and providing better control over illumination angle.

In images where conditions were favorable, it was possible to collect canopy reflectance measurements from the digital images such as in Figure 3.8. In this case, the images were calibrated for reflectance and co-registered. Portions of the images
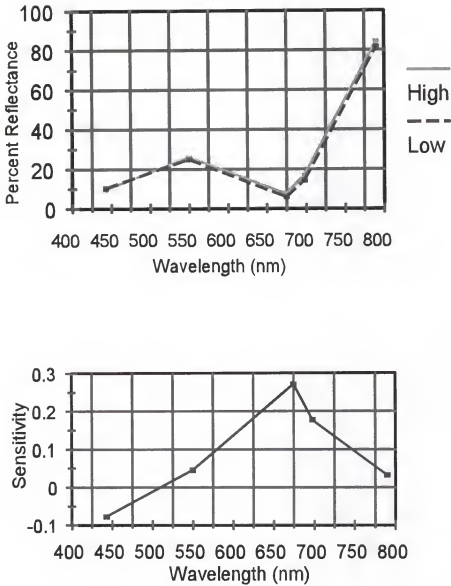
Figure 3.8 Percent reflectance and sensitivity to stress factors derived from canopy-scale images. The 5 bands were calibrated and coregistered, and a 1 m² section of the tree canopy was selected from the image and values averaged to obtain the numbers used.

representing sections of the canopies of trees that received different experimental treatments were selected, and when the mean values of the pixels in these selections are compared it may be noted that the wavelengths which show the highest sensitivity to stress factors, are in the red and far red, namely, at 675 nm and 700nm.

3.2.2 Calibration of LAI Measurement

Leaf area index (LAI) was measured under eight small citrus trees selected from a group of sixty at the Vero Beach citrus site using the Delta-T Canopy Analyzer, and the actual total leaf area of those trees was measured in the lab. Two trees were selected to represent each of the four classes of canopy condition, ranging from very poor to healthy. LAI was calculated by dividing the total leaf area of each tree by the area on the ground covered by canopy. The resulting calculated values are shown in Table 3.3., along with the measured and corrected values.

Table 3.3 Calculated and Measured LAI values. Calculated values were obtained by measuring total leaf area and dividing by ground cover area . Measured values were obtained by averaging 5 readings from the canopy analyzer, and corrected values were obtained by applying the correction formula (3.1).

Tree	Calculated	Measured	Corrected
E5	2.58	2.05	2.49
E6	2.60	2.00	2.44
E11	2.80	2.48	2.97
E19	3.10	2.53	3.03
W7	1.57	1.40	1.76
W13	1.36	1.05	1.37
W14	1.01	0.68	0.94
W18	2.90	0.95	1.25

A linear regression of the eight measured LAI values against the calculated values shows a rather poor fit, with $R^2 = 0.59$. When the data from tree W18 are removed from the regression, however, the fit improves to $R^2 = 0.97$. This indicates that the measurement of tree W18 may have been made improperly, and therefore may be considered an outlier that is not representative of the true relationship of measured to calculated LAI values.

A likely cause of the low measured value for tree W18 is the passing of a cloud that temporarily blocked direct sunlight. Although the change in total solar radiance is compensated for by the instrument, the increase in the proportion of indirect light reaching the probe meant that light arriving from the side, not passing through the tree canopy, becomes more important. It has been observed that under these conditions, the Delta-T SunScan probe should be held up as close as possible to the foliage to ensure that only light which had passed through the tree canopy is allowed to reach the probe. Another factor that may have made an accurate LAI measurement of tree W18 difficult is the small size of the tree canopy, just under 1 meter in diameter. Since the probe is 1 meter long, the whole probe did not quite fit under the tree canopy. It is assumed in the light penetration model that the whole probe is under the shade of the canopy, so an accurate measurement of a tree canopy less than 1 meter in diameter is not possible.

Figure 3.9 shows the plotted values along with the regression line. The equation of the regression line is:

$$\text{LAI (calculated)} = 1.127 \times \text{LAI (measured)} + 0.184 \qquad (3.1)$$
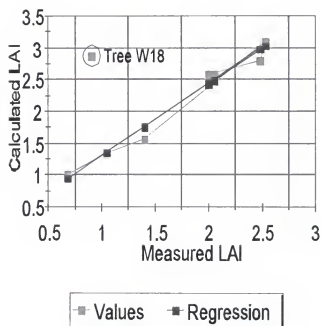
Figure 3.9 Calculated LAI vs. Measured LAI. Calculated values were obtained by stripping leaves from trees, summing their area, and dividing by canopy area. Measured LAI values were obtained with the canopy analyzer.

This indicates that to properly calibrate the measured LAI values for actual LAI, the measured values may be multiplied by 1.127, and 0.184 added to them. Such a correction would not be possible for very small LAI values, since it assumes that in the case of LAI less than 0.184, the measured values would be negative. LAI values of less than zero are not possible. This indicates that this method is not applicable to LAI values that are very small, and should not be used in such cases. The lowest LAI value that can be accurately measured is not clear from these results, however, the lowest LAI in the study, 1.01 was predicted as 0.94 after calibration, within 5% of agreement with physical leaf measurement .

3.3 Grove Scale Aerial Images

Results from the analysis of the airborne multispectral images captured on May 26, 1999 are described here. The bands had center wavelengths of 550 nm, 700 nm and 840 nm, with bandwidths of 10 nm. The images were processed by overlaying a GIS point coverage of the tree locations, and automatically extracting the digital numbers representing reflectance at specific wavebands from the image, and transferring them to a database for statistical analysis, according to the method described above.

3.3.1 Analysis of Variance

The statistical relationships between the reflectance values obtained and the experimental treatment groups in the citrus grove were analyzed. When reflectance values from the individual bands were grouped according to the level of irrigation salinity which

Table 3.4 Analysis of Variance for the simple ratios of 840nm/550nm, 550nm/700nm and 840nm/700nm by Rootstock.

```
840nm/550nm  (p<0.001)        Individual 95% CIs For Mean
                                  Based on Pooled StDev
Level     N     Mean    StDev  ---------+---------+---------+-------
CA      235    4.257    1.106                 (--*---)
CL      240    4.905    1.377                              (---*--)
SO      244    3.822    1.302  (---*--)
SW      241    4.932    0.951                              (--*---)
                               ---------+---------+---------+-------
Pooled StDev =   1.196             4.00      4.40      4.80
```

```
550nm/700nm  (p<0.001)          Individual 95% CIs For Mean
                                  Based on Pooled StDev
Level     N     Mean    StDev  ------+---------+---------+---------+
CA      235   0.9914   0.3740   (-----*----)
CL      240   1.2260   0.6788                       (----*----)
SO      244   0.9516   0.3194  (----*----)
SW      241   1.1102   0.4780              (-----*----)
                               ------+---------+---------+---------+
Pooled StDev =   0.4824          0.96      1.08      1.20      1.3
```

```
840nm/700nm  (p<0.001)          Individual 95% CIs For Mean
                                  Based on Pooled StDev
Level     N     Mean    StDev  ------+---------+---------+---------+
CA      235    4.456    2.799    (----*---)
CL      240    6.448    5.078                         (---*----)
SO      244    3.888    2.418  (----*---)
SW      241    5.684    3.448                (----*---)
                               ------+---------+---------+---------+
Pooled StDev =   3.583           4.0       5.0       6.0       7.0
```

the trees received, the differences between the groups were not significant, however, when simple ratios of each pair of bands (840nm/700nm, 840nm/550nm and 550nm/700nm) were compared, significant differences between treatment group means appeared (Table 3.4). When the trees were grouped by rootstock, there were significant differences (p < .0001) in mean reflectance values in each of the bands and also between the means of the simple ratios. When the trees were grouped according to fertilizer treatment, the differences in mean values of the simple ratios were also significant.

The most significant index derived from reflectance measurements in the three band images was a narrow-band normalized difference vegetation index (NDVI), derived from reflectances (R) in the 840 nm and 700 nm bands. This index is calculated by:

$$NDVI = \frac{R_{840} - R_{700}}{R_{840} + R_{700}} \tag{3.2}$$

Analysis of variance of the NDVI by salinity level grouping showed an overall effect with a significance level of p=0.062. Typically, a level considered significant is p<0.05, however, in agricultural studies, a level of p<0.1 is frequently considered significant, due to the many uncontrolled environmental factors in field experiments.

Only the highest salinity level show a significant reduction in NDVI compared with the other levels (Table 3.5). Part of the reason of this may be the fact that where a tree canopy is smaller or thin due to stress effects, understory vegetation such as grasses can grow and contribute to the NDVI detected by airborne imagery. Increased variability in tree response to salinity stress due to other factors, particularly as indicated for rootstock and fertilizer type, is also likely to confound the predictive power of NDVI with respect to salinity level unless these factors are accounted for in the analysis. Table 3.5 also shows the analysis of variance of the differences in NDVI caused by rootstock type. Here, differences are highly significant. This indicates the greater vulnerability of some rootstocks to salinity stress effects (and perhaps other stressors that my affect them). The 'sour orange' (SO) and 'Carrizo citrange' (CA) varieties are clearly distinguishable from the 'cleopatra mandarin' (CL) and 'Swingle citrumelo' (SW) varieties by their NDVI signatures.

In many experiments, the interaction of two factors can have a larger effect on the results than either factor individually. In order to get an understanding of the interaction of salinity, fertilizer and rootstock factors, interaction plots comparing the responses of measured canopy volume growth to each factor (Figure 3.10), and comparing the response in NDVI from aerial imagery to each factor (Figure 3.11) were created.

Table 3.5 Analysis of Variance for NDVI by Water Quality, Rootstock and Fertilizer Type.

```
NDVI by Water Quality (p=0.062)     Individual 95% CIs For Mean
                                     Based on Pooled StDev
Level      N      Mean    StDev   -+---------+---------+---------+--
1         240   0.5944   0.1826         (-------*-------)
2         240   0.6092   0.1836              (-------*-------)
3         240   0.5889   0.1779         (-------*-------)
4         240   0.5630   0.2156   (-------*-------)
                                  -+---------+---------+---------+--
Pooled StDev =   0.1905           0.540     0.570     0.600     0.630


NDVI by Rootstock (p<0.001)         Individual 95% CIs For Mean
                                     Based on Pooled StDev
Rootstock   N      Mean    StDev  -+---------+---------+---------+--
CA        235   0.5627   0.1707            (---*---)
CL        240   0.6452   0.1928                           (---*--)
SO        244   0.4968   0.2184   (---*---)
SW        241   0.6515   0.1246                           (---*--)
                                  -+---------+---------+---------+--
Pooled StDev =   0.1801            0.480     0.540     0.600     0.660


NDVI by Fertilizer Type (p=0.034)  Individual 95% CIs For Mean
                                     Based on Pooled StDev
Level      N      Mean    StDev  -+---------+---------+---------+-----
1         320   0.5902   0.1855          (-------*------)
2         320   0.5686   0.1844   (-------*-------)
3         320   0.6078   0.2010               (------*------)
                                 -+---------+---------+---------+-----
Pooled StDev =   0.1905           0.550     0.575     0.600     0.625
```

In an interaction plot, lines that remain parallel indicate no interaction between the factors, while lines that diverge or converge indicate an interaction. It may be seen from Figure 3.10 that water quality seems to interact with fertilizer type in creating differential canopy development. In particular, fertilizer number 2 ($Ca(NO_3)_2$ & $K NO_3$) has a pronounced effect in reducing canopy development in the presence of higher salinity concentrations (poorer water quality). At the highest salinity level, a reduction in average canopy volume appears in all fertilizer treatments, although to a lesser degree with fertilizer 3 (NH_4NO_3 & KCl (dry)). There is also some interaction between rootstock and water quality, with the 'cleopatra mandarin' rootstock showing the biggest interaction in the presence of poor water quality, although the 'sour orange' rootstock has produced the least canopy development, and 'Carrizo citrange' the second least. The interaction between fertilizer and rootstock is also pronounced, with the $Ca(NO_3)_2$ & $K NO_3$ treatment showing the greatest interaction reducing canopy development with all rootstocks except 'sour orange', where it appears to actually help increase canopy development somewhat.

Table 3.6 Significance levels of ANOVA separated by rootstock.

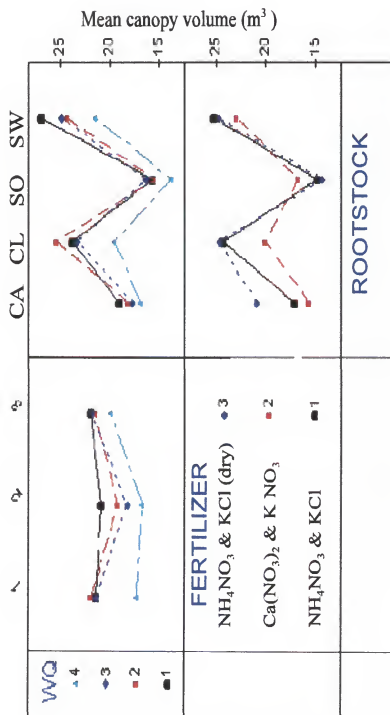| Test	Carrizo	cleopatra	sour orange	Swingle
Vol x WQ	0.472	0.015	0.641	0.002
Vol x Fert	0.000	0.008	0.313	0.181
NDVI x WQ	0.921	0.228	0.510	0.151
NDVI x Fert	0.001	0.448	0.274	0.328

Figure 3.10 Interaction plots of the effects of Water Quality (WQ), Rootstock and Fertilizer on Canopy Volume. Water quality values are 1 (500 mg/L), 2 (1600 mg/L), 3 (2700 mg/L) and 4 (3600 mg/L TDS. Rootstocks are CA ('Carrizo citrange'), CL ('cleopatra mandarin'), SO ('sour orange') and SW ('Swingle citrumelo'). The fertilizer treatments are indicated within the figure.
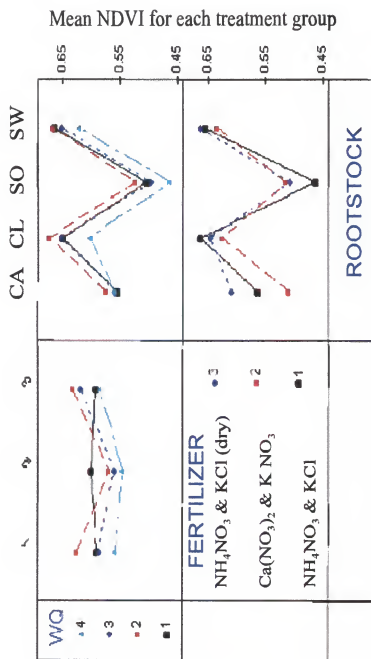
Figure 3.11 Interaction plots of the effects of Water Quality (WQ), Rootstock and Fertilizer on NDVI derived from aerial multispectral imagery. The symbols used are the same as in Figure 3.10.

The interaction plots with NDVI derived from airborne multispectral imagery as the effect (Figure 3.11) show similar types of interaction as those with canopy volume. Fertilizer 2 shows an interaction with all levels of water quality except the least saline, 'cleopatra mandarin' rootstock shows the strongest interaction with water quality, and fertilizer treatment 2 causes a reduction in NDVI in combination with all rootstocks except 'sour orange', although 'sour orange' has the worst performance overall.

3.3.2 Linear Regression Analysis

Regression analysis can provide a further indication of the usefulness of remote sensing to detect stress related effects at the scale of several hectares to several square kilometers, which is the area generally covered by a single airborne image. Tree growth has been shown to be slowed in situations where chronic salinity stress exists (Maas 1992). Reduced tree size among trees of similar age can therefore be an indicator of stress. The linear regression of tree size with NDVI shows a significant, although not a simple relationship. When tree canopy height is regressed against NDVI it has an r^2 of 0.487, indicating about half the variability in NDVI is due to the measured canopy height (Figure 3.12). Note that, as indicated above, weeds growing below weakened trees may contribute to the NDVI.

Canopy volume is normally considered to be a better indicator of yield potential of the trees than height, although the current method, where a single 0.9 meter square pixel is taken from the canopy to represent the tree, does not really capture information about the width of the canopy beyond the 0.81 m^2 the pixel covers. It stands to reason that
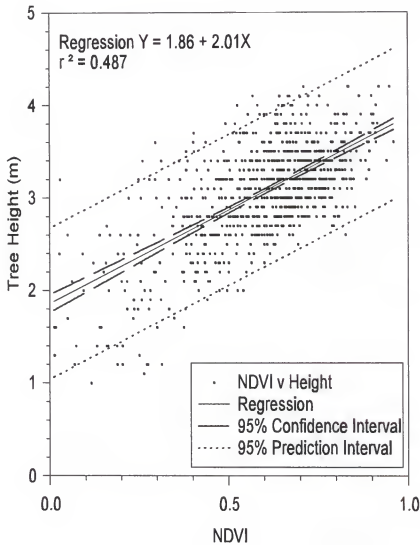
Figure 3.12 Linear regression of tree canopy height against NDVI. Missing trees and those less than 1 meter in height were removed from the data.
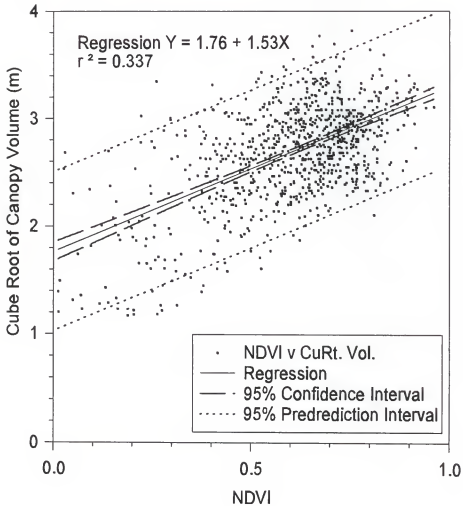
Figure 3.13 Linear regression of the cube root of tree canopy volume against NDVI. The same group of trees as in Figure 3.12 were used, excluding those less than 1 m in height, or missing.

the relationship between the cube root of canopy volume (the cube root is taken to linearize the relationship) is a weaker than the one between NDVI and tree height. This is seen in the linear regression of the cube root of canopy volume against NDVI, which has an r^2 of 0.337 (Figure 3.13).

Improved spatial resolution of the airborne image would make it possible to measure the width of the canopy as well. Sufficient spatial resolution to identify the horizontal extent of the tree canopy, combined with the estimate of tree height can provide a volume estimate for the trees.

3.3.3 Results of LAI Image Map Creation.

The LAI measurement calibration procedure was used obtain corrected LAI values for 60 small trees at the Kerr Center Vero Beach citrus grove. A radiometrically calibrated multispectral image with 500, 700 and 840 nm bands was then used to create a LAI map of the grove, shown in Figure 3.14. The LAI values range from 0 to over 13. The near zero LAI values of the lawn areas are due to the requirements of calibrating for small citrus trees. Bare soil, and buildings also have LAI of 0, whereas the taller grass, weeds and small trees have LAI of 1-3. Healthy mature citrus trees have LAI of 5-10, which is in agreement with values typical for citrus (Syvertsen and Lloyd 1994). The tall windbreak trees mostly have LAI of 6 or higher, although values of less than 5 or in excess of 13 are probably due to shading effects in the trees, and are not accurate. In general, this LAI map can be considered a good representation of true LAI, and can be a good indicator of tree condition.
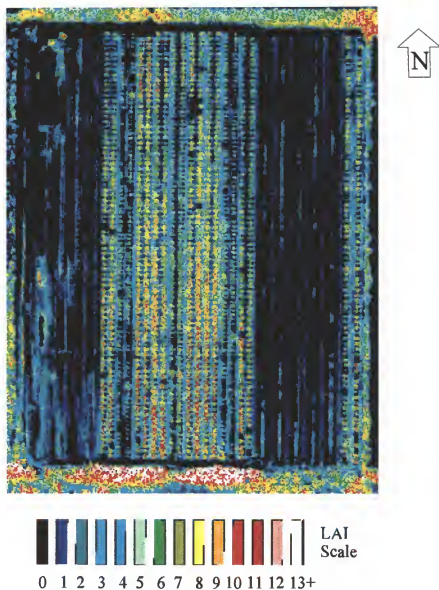
Figure 3.14 LAI image map of the Kerr Center citrus grove. Healthy, mature citrus trees have LAI of 5 to 10. LAI of greater than 13 in the windbreak trees are probably in error due to shading effects.

3.3.4 Results of Hyperspectral Image Analyses.

While the spatial resolution of the hyperspectral images acquired for this study was not ideal to provide comparisons between individual trees, observations at larger spatial scales are possible, utilizing the enhanced spectral resolution that they offer. Figure 3.15 shows a representation of the "hyperspectral cube" with a true color image of the Ft. Pierce citrus grove, and, at an angle to it, a mapping of the 64 layers of the image for the first row of pixels along the top. The center wavelengths of the bands are given in Table 3.7. the bands are approximately 8 nm in width. Vegetation reflectance in the visible range is generally between 5% and 10%, represented by dark blue and cyan colors, while reflectance in the infrared range is around 30% to 40%, represented by the yellow and red colors.

Table 3.7 Center wavelengths (λ) of the 64 bands (B) of the hyperspectral images.

| B	λ	B	λ	B	λ	B	λ	B	λ	B	λ
1	395	13	492	25	589	37	686	49	783	61	880
2	403	14	500	26	597	38	694	50	791	62	888
3	411	15	508	27	605	39	702	51	799	63	896
4	419	16	516	28	613	40	710	52	807	64	904
5	427	17	524	29	621	41	718	53	815		
6	435	18	532	30	629	42	726	54	824		
7	443	19	540	31	637	43	734	55	832		
8	451	20	548	32	645	44	743	56	840		
9	459	21	556	33	654	45	751	57	848		
10	467	22	564	34	662	46	759	58	856		
11	475	23	573	35	670	47	767	59	864		
12	484	24	581	36	678	48	775	60	872		
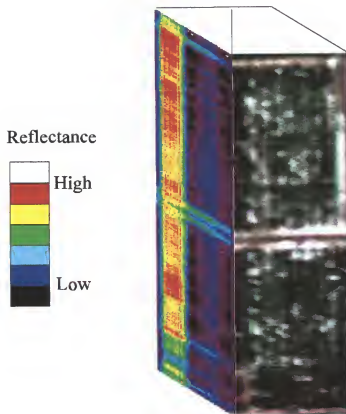
Figure 3.15 Hyperspectral cube representation of the Ft. Pierce citrus grove. The front face of the cube shows a color image in the 450, 550 and 670 nm bands. The left face shows reflectance values in all 64 bands for the leftmost column of pixels, longer wavelengths further to the left.

Four methods of analysis were performed on the hyperspectral image. These included two methods of image classification, maximum likelihood classification, and the spectral angle mapper, as well as a subpixel classifier, and a method was used to detect the red edge position, or the wavelength at which the increase in refelctance with increasing wavelength is maximum, for the vegetation throughout the citrus grove.

3.3.5 Comparison of Hyperspectral Classifiers.

The maximum likelihood classification method was applied to a subset of the image taken in the Ft. Pierce grove. The image used was captured with the airplane flying in an west-east direction, at 9:40 AM. (EDT) This hour was chosen in order to avoid the possibility of cloudy conditions in the afternoon, since several sites needed to be imaged on that day. This introduced a rather severe shadow effect, however, which can affect an image classification.

A visual comparison of these two methods (Figure 3.16) shows the maximum likelihood image has greater complexity, with finer details, and a check of accuracy in certain well defined locations indicates that it also has a more accurate ground cover classification. At the points labeled 1 in the images, a clump of vigorous non-citrus vegetation (weeds in a dry pond) is located outside of the grove. It is classified as other by the maximum likelihood method, but citrus by the spectral angle mapper method. At points labeled 2, an area of mostly sandy soil with sparse grass covering is classified as sand by the maximum likelihood method, but it is classified as grass by the spectral angle mapper method.
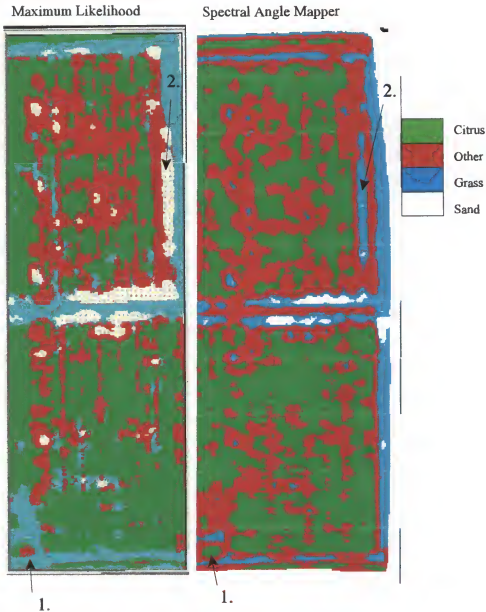
Figure 3.16 Comparison of hyperspectral image classification by maximum likelihood and spectral angle mapper methods. Areas misclassified by the spectral angle mapper include a clump of non-citrus vegetation (1) and an area with exposed soil (2).

3.3.6 <u>Results of subpixel classifier method.</u>

The subpixel classifier uses a completely different concept in classification than the previous two methods. Instead of assigning a pixel to one of several classes, it attempts to estimate the percentage of each pixel which is covered by one of several known types. The component ground cover types, or more precisely, the spectral signatures associated with these ground cover types, are known as endmembers. Endmembers may be collected by identifying areas in the image which have pixels with homogeneous ground cover , or they may be collected on the scene at the time of imaging using a spectroradiometer. When using the spectroradiometer method one must consider possible scaling effects, as the spectral signature on the ground may not correspond with what is captured during imaging, particularly for trees and other vegetation which has a complex geometry as well as a complex spectral signature.

Figure 3.17 shows the original hyperspectral image and three fraction images, showing citrus, grass and sandy soil fractions. Figure 3.18 shows close-up images of a corner of the grove. A citrus tree is identified in each image and marked as 1. It is bright in the citrus fraction, and dark in the other two images. A grassy area is marked 2 in each image, and appears much brighter in the grass fraction image than in the other two, although it may be noted that some bright "grass" pixels appear within the citrus. This is accurate, since there is grass all around the trees, and in the pathway between them.
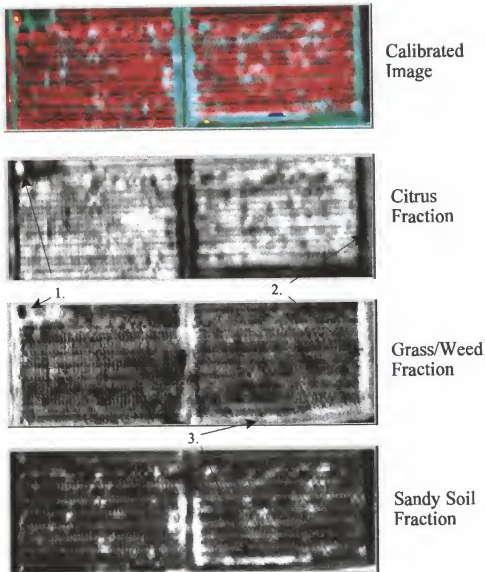
Calibrated Image

Citrus Fraction

Grass/Weed Fraction

Sandy Soil Fraction

Figure 3.17 Ground cover fraction images produced by the subpixel classifier. Note that combining grass and weeds in one class resulted in a clump of non-citrus vegetation (1) to be misclassified as citrus, while the grass covered road (2) and exposed sandy soil (3) are properly represented.
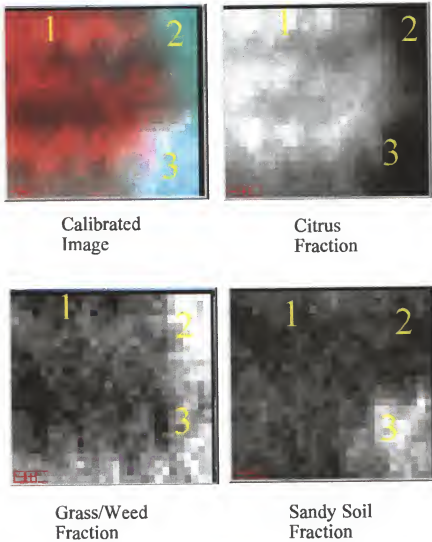
Calibrated
Image

Citrus
Fraction

Grass/Weed
Fraction

Sandy Soil
Fraction

Figure 3.18 Close-up images of subpixel classifier fraction images. A citrus tree is marked as 1, a grassy area is marked as 2, and a sandy area is marked as 3.

Citrus tree with measuring rod.

Grass and weeds in a drainage ditch.

Small plant in white sandy soil

Figure 3.19 Photographs of ground cover types, citrus, grass and weeds, and sandy soil.

Pictures taken at ground level show examples of the ground cover types that are identified as spectral endmembers (Figure 3.19). They include citrus, grass and weeds, and sandy soil. It may be noted that the classification methods used previously had four endmember classes, with a separate grouping for grass and for weeds and other non-citrus vegetation.

One of principal uses of subpixel analysis is to detect the presence of objects in locations where they would not be detectable by conventional classification, because they occupy less than half of the area covered by a pixel. The results are approximations, and there is always the risk of predicting the presence of some endmember which is not really there, especially if the endmember spectra are chosen from spectral libraries without actually visiting the study site. When the endmembers are collected locally or from within the image as was done here, the subpixel results can be a good estimator of their relative abundance .

3.3.7 Red edge position results.

The red edge position image (Figure 3.20) was created in ERDAS Imagine using the program listed in Appendix C section C-2. Red edge position is a characteristic of all normal vegetation spectra, and as is demonstrated here, it can provide a means to distinguish between different types and conditions of vegetation. (Jago et al. 1999). The colors used in the image were chosen to highlight grass (cyan), citrus (green), stressed citrus (red) and other vegetation (magenta).
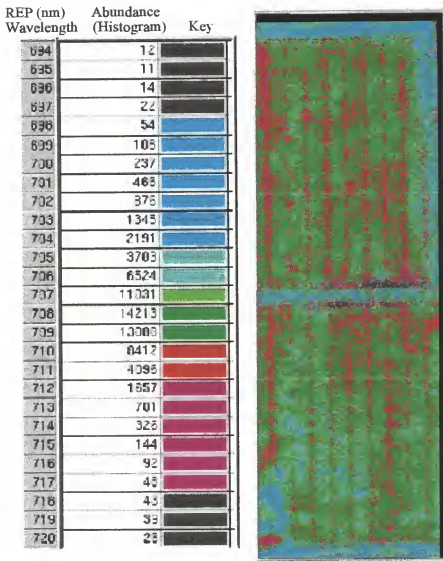
Figure 3.20 An image created from the red edge position of vegetation spectra. The key shows the colors assigned to each wavelength, and the abundance of pixels representing each wavelength in the image.

3.3.8 Results of ALSM Mapping.

The Kerr Center for Sustainable Agriculture Vero Beach research Station was oveflown with an airborne laser swath mapper in May, 2000, two weeks prior to the multispectral and hyperspectral imaging flight.

Point data in a citrus grove in Vero Beach, Florida were collected using the UF/FIU Airborne Laser Swath Mapping (ALSM) system in May, 2000. These data indicate a special property of ALSM. Typically, data points collected in one pass are approximately 1 meter apart, allowing the creation of a digital terrain model (DTM) with 1 meter grid cell size with no interpolation. Subsequent passes over the same area served to densify the point spacing, allowing the formation of accurate DTMs of finer spatial scale. The data collected in the citrus grove were from five sequential passes, creating an average point density of five per square meter. Interpolation by "tinning" or krigging can generate even finer scaled DTMs. In this case, the krigging method was used to create a DTM with 0.1 meter (10 cm) cell spacing, which provided sufficient spatial resolution to visualize the tree canopies in great detail. Figure 3.21 shows a view of the grove facing north with a multispectral image overlaying the DTM (no vertical exaggeration). Figure 3.22 shows a section of the southwest corner of the grove, the upper image (A) is the DTM, brighter shades indicating greater height, with a white box indicating the extent of the 3 dimensional surface (B). Figure 3.23 shows a closer view the same area, the spatial extent of the surface (B) is indicated by the white box above (A).
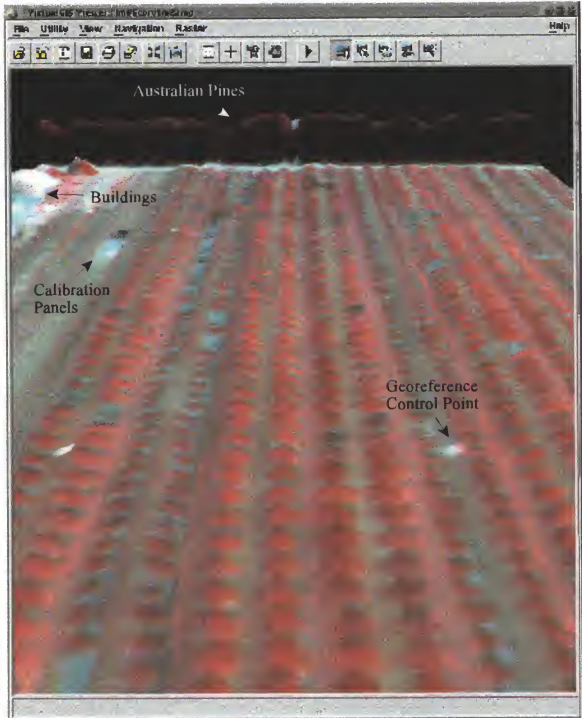
Figure 3.21 Digital terrain model draped with a multispectral image at Kerr Center grove. No vertical exaggeration is applied to the elevation data, to provide a realistic perspective. Australian pine windbreak row, buildings, radiometric calibration panels and a georeference target are indicated with arrows.
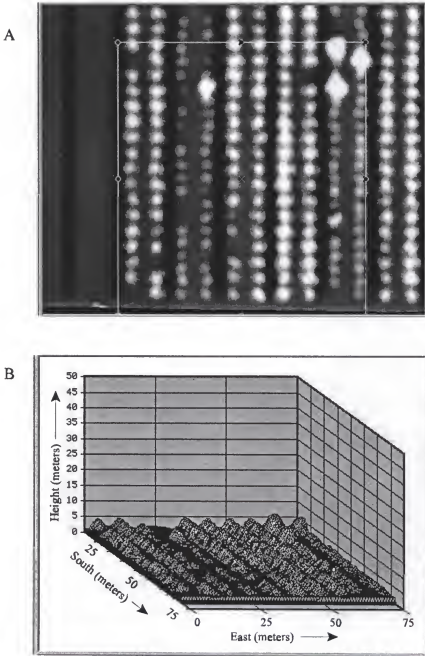
Figure 3.22 3 dimensional surface in southwest corner of the grove, the upper image (A) is the DTM, brighter shades indicating greater height, with a white box indicating the spatial extent of the surface (B).

The data conversion steps were performed using Arc/Info. First, the data, provided in as a flat ASCII text file listing x, y, z values in UTM coordinates, zone 17, WGS84 datum, GRS 1980 spheroid, were converted to an Arc/Info point coverage containing height values referenced to local ellipsoid heights. The point values of the coverage were then used to create a raster lattice at 0.1m cell spacing using the krigging method. Finally, the lattice was converted to a USGS format DEM for transportability to other programs.

The DEM was imported to ERDAS Imagine for further study. The original ellipsoid height values in the DEM were negative, since the area, located near the coast and just a few meters above sea level, is below the WGS84 ellipsoid level. In order to make the relative heights positive, an offset of 23 meters was added to them using ERDAS Imagine raster image processing. Three dimensional renderings of some of the citrus trees are shown in figures 2 and 4, while the corresponding areas in the citrus grove are shown in figures 1 and 3, respectively.

The figures show highly detailed images entirely created from elevation data. These images provide precise spatial and height information of the size and structure of the tree canopies. Using such data, it is possible to assess height of each tree and its diameter, and to generate information about the canopy volume. This information can be used to assess the relative growth vigor of the trees, and locate areas within the grove where tree growth is more or less successful, providing a unique contribution to the study of citriculture, and other types of tree crops.
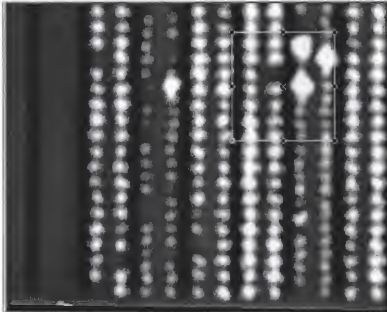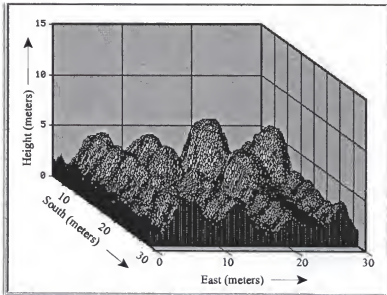
Figure 3.23 A closer 3 dimensional view of the same area. The white box in A indicates the spatial extent of the 3 dimensional surface (B). The three large trees in the upper right corner are neem (*Melia azadirachta*) trees planted to test their insect-repelling properties..

3.3.9 <u>Results of Multi-year Landsat Citrus Study.</u>

Despite the coarse spatial scale of Landsat images relative to the size of citrus trees, a multi-year comparison of images in a young citrus grove clearly shows the growth of the trees over time. Three winter Landsat images were obtained from 1993, 1996 and 2000. Since the grove was planted in 1990, these images represent three periods in the grove's development that are nearly equally spaced in time. The year 2000 image was calibrated for reflectance, and the other two were normalized to it. NDVI values were calculated from bands 3 and 4 of each image.

In the 1993 image, the NDVI values had a mean of 0.173 and ranged from 0.137 to 0.227. In the 1996 image, they had a mean of 0.276 and ranged from 0.192 to 0.341. In the 2000 image, they had a mean of 0.319 and ranged from 0.247 to 0.380. Figure 3.24 clearly shows the increase of NDVI in the citrus grove over the period covered by the Landsat images. Each 30m x 30m pixel covers 24-28 trees in the grove, so it represents the average reflectance or NDVI values of all those trees and whatever is between them, including some areas of bare soil, ditches and roads, as well as trees and weeds of various types. Furthermore, it is not possible to be certain that the corresponding pixels from one image to another cover exactly the same group of trees. Even with careful rectification and georeferencing, it is common for the location of a pixel to be off by up to ½ its width, in this case, 15 meters. Nevertheless, on the spatial scale of the whole grove and the time scale of 10 years, the groves's growth can be monitored using this method.
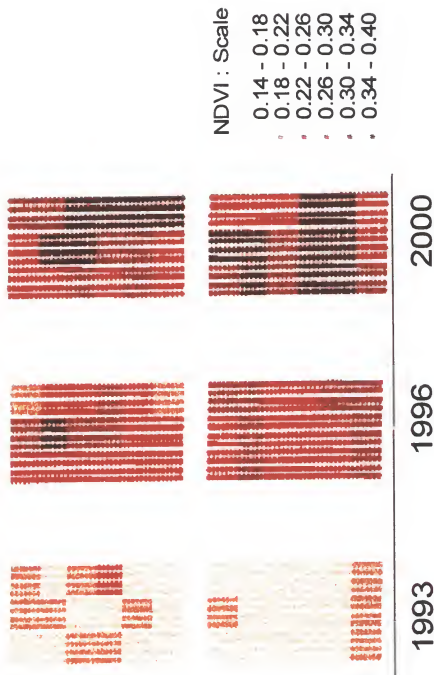
NDVI : Scale

0.14 - 0.18
0.18 - 0.22
0.22 - 0.26
0.26 - 0.30
0.30 - 0.34
0.34 - 0.40

2000

1996

1993

Figure 3.24 The development of the citrus grove at Ft. Pierce over the period from1993 to 2000 as detected by Landsat imagery. Trees were grouped according to the approximate ground coverage of a Landsat pixel, and were assigned the NDVI value calculated from bands 3 and 4 of that pixel.

3.4 Cypress Wetland Analysis Results

After performing a supervised classification of each image, several features become apparent. In both the 1992 (Figure 3.24) and 1994 (Figure 3.26) images, a substantial group of wetlands appear severely stressed in the northern portion of the study area, as well as a number of smaller wetlands scattered throughout the center of the region. A broad section of wetlands in the east of the region appear moderately stressed.

The total area of wetlands classified as "severely stressed" increased from 1843 hectares to 2163 hectares from 1992 image to the 1994 image. This may be explained by the fact that the months leading up to the 1994 imaging date saw less rainfall in the area than during the months prior to the 1992 imaging date. This might also be interpreted as a sign that some of the wetland areas are experiencing degradation due to prolonged hydraulic stress or other factors. Geologic studies of the region have indicated that the confining layer which isolates the surficial aquifer from the Floridan aquifer is thinner in the northern part of the region than in the south, making it more difficult for wetlands and lakes to remain hydrated when hydrostatic pressure is reduced in the lower aquifer during dry periods with heavy public water usage. The general agreement between the two image classifications as to the location of the most severely stressed wetlands is also apparent. The locations of the most severely stressed wetlands in this study are in strong agreement with those provided by field-based studies by the Southwest Florida Water Management District and others (Rochow 1998).
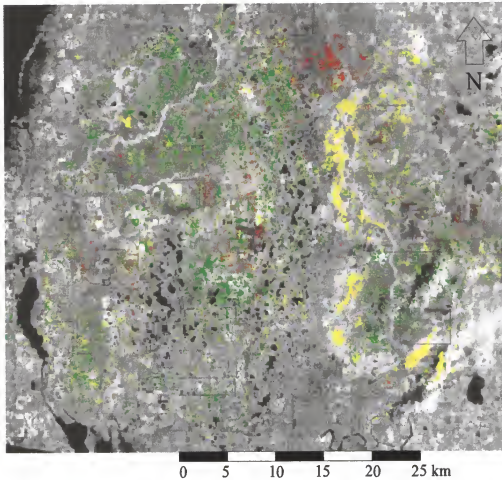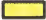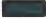
	Class Names	Hectares	Percent
	Good	6306	43.6
	Moderately Stressed	5957	41.2
	Severely Stressed	1843	12.7
	Cloud	197	1.4
	Shadow	162	1.1

Figure 3.25 Results from classification of the March 24, 1992 Landsat image. Areas in hectares were calculated at 11.1 pixels/ha. Percent values are the percentage of all cypress pixels in the image.
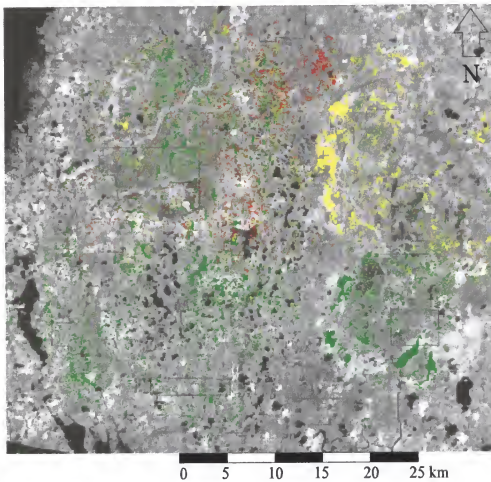
Class Names	Hectares	Percent
Good	7971	55.0
Moderately Stressed	4044	27.9
Severely Stressed	2163	14.9
Cloud	300	2.1
Shadow	15	0.0

Figure 3.26 Results from classification of the March 14, 1994 Landsat image. Total area and percent area were calculated as in Figure 3.25.

There appears to be disagreement between the classification results in the southeastern portion of the images. The 1992 image shows the band of "moderately stressed" wetlands extending along the entire eastern portion of the image, whereas the 1994 image shows most of the wetlands in the southeastern quadrant as being in "good" condition. The apparent "improvement" of wetland condition in the southeastern region would seem to run counter to the notable increase in severely stressed wetlands elsewhere. Another explanation for this discrepancy is that the classification method is not adequate to distinguish reliably between wetlands classified as "good" and those classified as "moderately stressed". Figure 3.27 illustrates this with the spectral signatures derived from the reference wetlands. It may be seen that there is little difference between the spectral signatures of the wetlands identified as "good" and "moderately stressed" during field visits. There is, however, a much larger difference between the spectral signatures of these two groupings and those which were grouped as "severely stressed".

It was also noted above that one of the sources of error in defining the boundaries of cypress wetlands, or indeed any other land cover classification, is the level of purity of the land cover classification. As much as 10% of the total area designated as "cypress wetlands" in the region may in fact be mixed stands of wetland forest, predominantly cypress, but including some percentage of other tree species. The presence of mixed stands can additionally explain the difficulty of distinguishing "good" from "moderately stressed" wetlands in the eastern portion of the study area.
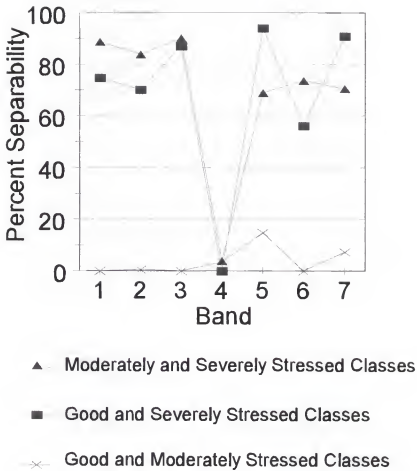
Figure 3.27 Percent separability of pairs of classes calculated using the Transformed Divergence method. The "Severly Stressed" class is separable from either "Good" or "moderately Stressed" class in all Landsat TM bands except band 4. The "Good" and "Moderately Stressed" classes are not separable.

3.4.1 <u>Accuracy Assessment</u>

  The degree to which the polygons of the assessed cypress wetlands correctly overlaid the corresponding wetland areas in the Landsat image is an issue that affects the accuracy of the stress detection. An accuracy assessment was conducted on the match between the polygon coverage and both the 1992 and 1994 Landsat images. Two thousand random points were selected from within the cypress areas of the polygon coverage. These points were overlaid on the Landsat image displayed in bands 2, 3 and 4 in the ERDAS Imagine viewer, together with the cypress polygon coverage. The image was zoomed in, displaying 1/16 of the image per screen, in addition to a "magnifier window" which allowed closer inspection of certain areas of the image, revealing individual pixels. The match between the polygons and the cypress areas of the image was assessed by counting the number of these pre-selected random points which corresponded to one of Five categories of errors as follows:

  (1) Evidence of land use change since the creation of the polygon coverage. Only conversions of natural areas to urban or residential land use were considered, since conversion of cypress to other natural land cover by ecological succession may be the result of stress. About 0.8% of the cypress in the 1992 image, and 1.0% in the 1994 image appears to have been affected in this way.

  (2) Error in delineating the polygon boundary made during the creation of the polygon coverage, or in registration between the polygon coverage and the image. Both of these error types have the same effect of causing non-cypress areas to be included in the

analysis. The accuracy assessment revealed that 2.5% of the cypress area in 1992 and 2.2% in 1994 were incorrectly included in the analysis.

(3) In some cases, a cypress area completely encircles a non-cypress area, such as a lake, or a hardwood hammock. These encircled areas were sometimes incorrectly included in the analysis, representing 0.9% of the area in 1992, and 0.8% in 1994.

(4) A substantial percentage of the area identified as cypress in the eastern third of the image may in fact be composed of a mix of cypress and evergreen tree species. This appears to have affected the analysis of approximately 10% of the cypress in both 1992 and 1994.

(5) Areas affected by cloud or shadow corresponded to 2.3% of the cypress in 1992 and 1.6% in 1994. This should not have any impact on the results of the study, however, since the cloud and shadow areas were separately classified and eliminated from the study. These results are summarized in Table 3.8.

Table 3.8 Types of differences between Landsat images and Land Use coverage.

Type of Error	1992 pixels	1992%	1994 pixels	1994%
Land Use Change	16	0.8	19	4.0
Boundary error	50	2.5	44	2.2
Internal Polygon	18	0.9	16	0.8
Subtotal	84	4.2	79	4.0
Not Pure Cypress	200	10	200	10
Total Error	284	14.2	279	13.95

3.4.2 National Wetlands Inventory Database Comparison

The second portion of this study determined whether similar classification results could be obtained when different GIS databases are used to define the wetland boundaries. To test this, the March 14, 1994 Landsat image was analyzed using the National Wetlands Inventory GIS database from the United States Fish and Wildlife Service in addition to that from the Southwest Florida Water Management District. The two GIS databases were constructed in similar manner; starting from aerial photographs, the wetlands and other land cover types were manually delineated by photointerpretation experts, transferred to 1:24,000 scale maps, then manually digitized. The final digital maps may differ from one another as result of different dates that the aerial photography was flown, different classification schemes, different decisions made by the photointerpretation experts, or errors in digitizing and data processing.

A two level supervised classification was used for this portion of the study, separating the cypress wetland areas into those which are severely stressed, and those which are in good condition, or moderately stressed. The classified images (Figures 3.28A and 3.28B) indicate some differences, but substantial agreement between the results of the two methods. It may be noted that a concentration of severely stressed wetlands appears in the northern portion of the study area in both images. Also, there are severely stressed wetlands interspersed between those in better condition in the central portion of the study area. This is in agreement with the results from the three-level classification noted above. It is also apparent, however, that there is less total area of cypress wetlands reported in the
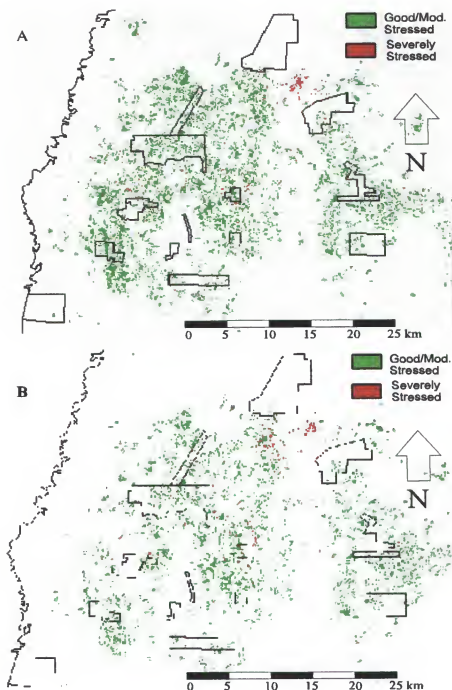
Figure 3.28 Comparison of the 1994 Landsat image classified with wetland boundaries defined by different GIS databases. The Southwest Florida Water Management District GIS data (A) and the same image created with wetland boundaries delineated by the National Wetlands Inventory database (B).

National Wetlands Inventory database (Figure 3.28B) than that from the Southwest Florida Water Management District. This is likely due to the application of different standards of delineation during the photointerpretation process, with the result that some of the areas delineated as cypress in the Southwest Florida Water Management District database are instead considered to be mixed forested wetlands by the National Wetlands Inventory database. This includes some of the wetlands in the eastern portion of the study area that were perhaps erroneously classified as "moderately stressed" in the three-level classification.

CHAPTER 4
CONCLUSIONS AND RECOMMENDATIONS

4.1 <u>Conclusions</u>

In this study, various techniques for detecting vegetation stress were explored, which operate on vastly different scales, from that of a leaf to an area of thousands of square kilometers. It was shown that carefully controlled observation of individual leaves using a spectroradiometer results in very sensitive measures of spectral reflectance, which can reveal early and subtle indications of plant stress. There is no indication from this research that the different factors of stress can be easily distinguished from one another. For example, from the citrus salinity study, it was shown that rootstock type, and fertilizer type can interact with water quality, to produce stress. The stress may be detected from the spectral reflectance study of leaves, but it was not shown in this study that stress caused by different agents can be distinguished spectrally from one another. Other stress factors, such as disease, subsoil, or drought conditions, were not included in the scope of this study.

At the scale of tree canopies, precise measurement of spectral reflectance is more difficult. This is due to the variability of leaf angle, sun angle, canopy density, leaf movement, etc. As a result of this greater variability, indications of early stress are more difficult to detect than with single leaf studies, however, more advanced stress conditions may be detected.

147

Citrus grove-scale multispectral aerial imagery used in combination with ground-based measurements was shown to be effective in detecting stress effects. A narrow-band NDVI derived from the 840 nm (infrared) and 700 nm (red) bands provided the best correlation with tree size, which, for trees of equal age, is known to be a long-term effect of stress. The integration of GIS and spectral reflectance data from airborne imagery was found to be effective in gathering, analyzing and presenting the remotely sensed data in conjunction with ancillary information about the individual citrus trees.

At the regional scale, this study has shown the potential of combining vector GIS data with remotely sensed imagery to improve the ability to interpret the imagery for wetland quality assessment. The limitations of the assessment methodologies are also apparent. Factors that may diminish the accuracy of any wetland quality assessment include limitations of the spatial and spectral resolution and cloud-free quality of the remotely sensed imagery, as well as the spatial resolution, positional accuracy, and the accuracy of land cover type classification of the vector land cover data. It was further shown that despite such limitations, the methods used were robust enough to determine the location of severely stressed cypress wetlands in a large regional study.

4.2 Recommendations

The primary goal of this research was not to develop citrus management practices, but to better understand the remote sensing methods which may be applicable to stress detection, and the spatial and temporal scales on which they operate. Some of the conclusions reached in this study, however, point to possible recommendations for citrus

management practices to avoid severe effects from high salinity in irrigation water. The comparisons of rootstock varieties, for example, suggest that the 'Swingle citrumelo' and 'cleopatra mandarin' rootstocks are better at supporting tree canopy development than the 'sour orange' and 'Carrizo citrange' rootstocks. These results are certainly not definitive, however, as there are many other factors not addressed, such as resistance to specific diseases, which are also important when choosing a rootstock on which to plant grapefruit.

This research has indicated many avenues for further study. The use of high resolution terrain mapping, such as the ALSM system used at the Kerr Center citrus grove shows promise. A future study to develop algorithms for automatic tree location identification, tree height and canopy volume would be useful, and also the correlation of these data with stress factors. Further study of red edge detection applications is also needed. It is likely that red edge position is dependant on plant species, in addition to plant condition, so that further research is needed to identify the appropriate scaling of the red edge detection algorithm to best discriminate changes in red edge position of a particular species as a result of stress.

Leaf area index mapping is also of interest and bears further study to provide the appropriate scaling factors for different types of plants and canopy structures. Leaf area index is commonly used as a parameter for simulation modeling of plant growth , evapotranspiration, and crop yield. Spatially explicit LAI values can be used to parameterize or validate more complex and realistic spatial dynamic models, to be used in precision agriculture or natural resource management applications.

APPENDIX A
GLOSSARY

ALSM – Airborne Laser Swath Mapper. Also referred to as Lidar, it is an airborne system for high resolution and high accuracy mapping of elevations of a ground surface, by measuring the travel time of laser light pulses reflected off the surface and back to the aircraft.

BDRF – Bidirectional Reflectance Distribution Function. Energy reflected from a surface may not be evenly disbursed in a hemispherical patter, as is assumed by the Lambertian model. Instead, the reflected energy depends on the angle of the light source and the angle of the detector in relation to the surface, and to each other.

Exposure Falloff – An effect which causes a photographic or digital image to be brightest at the center point and attenuated at radial distances from the center, due to the effectively smaller aperture size for light rays entering the lens at an angle, as well as the longer distance the ray travels within the camera to reach the edge of the focal plane, and the dilution of light intensity of a ray which strikes the focal plane at an angle.

FWHM – Full Width Half Maximum. For bandpass filters, it is the full width of the pass band measured at one-half the peak transmittance, expressed in nanometers, or microns.

Hydroperiod – The length of time during which a wetland is flooded in a typical year.

LAI – Leaf Area Index. The total quantity of leaf surface area which covers a unit area on the ground (unitless).

NTSC – National Television Standards Committee. Also, the standard for television picture transmission used in North America, and certain other regions.

Pixel – Picture element.

Reflectance – The fraction of radiant energy that is reflected from a surface.

Solar Azimuth – The point on the horizon where a vertical circle passing through the sun meets it, reckoned from the south point of the horizon around by the west from 0° to 360°.

Solar Elevation – The distance in degrees of the sun above the horizon, or the arc of a vertical circle intercepted between it and the horizon.

Specular Reflectance – Results from the reflection of parallel light rays off of a smooth surface, such as a mirror.

TDS – Total Dissolved Solids, the sum of the concentrations of all substances dissolved in water.

TIFF – Tagged Image File Format. A file structure for the transfer of digital images which may be compressed, but does not degrade image quality when compressed.

Vignetting – An effect that causes the edges of a photographic image to appear less bright than the center of the image, due to shadowing by internal aperture surfaces within the camera.

Energy source from outside the system.

Heat sink. The energy which is degraded in a process disburses to the environment.

Storage of energy or matter.

Consumer unit. Uses high quality energy and is self-maintaining.

General-purpose box for any subunit needed.

Producer unit. Converts and concentrates solar energy; it is self-maintaining.

Interaction. Two kinds of energy are required to produce a higher-quality energy flow.

Switching unit. Turns flows on or off according to control actions specified for the unit.

Energy-money transaction.

APPENDIX C
ERDAS IMAGE PROCESSING PROGRAMS

C.1 Hyperspectral Image Calibration Program


```
# set cell size for the model
#
SET CELLSIZE MIN;
#
# set window for the model
#
SET WINDOW UNION;
#
# set area of interest for the model
#
SET AOI NONE;
#
# declarations
#
Integer RASTER n1_fpwe_sub FILE OLD NEAREST NEIGHBOR AOI NONE
"/export/home/jcraig/fpwe_sub.img";
Float RASTER n67_fpwe_cal_new FILE DELETE_IF_EXISTING USEALL
ATHEMATIC FLOAT SINGLE "/export/home/jcraig/fpwe_cal_new.img";
{
#
# function definitions
#
#define n65_memory Float((($n1_fpwe_sub(64) - 371.91) / 10.16))
#define n64_memory Float((($n1_fpwe_sub(63) - 391.4) / 10.44))
#define n63_memory Float((($n1_fpwe_sub(62) - 415.82) / 10.93))
#define n62_memory Float((($n1_fpwe_sub(61) - 425.5) / 11))
#define n61_memory Float((($n1_fpwe_sub(60) - 412.57) / 10.43))
#define n60_memory Float((($n1_fpwe_sub(59) - 379.51) / 7.86))
#define n59_memory Float((($n1_fpwe_sub(58) - 323.31) / 6.41))
#define n58_memory Float((($n1_fpwe_sub(57) - 317.16) / 5.45))
```

```
#define n57_memory Float((($n1_fpwe_sub(56) - 301.96) / 6.78))
#define n56_memory Float((($n1_fpwe_sub(55) - 342.78) / 6.68))
#define n55_memory Float((($n1_fpwe_sub(54) - 323.78) / 7.25))
#define n54_memory Float((($n1_fpwe_sub(53) - 326.22) / 7.27))
#define n53_memory Float((($n1_fpwe_sub(52) - 309) / 7.58))
#define n52_memory Float((($n1_fpwe_sub(51) - 392.8) / 9.77))
#define n51_memory Float((($n1_fpwe_sub(50) - 476.88) / 12.9))
#define n50_memory Float((($n1_fpwe_sub(49) - 509.22) / 14.18))
#define n49_memory Float((($n1_fpwe_sub(48) - 544.96) / 16.79))
#define n48_memory Float((($n1_fpwe_sub(47) - 628.3) / 19.54))
#define n47_memory Float((($n1_fpwe_sub(46) - 633.59) / 19.14))
#define n46_memory Float((($n1_fpwe_sub(45) - 462.86) / 12.33))
#define n45_memory Float((($n1_fpwe_sub(44) - 751.56) / 13.58))
#define n44_memory Float((($n1_fpwe_sub(43) - 782) / 27.1))
#define n43_memory Float((($n1_fpwe_sub(42) - 785.22) / 25.86))
#define n42_memory Float((($n1_fpwe_sub(41) - 623.02) / 22.03))
#define n41_memory Float((($n1_fpwe_sub(40) - 613.97) / 21.47))
#define n40_memory Float((($n1_fpwe_sub(39) - 798.66) / 30.78))
#define n39_memory Float((($n1_fpwe_sub(38) - 775.58) / 31.98))
#define n38_memory Float((($n1_fpwe_sub(37) - 731.2) / 32.02))
#define n37_memory Float((($n1_fpwe_sub(36) - 720.43) / 34.43))
#define n36_memory Float((($n1_fpwe_sub(35) - 808.44) / 41.97))
#define n35_memory Float((($n1_fpwe_sub(34) - 834.01) / 44.8))
#define n34_memory Float((($n1_fpwe_sub(33) - 872.69) / 46.9))
#define n33_memory Float((($n1_fpwe_sub(32) - 842.59) / 46.46))
#define n32_memory Float((($n1_fpwe_sub(31) - 906.28) / 51.97))
#define n31_memory Float((($n1_fpwe_sub(30) - 982.86) / 57.26))
#define n30_memory Float((($n1_fpwe_sub(29) - 1019.85) / 59.13))
#define n29_memory Float((($n1_fpwe_sub(28) - 1077.95) / 63.1))
#define n28_memory Float((($n1_fpwe_sub(27) - 1139.19) / 66.92))
#define n27_memory Float((($n1_fpwe_sub(26) - 1196.6) / 71.2))
#define n26_memory Float((($n1_fpwe_sub(25) - 1185.48) / 70.2))
#define n25_memory Float((($n1_fpwe_sub(24) - 1144.45) / 67.67))
#define n24_memory Float((($n1_fpwe_sub(23) - 1245.95) / 61.38))
#define n23_memory Float((($n1_fpwe_sub(22) - 1245.35) / 75.02))
#define n22_memory Float((($n1_fpwe_sub(21) - 1293.35) / 73.95))
#define n21_memory Float((($n1_fpwe_sub(20) - 1333.85) / 74.35))
#define n20_memory Float((($n1_fpwe_sub(19) - 1390.39) / 73.95))
#define n19_memory Float((($n1_fpwe_sub(18) - 1381.75) / 73.03))
#define n18_memory Float((($n1_fpwe_sub(17) - 1397.41) / 73.55))
#define n17_memory Float((($n1_fpwe_sub(16) - 1360.21) / 73.3))
#define n16_memory Float((($n1_fpwe_sub(15) - 1277.22) / 67.07))
#define n15_memory Float((($n1_fpwe_sub(14) - 1232.116) / 66.89))
```

```
#define n14_memory Float((($n1_fpwe_sub(13) - 1145.83) / 59.5))
#define n13_memory Float((($n1_fpwe_sub(12) - 1087.48) / 53.82))
#define n12_memory Float((($n1_fpwe_sub(11) - 986.78) / 45.62))
#define n11_memory Float((($n1_fpwe_sub(10) - 961.87) / 43.47))
#define n10_memory Float((($n1_fpwe_sub(9) - 930.87) / 38.7))
#define n9_memory Float((($n1_fpwe_sub(8) - 905.67) / 36.47))
#define n8_memory Float((($n1_fpwe_sub(7) - 876.92) / 31.3))
#define n7_memory Float((($n1_fpwe_sub(6)  - 632.68) / 19.23))
#define n6_memory Float((($n1_fpwe_sub(5) - 285.24) / 6.29))
#define n5_memory Float((($n1_fpwe_sub(4) - 155.41) / 5.0))
#define n4_memory Float((($n1_fpwe_sub(3) - 116.4) / 5.0))
#define n3_memory Float((($n1_fpwe_sub(2) - 110.8) / 5.0))
#define n2_memory Float((($n1_fpwe_sub(1) - 106.52) / 5.0))
```

C.2 Hyperspectral Red Edge Detection Program

```
PAGESIZE 6, 9.06667 INCHES;
CELLSIZE MINIMUM;
PRINTERPAGESIZE 8.5, 11;
MARGINS 0.5, 0.5, 0.5, 0.5;
ORIENTATION PORTRAIT;
PRINTSCALE 100;
WINDOW UNION;
PROJECTION DEFAULT;
AOI NONE;
OPTIMIZE NO;
RASTER {
       ID 1;
       TITLE "n1_fpwe_cal_new_sub";
       POSITION 2.41111, 0.822222;
       FILENAME "/export/home/jcraig/fpwe_cal_new_sub.img";
       INTERPOLATION NEAREST;
       ATHEMATIC;
       DATATYPE FLOAT;
       DECLARE "Float";
       COMPRESSION UNCOMPRESSED;
       COORDINATES MAP;
       AOI NONE;
       RECODE NO;
       CHILD 3, 7;
}
```

```
RASTER {
      ID 2;
      TITLE "n2_fpwe_new_sub_rep";
      POSITION 1.56667, 4.3;
      FILENAME "/export/home/jcraig/fpwe_new_sub_rep.img";
      DELETEFILE;
      IGNORE 0;
      INTERPOLATION NEAREST;
      ATHEMATIC;
      DATATYPE UNSIGNED16;
      DECLARE "Integer";
      COMPRESSION UNCOMPRESSED;
      COORDINATES MAP;
      RECODE NO;
      CHILD 4;
}
FUNCTION {
      ID 3;
      TITLE "$n1_fpwe_cal_new_sub";
      POSITION 1.9, 2.45556;
      VALUE "((($n1_fpwe_cal_new_sub(35) + $n1_fpwe_cal_new_sub(44)) / 2 -
$n1_fpwe_cal_new_sub(37)) / (($n1_fpwe_cal_new_sub(41) -
$n1_fpwe_cal_new_sub(37)) / 33)) + 686";
      AREA UNION;
      CHILD 2;
}
FUNCTION {
      ID 4;
      TITLE "$n2_fpwe_new_sub_rep - 675) * 5";
      POSITION 1.43333, 6.11111;
      VALUE "($n2_fpwe_new_sub_rep - 675) * 5";
      AREA UNION;
      CHILD 5;
}
RASTER {
      ID 5;
      TITLE "n5_fpwe_rep_8bit";
      POSITION 1.23333, 7.56667;
      FILENAME "/export/home/jcraig/fpwe_rep_8bit.img";
      DELETEFILE;
      IGNORE 0;
      INTERPOLATION NEAREST;
      ATHEMATIC;
```

```
      DATATYPE UNSIGNED8;
      DECLARE "Integer";
      COMPRESSION UNCOMPRESSED;
      COORDINATES MAP;
      RECODE NO;
}
RASTER {
      ID 6;
      TITLE "n6_fpwe_rep_16them";
      POSITION 3.87778, 4.13333;
      FILENAME "/export/home/jcraig/fpwe_rep_16them.img";
      NEWFILE;
      IGNORE 0;
      INTERPOLATION NEAREST;
      THEMATIC;
      DATATYPE UNSIGNED16;
      DECLARE "Integer";
      COMPRESSION UNCOMPRESSED;
      COORDINATES MAP;
      RECODE NO;
}
FUNCTION {
      ID 7;
      TITLE "$n1_fpwe_cal_new_sub";
      POSITION 3.57778, 2.52222;
      VALUE "(((($n1_fpwe_cal_new_sub(35) + $n1_fpwe_cal_new_sub(44)) / 2 -
$n1_fpwe_cal_new_sub(37)) / (($n1_fpwe_cal_new_sub(41) -
$n1_fpwe_cal_new_sub(37)) / 33)) + 686";
      AREA UNION;
      CHILD 6;
}
```

C.3 Landsat 7 Calibration Program

```
# LANDSAT-7 INPUT RASTER IMAGE
# SOLAR ZENITH ANGLE (rad)
# LAYERS STACK
# CONVERSION TO RADIANCE
# RADIANCE TO REFLECTANCE
# EARTH-SUN DISTANCE
# CALIBRATED OUTPUT RASTER IMAGE
```

```
#
# set cell size for the model
#
SET CELLSIZE MIN;
#
# set window for the model
#
SET WINDOW UNION;
#
# set area of interest for the model
#
SET AOI NONE;
#
# declarations
#
Integer RASTER n1_tm700_utm FILE OLD NEAREST NEIGHBOR AOI NONE
"/export/home/jcraig/citmap/tm700_utm.img";
Integer RASTER n29_tm700_utm_refl FILE NEW IGNORE 0 ATHEMATIC 8 BIT
UNSIGNED INTEGER "/export/home/jcraig/citmap/tm700_utm_refl.img";
FLOAT SCALAR n27_Float;
FLOAT SCALAR n47_Float;
#
# load scalar n27_Float
#
n27_Float = 0.893609;
#
# load scalar n47_Float
#
n47_Float = 0.9864;
#
# function definitions
#
#define n8_memory Float((10.8+0.35)*$n1_tm700_utm(6)/255-0.35)
#define n21_memory
Float((3.14159265*$n8_memory*($n47_Float^2))/(80.530*COS($n27_Float))*255)
#define n7_memory Float((31.06+1.0)*$n1_tm700_utm(5)/255-1.0)
#define n22_memory
Float((3.14159265*$n7_memory*($n47_Float^2))/(227.100*COS($n27_Float))*255)
#define n6_memory Float((241.1+5.1)*$n1_tm700_utm(4)/255-5.1)
#define n23_memory
Float((3.14159265*$n6_memory*($n47_Float^2))/(1047.000*COS($n27_Float))*255)
#define n5_memory Float((152.9+5.0)*$n1_tm700_utm(3)/255-5.0)
```

```
#define n24_memory
Float((3.14159265*$n5_memory*($n47_Float^2))/(1555.000*COS($n27_Float))*255)
#define n4_memory Float((196.5+6.4)*$n1_tm700_utm(2)/255-6.4\
)
#define n25_memory
Float((3.14159265*$n4_memory*($n47_Float^2))/(1843.000*COS($n27_Float))*255)
#define n3_memory Float((191.6+6.2)*$n1_tm700_utm(1)/255-6.2)
#define n26_memory
Float((3.14159265*$n3_memory*($n47_Float^2))/(1970.000*COS($n27_Float))*255)
n29_tm700_utm_refl = STACKLAYERS
($n26_memory,$n25_memory,$n24_memory,$n23_memory,$n22_memory,$n21_memor
y);
QUIT;
```

C.4 Hyperspectral Wavelength Calibration File

```
tm {
        SensorName "NASA Stennis Hyperspectral";
        BandUnits "nanometers";
        BandMeasurement "Wavelength";
        BandCount 64;

        Band 1 { Value 395; Width 8.095; }
        Band 2 { Value 403.095; Width 8.095; }
        Band 3 { Value 411.95; Width 8.095; }
        Band 4 { Value 419.285; Width 8.095; }
        Band 5 { Value 427.38; Width 8.095; }
        Band 6 { Value 435.475; width 8.095; }
        Band 7 { Value 443.57; width 8.095; }
        Band 8 { Value 451.665; Width 8.095; }
        Band 9 { Value 459.76; Width 8.095; }
        Band 10 { Value 467.855; Width 8.095; }
        Band 11 { Value 475.95; Width 8.095; }
        Band 12 { Value 484.045; width 8.095; }
        Band 13 { Value 492.14; width 8.095; }
        Band 14 { Value 500.235; Width 8.095; }
        Band 15 { Value 508.33; Width 8.095; }
        Band 16 { Value 516.425; Width 8.095; }
        Band 17 { Value 524.52; Width 8.095; }
        Band 18 { Value 532.615; width 8.095; }
        Band 19 { Value 540.71; width 8.095; }
```

Band 20 { Value 548.05; Width 8.095; }
Band 21 { Value 556.9; Width 8.095; }
Band 22 { Value 564.995; Width 8.095; }
Band 23 { Value 573.09; Width 8.095; }
Band 24 { Value 581.185; width 8.095; }
Band 25 { Value 589.28; width 8.095; }
Band 26 { Value 597.375; Width 8.095; }
Band 27 { Value 605.47; Width 8.095; }
Band 28 { Value 613.565; Width 8.095; }
Band 29 { Value 621.66; Width 8.095; }
Band 30 { Value 629.755; width 8.095; }
Band 31 { Value 637.85; width 8.095; }
Band 32 { Value 645.954; Width 8.095; }
Band 33 { Value 654.04; Width 8.095; }
Band 34 { Value 662.135; Width 8.095; }
Band 35 { Value 670.23; Width 8.095; }
Band 36 { Value 678.325; width 8.095; }
Band 37 { Value 686.42; width 8.095; }
Band 38 { Value 694.515; Width 8.095; }
Band 39 { Value 702.61; Width 8.095; }
Band 40 { Value 710.705; Width 8.095; }
Band 41 { Value 718.8; Width 8.095; }
Band 42 { Value 726.895; width 8.095; }
Band 43 { Value 734.99; width 8.095; }
Band 44 { Value 743.085; Width 8.095; }
Band 45 { Value 751.18; Width 8.095; }
Band 46 { Value 759.275; Width 8.095; }
Band 47 { Value 767.37; Width 8.095; }
Band 48 { Value 775.465; width 8.095; }
Band 49 { Value 783.56; width 8.095; }
Band 50 { Value 791.655; Width 8.095; }
Band 51 { Value 799.75; width 8.095; }
Band 52 { Value 807.845; width 8.095; }
Band 53 { Value 815.94; Width 8.095; }
Band 54 { Value 824.035; Width 8.095; }
Band 55 { Value 832.13; Width 8.095; }
Band 56 { Value 840.225; Width 8.095; }
Band 57 { Value 848.32; width 8.095; }
Band 58 { Value 856.415; width 8.095; }
Band 59 { Value 864.51; Width 8.095; }
Band 60 { Value 872.605; Width 8.095; }
Band 61 { Value 880.7; Width 8.095; }
Band 62 { Value 888.795; Width 8.095; }

```
        Band 63 { Value 896.89; width 8.095; }
        Band 64 { Value 904.985; width 8.095; }

}
```

C.5 <u>Leaf Area Index Calculation Program</u>

```
# Min NDVI
# Max NDVI
# K
#
# set cell size for the model
#
SET CELLSIZE MIN;
#
# set window for the model
#
SET WINDOW UNION;
#
# set area of interest for the model
#
SET AOI NONE;
#
# declarations
#
Float RASTER n1_lm64_refl_sub FILE OLD NEAREST NEIGHBOR AOI NONE
"/export/home/jcraig/lm64_refl_sub.img";
Float RASTER n14_kerr_LAI FILE DELETE_IF_EXISTING USEALL ATHEMATIC
FLOAT SINGLE "/export/home/jcraig/kerr_LAI.img";
FLOAT SCALAR n6_Float;
FLOAT SCALAR n7_Float;
FLOAT SCALAR n8_Float;
#
# load scalar n6_Float
#
n6_Float = 0.35;
#
# load scalar n7_Float
#
n7_Float = 1;
#
```

```
# load scalar n8_Float
#
n8_Float = -0.11;
#
# function definitions
#
#define n5_memory Float(($n1_lm64_refl_sub(3) - $n1_lm64_refl_sub(2)) /
($n1_lm64_refl_sub(3) + $n1_lm64_refl_sub(2)))
#define n10_memory Float(LOG ( ($n5_memory - $n7_Float) / ($n6_Float - $n7_Float ) )
/ $n8_Float)
n14_kerr_LAI = EITHER $n10_memory IF ($n10_memory > 0) OR  0 OTHERWISE ;
QUIT;
```

LIST OF REFERENCES

Arino, O. , C. Brockman, B. Versini and G. Pittella. 1994. ESA products and processing algorithms for Landsat-TM. *ESA Technical Note TM-TN-DPE-OT-OA-001* May 31, 1994. ESA/ESRIN Earth Observation Division, Frascatti, Italy.

Barry, John M. 1980. *Natural vegetation of South Carolina.* University of South Carolina Press, Columbia.

Beadle, C.L., M.M. Ludlow and J.L. Honeysett. 1993. Water relations. In D.O. Hall, J.M.O. Scurlock, H.R. Bolhar-Nordenkampf, R.C. Leegood and S.P. Long (ed.) *Photosynthesis and production in a changing envioronment. A field and Laboratory manual*. Chapman & Hall.

Bielorai, H., J. Shalhevet and Y. Levy. 1978. Grapefruit response to variable salinity in irrigation water and soil. *Irrig. Sci.* 1:61-70.

Bolton, J. 1999. *Characterization of an Airborne Imaging Spectrometer System.* Fourth International Airborne Remote Sensing Conference and Exhibition held in conjunction with the 21st Canadian Symposium on remote sensing 1999. ERIM International, Inc. Ann Arbor.

Boman, B.J. 1993. First-year response of Ruby Red grapefruit on four rootstocks, to fertilization and salinity. *Proc. Florida State Hort. Soc.* 106:12-28.

Brandt, K., and K. C. Ewel. 1989. *Ecology and management of cypress swamps: A review.* Bull. 252. Fl. Coop. Ext. Serv. IFAS. Univ. Florida. Gainesville

Brown, M.J. 1995. *Forest statistics for Florida,* 1995. USDA For. Serv., Southern Res. Sta., Res. Bull. SRS-6.

Brown, M.J. 1987. *Forest statistics for Florida,* 1987. USDA For. Serv., Southeastern For. Exp. Sta. Res. Bull. SE-96-100.

Brown, Sandra. 1981. A comparison of the structure, primary productivity, and transpiration of cypress ecosystems in Florida. *Ecological Monographs* 51(4):403-427.

Burns, A.C. 1980. Frank B. Williams: Cypress lumber king. *J. For. Hist.* 24:127-133.

Cao, C. and N. S. Lam. 1997. Understanding the scale and resolution effects in Remote Sensing and GIS. In: D.A. Quattrochi and M.F. Goodchild, eds., *Scale in Remote Sensing and GIS*. CRC Press, Boca Raton, Florida.

Carter, G. A. 1998. Reflectance wavebands and indices for remote estimation of photosynthesis and stomatal conductance in pine canopies. *Remote Sens. Environ.* 63:61-72.

Carter, G. A. 1994. Ratios of leaf reflectances in narrow wavebands as indicators of plant stress. *Int. J. of Remote Sensing*. 15(3):697-703.

Carter, G. A. 1993. Responses of leaf spectral reflectance to plant stress. *American J. of Botany*. 80(3):239-243.

Carter, G. A. 1991. Primary and secondary effects of water content on the spectral reflectance of leaves. *American J. of Botany*. 78:916-924.

Carter, G. A.,. T. R. Dell and W. G. Cibula. 1996. Spectral reflectance characteristics and digital imagery of a pine needle blight in the southeastern United States. *Can. J. of Forest Resources*. 26:402-407.

Carter, G. A., W. G. Cibula and R. L. Miller. 1996. Narrow-band Reflectance imagery compared with thermal imagery for early detection of plant stress. *J. Plant Physiol.* 148:512-522.

Christiansen, M. N. 1979. Organization and conduct of plant stress research to increase agricultural productivity. In: H. Mussell and R. C. Staples, Eds., *Stress physiology in crop plants*. John Wiley and Sons, New York.

Conner, William H., and John W. Day, Jr. 1976. Productivity and composition of a baldcypress-water tupelo site and a bottomland hardwood site in a Louisiana swamp. *American J. of Botany* 63(10):1354-1364

Craig, J. C. 1996. *Cumulative impact of water withdrawal and urbanization on wetlands in the northern Tampa Bay region of Florida*. Master's Thesis, University of Florida, Gainesville, FL.

Craig, J. C., S. F. Shih, B. J. Boman and G. A. Carter. 2000. Multispectral aerial imaging for detection of salinity stress in citrus. Presented at the Second International Conference on Geospatial Information in Agriculture and Forestry, Lake Buena Vista, Florida, 10-12 January, 2000.

Craig, J. C., S. F. Shih, B. J. Boman and G. A. Carter. 1998a. Detection of salinity stress in citrus trees using narrow-band multispectral imaging.. Presented at the First International Conference on Geospatial Information in Agriculture and Forestry, Lake Buena Vista, Florida, 1-3 June, 1998.

Craig, J. C., S. F. Shih, B. J. Boman and G. A. Carter. 1998b. Detection of salinity stress in citrus trees using narrow-band multispectral imaging.. Presented at the American Society of Agricultural Engineers Annual International Meeting, July 12-16, 1998.

Craig, J. C. and S. F. Shih. 1998. The spectral response of stress conditions in citrus trees: development of methodology. *Soil Crop Sci. Soc. Florida Proc.* 57:16-20 (1998).

Curran, P. J., G. M. Foody and P. R. van Gardingen. 1997. Scaling up. In: P.R. van Gardingen, G. M. Foody and P. J. Curran, eds. *Scaling up: from cell to landscape.* Cambridge University Press., Cambridge, UK.

Dasberg, S., H. Bielorai and Y. Erner. 1991. The effect of saline irrigation water on shamouti oranges. *Acta Hortic.* 228:305.

Duryea, M. L. and L. A. Hermansen. 2000. *Cypress: Florida's Majestic and Beneficial Wetlands Tree.* Circular 1186-University of Florida Cooperative Extension Service, Institute of Food and Agricultural Sciences, Gainesville, FL.

ERDAS 1999. *Field Guide, 5th edition.* ERDAS, Atlanta, GA.

Ewel, K.C., H.T. Davis, and J.S. Smith. 1989. Recovery of Florida cypress swamps from clearcutting. *South. J. Appl. For.* 13(3):123-126.

FDOT. 1985. *Florida land use, cover and forms classification system.* Florida Dept. of Transportation, State Topographic Mapping Bureau, Thematic Mapping Section, Tallahassee

Friedel, M. A. 1997. Examining the effects of sensor resolution and sub-pixel heterogeneity on spectral vegetation indices: implications for biophysical modelling. In: D. A. Quattrochi and M. F. Goodchild, Eds. *Scale in remote sensing and GIS.* CRC Press, Boca Raton, Florida

GER, 1996. GER 1500 *Spectroradiometer User Manual Release 2.0,* Geophysical and Environmental Research Corporation, Millbrook, NY.

Guyot, G. and F. Baret. 1988 Utilisation dela haute resolution spectral pour suivre l'etat des couvert vegetauz. In *Proceedings of the Fourth International Colloquium on*

Physical Measurements and Signatures in Remote Sensing, ESA SP-287, European Space Agency, Noordwijk, pp. 279-286.

Heller, J., J. Shalhevet, and A. Goell. 1973. Response of a citrus orchard to soil moisture and soil salinity. p. 409—419. *In* A. Hadas et al. (ed.) *Physical aspects of soil water and salts in ecosystems. Ecol. Stud. 4.* Springer-Verlag, Berlin.

Houghton Mifflin. 1996. *The American Heritage Dictionary of the English Language, Third Edition.* Houghton Mifflin Company.

Hutton, J. J. , T. Savina and E. Lithopoulos. 2000. *Photogrammetric application of Applanix's Position and Orientation System (POS).* Applanix Cororation, Markham, ON, Canada.

Jago, R. A., M. E. J. Cutler, P. J. Curran. 1999. Estimating canopy chlorophyll concentration from field and airborne spectra. *Remote Sens. Environ.* 68:217–224

Jensen, J. R. 2000. *Remote sensing of the environment an Earth resource perspective.* Prentice Hall, Upper Saddle River, NJ.

Kaplan, H. 1996. Machine vision: photonics advances drive an exploding applications market. *Photonics*, December, 1996:72-79.

Kennedy, Harvey E., Jr. 1972. Baldcypress-an American wood. USDA Forest Service, FS-218. Washington, DC. 5 p.

Kramer, P.J. 1983. *Water Relations in Plants.* Academic Press, New York.

Lang, A.R.G. 1969. Osmotic coeficients and water potentials of sodium chlirida solutions from 0 to 40 °C. *Australian Journal of Chemistry* 20:2017-2023.

Lillesand, T. E. and R. W. Kiefer. 1994. *Remote Sensing and Image Interpretation, Third Edition*. John Wiley and Sons. New York.

Leopold, A. 1937. A biotic view of land. *Journal of Forestry* 37:727-730.

Lesser, P.F. 1997. *Florida Citrus Outlook: The 1997-98 Season: A Presentation to the Florida Citrus Commission October 29, 1997.* Florida Department of Citrus, Lakeland, Florida.

Levy, Y., H. Bielorai, and J. Shalhevet. 1978. Long-term effects of different irrigation regimes on grapefruit tree development and yield. *J. Am. Soc. Hortic. Sci.* 103:680—683.

Lunetta, R., R. Congalton, L. Fenstermaker, J. Jensen, K. McGuire, L. Tinney. 1991. Remote sensing and geographic information system data integration: rror sources and research issues. Photogrammetric Engineering and Remote Sensing. 57(6):677-687.

Maas, E. V.. 1992. Salinity and Citriculture. In: *Proc Int. Soc. Citriculture.* (3):1290-1301

Mao, C., and D. Kettler 1995. Digital CCD cameras for airborne remote sensing. *Proceedings, 15 th Biennial Workshop on Videography and Color Photography in Resources Assessment, 1-3 May, 1995, Terre Haute, Indiana,* Amer. Soc. Photogram. Remote Sens., pp. 1-12.

McClave, J.T. and F.H. Dietrich, II. 1982. *Statistics, 2nd ed.* Dellen Publishing Co., Santa Clara, California.

Miller, J. A. 1990. Groundwater Atlas of the United States Segment 6 Alabama, Georgia, Florida and South Carolina. *Hydrological Investigations Atlas 730-G,* U. S. Geological Survey, Washington.

Miller, J. R. , E. W. Hare, and J.Wu. 1990. Quantitative characterization of the vegetative red edge reflectance: an inverted-Gaussian reflectance model. *Int. J Remote Sens.* 11:1755–1773.

Moore, D.G., M.L. Horton, J.J. Russel, and V.I. Meyers, 1975. Evaluation of Thermal X/5 Skylab S-192 Data for Estimating Evapotranspiration and Thermal Properties of Soils for Irrigation and Management. *Proc. of the NASA earth resources survey symposium,* Houston, Texas, NASA TX X-58168, pp. 2561-2583.

Morton, J. 1987. Grapefruit. p. 152-158. In: *Fruits of warm climates.* Julia F. Morton, Miami, FL.

Myers, R.L. and J.J. Ewel (editors). 1990. *Ecosystems of Florida.* University of Central Florida Press, Orlando, Florida.

Research Systems 2000. *ENVI 3.4 User's Guide.* Research Systems, Inc. Boulder, CO.

Rock, B.N., T. Hoshizaki, and J.R. Miller. 1988. Comparison of in situ and airborne spectral measurements of the blue shift associated with forest decline. *Remote Sensing of Environment.* 24:109-127.

Rochow, T.F. 1985. Hydrologic and vegetational changes resultig from underground pumping at the Cypress Creek Wellfield, Pasco County, Florida. *Fla. Sci.* 48(2):65-80.

Rochow, T.F. 1996. *The effects of water table level changes on fresh-water marsh and cypress wetlands in the Northern Tampa Bay Region--A review*, Technical Report 1996-1, Southwest Florida Water Management District, Brooksville.

Rouse, J. W., R.H. Haas, J. A. Schell and D.W. Deering. 1974. Monitoring vegetation systems in the Great Plains with ERTS. Proceedings, Third Earth Resource Technology Satellite-1 symposium, Greenbelt, MD. NASA SP-351, 310-317.

Salisbury, F.B. and C.W. Ross. 1992. *Plant Physiology, 4th ed.* Wadsworth Publishing Co., Belmont, California.

Schreiber, U. 1997. *Chlorophyll fluorescence and photosynthetic energy conversion: Simple introductory experiments with the TEACHING-PAM Chlorophyll Fluorometer.* Heinz Walz GmbH, Effeltrich, Germany.

Shih S.F. and J.D. Jordan. 1992. Landsat mid-infrared data and GIS in regional surface soil-moisture assessment. *Water Resources Bulletin*, 28(4):713-719.

Shih, S.F., D.L. Myher, G.J. Edwards, C.H. Blasquez and J.M. Gardner. 1985. Wavelength intensity indices in relation to tree conditions and leaf nutrient content. *Proc. 11th International Symposium on Machine processing of Remotely Sensed Data*. Purdue University, Laboratory of Application of Remote Sensing, West Lafayette, Indiana, pp. 350-356.

Shalhevet and Levy. 1990. Citrus Trees. P. 951-986. In: B.A. Stewart and D.R. Nielsen (eds.) *Irrigation of Agricultural Crops*. Chapt. 32. Agronomy Monograph 30. Amer. Soc. Agron. Madison, WI.

Shrestha, R. L. and B. Carter. 1998. Instant evaluation of beach storm damage using airborne laser terrain mapping. *EOM*. March, 1998:42-44.

Steven, M. D. 1993. Satellite remote sensing for agricultural management: opportunities and constraints. *ISPRS J. of Photogrammetry & Remote Sensing*. 48(4):29-34.

Storey, R. 1995. Salt tolerance, ion relations and the effects of root medium and the response of citrus to salinity. *J. Exp. Bot.*, 38:1769.

Syvertsen, J. P. and J. J. Lloyd. 1994. Citrus. In: Schaffer B. and P. C. Andersen, eds. *Handbook of environmental physiology of fruit crops, vol. II subtropical and tropical crops*. CRC Press, Boca Raton, FL. USA

Syvertsen, J.P., B. Boman and P.H. Tucker. 1989. Salinity in Florida citrus production. *Proc. Fla. State Hort. Soc.*, 102:61.

SWFWMD 1996. *Northern Tampa Bay Water Resources Assessment Project.* Vol 1: Surface Water/Ground-Water Interrelationships. Resource Evaluation Section, Southwest Florida Water Management District, Brooksville.

Tozlu, I. 1997. *Salinity stress responses and mapping QTL involved in growth, dry matter, and ion uptake in salinized and non-salinized Citrus and Poncirus.* Doctoral dissertation, University of Florida, Gainesville.

USGS 2000. *United States national map accuracy standards, revised 1947.* Available online at http://rmmcweb.cr.usgs.gov/public/nmpstds/nmas.html

Wehr, A. and U. Lohr. 1999. Airborne laser scanning–an introduction and overview. *ISPRS J. of Photogrammetry & Remote Sensing* 54(1999):68-82.

Whitfield, D. M. 1986. A simple model of light penetration into row crops. *Agricultural and Forest Meteorology.* 36:297-315.

Wilhite, L. P. and J. R. Toliver. 1990. Baldcypress In: Burns, Russell M., and Barbara H. Honkala, eds. *Silvics of North America: Volume 1. Conifers.* Agriculture Handbook 654. U.S. Department of Agriculture, Forest Service, Washington, DC.

Williston, H.L., F.W. Shropshire, W.E. Balmer. 1980. *Cypress Management: Forgotten Opportunity.* USDA For. Rept. SA-FR 8.

BIOGRAPHICAL SKETCH

John C. Craig was born on April 7, 1960, in Rochester, New York. Mr. Craig has lived and worked for extended periods in Brazil and the Caribbean. He received a Bachelor's degree in Physics from the State University of New York College at Fredonia, and a Master's degree in Environmental Engineering Sciences from the University of Florida. He was awarded a NASA Graduate Student Researchers Program fellowship with the John C. Stennis Space Center to study vegetation stress detection with remote sensing. Mr. Craig is a member of the Ecological Society of America, and Gamma Sigma Delta, the national honor society for agriculture and natural resources related professions.

I certify that I have read this study and that in my opinion it conforms to acceptable standards of scholarly presentation and is fully adequate, in scope and quality, as a dissertation for the degree of Doctor of Philosophy.

Jonathan D. Jordan, Chairman
Assistant In Agricultural and Biological
Engineering

I certify that I have read this study and that in my opinion it conforms to acceptable standards of scholarly presentation and is fully adequate, in scope and quality, as a dissertation for the degree of Doctor of Philosophy.

Larry O. Bagnall
Professor Emeritus of Agricultural and
Biological Engineering

I certify that I have read this study and that in my opinion it conforms to acceptable standards of scholarly presentation and is fully adequate, in scope and quality, as a dissertation for the degree of Doctor of Philosophy.

Brian J. Boman
Associate Professor of Agricultural and
Biological Engineering

I certify that I have read this study and that in my opinion it conforms to acceptable standards of scholarly presentation and is fully adequate, in scope and quality, as a dissertation for the degree of Doctor of Philosophy.

Mark T. Brown
Assistant Professor of Environmental
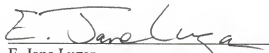Engineering Sciences

I certify that I have read this study and that in my opinion it conforms to acceptable standards of scholarly presentation and is fully adequate, in scope and quality, as a dissertation for the degree of Doctor of Philosophy.

Gregory A. Carter
Research Scientist, John C. Stennis Space
Center, National Aeronautics and Space
Administration

This dissertation was submitted to the Graduate Faculty of the College of Agricultural and Life Sciences and to the Graduate School and was accepted as partial fulfillment of the requirements for the degree of Doctor of Philosophy.

May, 2001

E. Jane Luzar
Dean, College of Agricultural and Life
Sciences

Winfred M. Phillips
Dean, Graduate School